UNIVERSITA' DEGLI STUDI DI ROMA

"TOR VERGATA"

FACOLTA' DI SCIENZE MATEMATICHE, FISICHE E NATURALI

DOTTORATO DI RICERCA IN FISICA

XXI CICLO

Electronic Correlations: an Insight by New Models for Auger and Coster-Kronig Transitions

Simona Ugenti

A.A. 2008/2009

Docente Guida/Tutor:
Prof. Michele Cini

Coordinatore:
Prof. Piergiorgio Picozza

Contents

Acknowledgements

Before beginning the journey into the protean world of Auger transitions from strongly correlated materials armed with new models and hunger knowledge, I would like to spend a few words to thank all the people without whom this enterprise certainly would have not been possible.

First of all I would like to thank my scientific advisor, Prof. Michele Cini, who worked hard on this project and always trusted and encouraged me since the very beginning of the adventure of this Ph.D. thesis.

I thank here also the stimulating group of research to which I belong, made up of Dr.s Enrico Perfetto and Gianluca Stefanucci, for their support and precious help.

I'm also grateful towards Dr. Josè Lorenzana of the ISC-CNR (Istituto Sistemi Complessi) of Rome and Prof. Götz Seibold of the Institut für Physik of the BTU (Brandenburgische Technische Universität) of Cottbus, for their fruitful discussions and precious advices: without them I would have risked to loose my direction in the tricky sea of the Gutzwiller's theory and its most recent developments.

During my Ph.D. studies I was involved in very fruitful cooperations with many valuable scientific groups and I would take advantage of this dedicated space to thank them all. In particular I'm grateful towards the group of Prof. Giovanni Stefani of the University "Roma Tre", Dr. Roberto Gotter of the TASC-INFM National Laboratory of the Synchrotron ELETTRA in Trieste and the group of Prof. Calogero Natoli of the National Laboratories of Frascati (LNF).

A special thank goes to all my venture-fellows of the awesome *Stanza Dottorandi* and in particular to Dr.s Giulia Festa, Antonio Racioppi, Marine Samsonyan and Francesco Stellato, who shared with me these three years of Ph.D. making them something much more than only years of study.

I would like to take advantage of this dedicated space to thank also my friends Orazio, Gianfabio, Luca and Alessandro for having supported me during the last months of my Ph.D. and for the smile they gave me lightening so many days of hard work.

I'm grateful towards Giovanni, Claudia and Tatiana too, for their amusing gags and above all their fondness and friendship.

I could never forget to thank my family (including Kikki, my cats) who built up every little brick of my essence with their love, support, craziness and a sprinkle of feline purr.

I dedicate this thesis and all my work to my grandfather Santo, who always trusted in the importance of education as the real solid backbone of human beings. Everywhere he is, I know that now he is laughing with my heart because he is crossing this tape with me.

A very very special thank goes to Francesco whose love and unshakeable faith in me are and have always been the only fixed stars in that chaotic firmament of my life and thoughts.

Fulled by all the extraordinary quality of all this people surrounding me, I need nothing else: I'm ready to face whatever new venture the future will propose - or impose - to me, so...

..I'm only left to say..

...avanti coi carri[1]!

[1] "Tanks go on!"...The Ugenti's battle cry.

1 Introduction

Electronic correlations have always played a fundamental role within Physics in general and in the field of condensed matter in particular. As an example for the latter it is enough to think about the agreed but not yet understood key role of correlations in superconductivity both from carbon nanotubes [1] and CuO_2 compounds [2, 171], as far as the so-called high T_c superconductors are concerned. Moreover electronic correlation is stated by many as the main cause of the breakdown of one-hole picture in the electronic structure of transition metal mono-oxides like NiO and CoO, which resulted in the introduction of the now famous Mott-Hubbard picture of insulators [4, 5, 6]. In these cases an extra complication arises from the remarkable contribution of magnetic ordering. The AF (Anti-Ferromagnetic) one in fact is another interesting correlation phenomenon occurring in these oxides [1], which contributes to complicate diagnosis for these materials.

From the few above examples one can already understand the growing interest into the deepening of our knowledge about this topic. To this end the well known property of being a local probe for electronic correlations qualifies the Auger spectroscopy as the most suitable instrument to draw out such a kind of information from the measured spectra. In particular Auger spectra from solids with incompletely filled valence bands, which represent a theoretically still unsettled field, are promising from this point of view. They are characterized in fact by many complications besides the ones which are typical for closed band materials. They just arise from the increased number of degrees of freedom that are available for holes delocalization and so are all deeply rooted in correlation mechanisms.

[1] NiO and CoO are both AF insulators below their Neèl temperatures, at 525 and 289 K respectively.

The present work is set within this framework and its task is to gain a deeper view on electronic correlations trying to explain Auger spectra from open band materials. Each one of the models we developed, and which will be presented in Chapter 4, represents in fact a little step forward towards a full understanding of the manifold and complex structures which populates this kind of spectra.

To this end we started modifying models for closed band solids so as to apply them to materials with not completely filled valence bands, such as for example the case of Copper, HOPG Graphite and single walled carbon nanotubes. After having built up an ab-initio approach to set free theoretical Auger patterns from experimentally determined parameters, we concentrate on the first application of a new time-dependent approach, the Gutzwiller approximation, to CuO_2 planes, having a quite half filled valence band. This case represents the maximum level of complication one can currently deal with as far as Auger spectra from open bands are concerned. For this level of filling in fact there are no existing theories which are able to explain this kind of spectra and surely closed bands approaches cannot be confidently applied.

The last model that will be presented is aimed to disentangle some of the sharpest features that may be present in an Auger spectrum from the ones due to the corresponding parent diagrammatic lines. These peaks are due to three holes structures originating from Coster-Kronig preceded Auger transition and, as it will be shown in Chapter 4, both their shape and position on the kinetic energy scale are strongly influenced by the magnitude of Coulomb interactions; similar remarks are known to hold for the two holes structures produced by the simpler Auger transitions.

My contribution to this project has been to help the development of several of the theoretical models which my group has worked upon, and most importantly to analyze the findings of our computations and simulations. The research has involved many modeling decisions, a thorough study of the equations and the creation of software (in many cases directly from scratch) to solve these equations.

In summary, I have been involved in nearly all phases of the project from its very beginning, including the presentation of the results to conferences and the writing-up of the research papers, both published and in preparation.

This thesis work is organized as follows: the first two chapters are devoted to build the theoretical basis for the models which have been developed and discussed within this thesis. The aim of Chapter 2 is in fact to draw an introduction to the basic features of Auger transitions and the theories used till today to predict the characteristic spectra they

produce. Chapter 3 instead focuses on the description of the Gutzwiller approximation: a time-dependent theory we used for the first time as an alternative approach to foresee Auger spectra from materials whose valence bands are not completely filled.
Chapter 4 is entirely dedicated to the description of the models we developed and their applications, while at last Chapter 5 recollects together all the achieved results drawing some conclusions.

2

A Little Bit of Augerology

Diving into the main features of the Auger processes to discover and deepen the promising information they give is the aim of this chapter. Since decades in fact the study of this kind of transition has played a fundamental role in improving our knowledge about the nature and magnitude of electronic correlations. These processes were known and studied since the first half of twentieth century. Despite that they are not still completely understood especially for open bands materials and reveals some surprises till today as it will be shown with this thesis work.

This chapter is organized as follows: in the first section some general features typical of an Auger process will be introduced. The following paragraphs instead will be devoted to describe Auger transitions from isolated atoms and solids, focusing in particular on the latter case. The final sections are centered on the challenge represented by the modeling of Auger transitions from open bands solids, which is still an open problem at the state of the art today.

2.1 The Auger Process

The Auger process [7, 8] is a radiationless autoionization event leading to a final two hole state in the considered target atom. Despite the fact it was firstly discovered in 1923 by Lise Meitner [9], because of the women′s condition of the time it took its name from Pierre Auger who independently discovered this kind of transitions two years later.

If a two-step approximation is valid this effect can be schematized as a first ionization event followed by a second emission of a free electron which is named Auger electron. After

the creation of the first core hole in fact, the other passive electrons of the target atom re-adjust their configuration because of the changed potential: one electron of the outer shells fills the initial vacancy and the energy gained in this transition is given to another outer electron, which will be our second free electron, the Auger one. This kind of transition can be schematized as:

$$\begin{aligned} h\nu + A \longrightarrow \quad & A^{+} \quad + e_1^{-} \\ \hookrightarrow \quad & A^{++} + e_2^{-} \end{aligned} \tag{2.1}$$

where $h\nu$ represents the photons of frequency ν impinging on the sample, while A, A^{+} and A^{++} describe the target atom respectively in its neutral, ionized and doubly ionized state; e_1^{-} and e_2^{-} are the emitted photo[1] and Auger electrons.

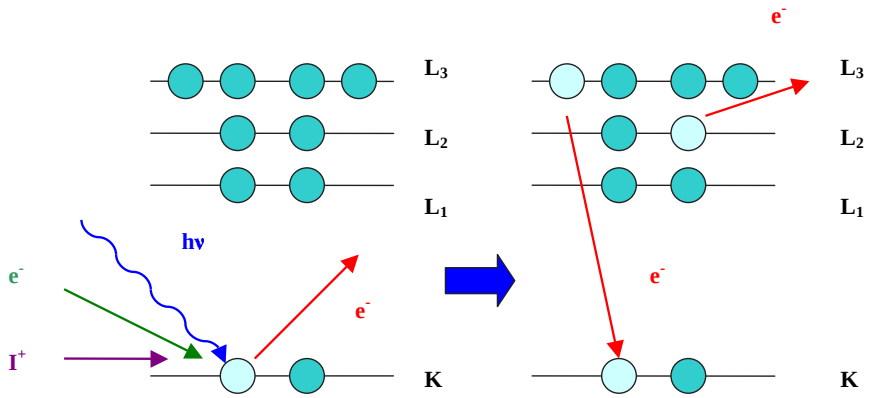

Figure 2.1. *Schematic representation in a two step approach of a KL_2L_3 Auger transition. The initial core hole is created in the K shell ($1s$) and it is filled by an electron coming from the L_2 shell ($2p_{1/2}$) because of relaxation of the other passive electrons. This process is followed by the emission of a L_3 electron ($2p_{3/2}$) which gained the energy of the core hole decay.*

Fluorescence and the Auger effect are the two main competing ways for a core hole decay. These two processes differ one to the other both in the nature of the operator responsible for the decay and in the possible achievable kind of final states. In fluorescence (which is the dominant core hole decay for heavy atoms) in fact the core hole is filled by an outer

[1] A photoelectron is an electron emitted because of the absorption of a photon impinging on the target atom which has enough energy to set it free.

shell electron and the energy gained in this relaxation process is communicated to a released photon: so the operator responsible for this transition is the electromagnetic interaction and it leads to a singly ionized final state plus the emission of a free photon. In an Auger decay (dominant for lighter atoms) instead the interaction which provokes the relaxation of at least the other two active electrons is the Coulomb operator and the final state is a two hole one.

Labeling with $|i\rangle$ and $|f\rangle$ respectively the initial and final states of the considered system and treating the Coulomb interaction as a small perturbation, the Auger transition probability P_{if} can be written using the Fermi golden rule [7]:

$$P_{if} = \frac{2\pi}{\hbar}|M_{if}|^2\delta(E_i - E_f), \tag{2.2}$$

where:

$$M_{if} = \sum_{m<n}\langle i|\frac{e^2}{r_{mn}}|f\rangle, \quad r_{mn} = |\overrightarrow{r}_m - \overrightarrow{r}_n|, \tag{2.3}$$

and where E_i and E_f are respectively the energies of the states $|i\rangle$ and $|f\rangle$ which describe the ionized system with a core hole and the doubly ionized system with two final holes plus a free electron of energy E_C. Summation in Eq.(2.3) runs over the N electrons of the target atom.

A rigorous calculation of $|i\rangle$ and $|f\rangle$ for a correlated N electrons system is a quite difficult task and in the following section several ways to do that or other alternative approaches to evaluate Auger intensities will be presented.

For heavy atoms Eq.(2.2) gives no more an accurate description of the Auger probability and a relativistic approach [10] is needed both for the involved states and for the interaction. The latter one in this case has to be described as scattering process between the two final holes (Möller scattering) which is mediated by a virtual photon having an energy $\hbar\omega$ equal to the one emitted by the corresponding radiative decay. The transition amplitude obtained this way can be interpreted in a semiclassical picture as due to an effective potential, $V(r_{12})$, acting on Dirac four components wave functions:

$$V(r_{12}) = \left[1 - \alpha_1 \cdot \alpha_2 f + c^2(\alpha_1 \cdot \nabla_1)(\alpha_2 \cdot \nabla_2)\frac{(f-1)}{\omega^2}\right]\frac{e^2}{r_{12}}. \tag{2.4}$$

Here the several α_i represent the Dirac's velocity matrices, c is the light speed in vacuum

and $f = exp(i\omega r_{12}/c)$ describes retardation effects. It can be shown that in a non relativistic limit the last two terms of Eq.(2.4) are negligible and $V(r_{12})$ reduces to the Coulomb potential.

From the point of view of nomenclature an Auger transition is identified by using the symbols of only the shells of the three active electrons written in the spectroscopic notation[2] and firstly indicating the shell of the initial deep hole. For instance if the initial core hole is produced in the K shell ($1s$), as the case reported in fig.(2.1), and the final state is characterized by two final holes in the L_2 ($2p_{1/2}$) and L_3 ($2p_{3/2}$) shells, the corresponding Auger transition is named KL_2L_3. In particular if the electron filling the initial deep hole or both the two relaxing electrons belong to the same shell of the core hole, the corresponding Auger decay is named respectively *Coster-Kronig* and *super Coster-Kronig* transition.

The kinetic energy of the electron ejected as a result of the Auger process ABC, where A is the shell in which initial ionization takes place and B and C are the shells of the two final holes, is given by:

$$E_{kin} = E_A^{(N-1)} - E_{BC}^{(N-2)}, \tag{2.5}$$

where $E_A^{(N-1)}$ and $E_{BC}^{(N-2)}$ are the energies respectively of the initial singly ionized and the final doubly ionized states. To take into proper account the relaxation of the other passive electrons, Eq.(2.5) usually is written in terms of the binding energies of the three active holes (ε_i with $i = A,B,C$) plus a correction term, ΔE, whose aim is to contain correlation and relaxation effects:

$$E_{kin} = \varepsilon_A - (\varepsilon_B + \varepsilon_C + \Delta E). \tag{2.6}$$

During the past decades several methods were developed to evaluate ΔE in a realistic way, which is a quite complicated task. A deep and detailed discussion about them is left to a dedicated section in [11].

[2]The conventional X-ray or spectroscopic notation is a scheme of classification for single particle spin-orbitals based on the principal quantum number n and on the electronic quantum numbers relative to the orbital and the total angular momenta, l and j. Within this scheme each single particle orbital is labeled by a capital letter representing n (i.e. n = 0,1,2,... correspond to K, L, M,...) and a number referring to the energy ordering of orbitals having the same n but different l and j. For example $1s_{1/2} \rightarrow K$, $2s_{1/2} \rightarrow L_1$, $2p_{1/2} \rightarrow L_2$, $2p_{3/2} \rightarrow L_3$, $3s_{1/2} \rightarrow M_1$ and so on.

Eqs.(2.5) and (2.6) are useful to give evidence to another important and typical feature of the Auger transitions. In these expressions in fact E_{kin} results to be completely lacking in any kind of information about the probe which causes the initial ionization event. This means that the kinetic energy of the emitted Auger electron is completely insensitive to whatever will be the energy of the used probe, whose nature influences only the probability to observe the process of interest. Furthermore from Eq.(2.6) it clearly appears that E_{kin} is characteristic of the atom in which the process ABC has taken place, and also that each atom will have a characteristic and unique spectrum of Auger energies. No two atoms in fact can have the same set of electronic binding energies. This qualifies the Auger Electron Spectroscopy (AES) as a standard tool used to check the cleanness and chemical composition of surfaces [12].

At the very beginning of this section the two step approach has been introduced to give a pictorial image of an Auger transition. Notwithstanding it has the advantage of keeping complications to a minimum in the description of this kind of processes, it has to be underlined that it is only an approximation whose accuracy depends on the comparison between the mean life time of the core hole and the relaxation time of the other passive electrons. The two step picture in fact treats the first ionization event and the following Auger decay of the core hole as two incoherent events and this represents a good approximation only if the autoionization process starts when the system has achieved a fully relaxed state. In the 80's Gunnarsson and Schönhammer developed a more general theory [13] describing the quadratic response of the system to photon probe in which photoemission and Auger decay are treated as a unique process in what can be referred to as a one step approach. To describe the spectrum in this picture, the whole set of possible excited initial states with a core hole has to be considered besides the fully relaxed one. The transition amplitudes and a sort of quantum coherence phenomenon occurs. This one step approach involves mathematics of increased complexity but represents the only instrument to gain theoretical access to the great quantity of information given by coincidence electron spectroscopies, i.e. APECS (Auger PhotoElectron Coincidence Spectroscopy) and AR-APECS (Angular Resolved - APECS) [14, 15, 16, 17].

2.2 The Auger Decay in Isolated Atoms

The theoretical formalism for the calculation of transition probabilities in isolated atoms [18] has long been known, having been laid down by Wentzel [19] in 1927 and elaborated by

Burhop [20] in the 50's. The basis of their simple approach was the use of time-independent first-order and non relativistic perturbation theory which makes suitable a calculation of the Auger transition probability via the Fermi Golden Rule, Eq.(2.2). Within this frame the chosen initial state describes a deep core hole and the other two active electrons belonging to outer shells and moving in the field of the nucleus and of all the other electrons in the atom. The final state instead represents the electron added to the inner shell and the other one ejected into the vacuum continuum. This means that actually Wentzel considered the problem from the point of view of the autoionization of hydrogenic states in which a doubly excited state interacts with a singly ionized continuum. The Auger probability per unit time is thus written taking into account only four electron orbitals which take part in the radial integral needed to evaluate the Auger matrix element M_{if} (see Eq.(2.3)).

Subsequent calculations of Auger intensities took the level of sophistication further and quite all the following recipes were based on an Hartree-Fock Slater atomic model firstly introduced by Asaad [21] and Listengarten [22]. In their approach the initial and final state wave functions were calculated assuming that the spin-orbitals of all the passive electrons remain unchanged before and after the Auger transition has taken place. The problem reduces this way again to a two body one and M_{if} can be easily written as:

$$M_{if} = D - E, \tag{2.7}$$

where for an ABC Auger transition:

$$D = \langle \varphi_A(1)\varphi_{ph}(2)|\frac{e^2}{r_{12}}|\varphi_B(1)\varphi_C(2)\rangle \tag{2.8}$$

is the direct term, while E is the exchange one, which can be obtained by swapping φ_B and φ_C in Eq.(2.8). The one particle spin orbital φ_A appearing in Eq.(2.8) represents the initial core hole, while φ_{ph} is that one of the emitted photoelectron. φ_B and φ_C represent instead the spin orbitals of the two final holes produced in the B and C shells.
As it can be seen from Eq.(2.8) the most intense transitions correspond to processes characterized by one particle spin orbitals having similar radial extension. This is the reason why in an Auger spectrum the Coster-Kronig and super Coster-Kronig transitions are usually the dominant ones, provided that they are energetically allowed.

A deep and accurate discussion about the several theories developed after the ones by Assad and Listengarten can be found in [18]. As we anticipated a few lines ago, all these

methods were based on the use of Eq.(2.7). The only differences between one kind of approach and another stem in:

- the way the initial and final wave function were evaluated;
- the choice for the best type of central potential used to calculate one particle spin orbitals, i.e. the IPM (Green's atomic Independent-Particle Model) used by Chen and Crasemann [23] or the Kohn-Sham-Gaspar exchange approximation, KSG, handled by Walters and Bhalla [24, 25, 26];
- the type of coupling (jj, Roussel-Saunders or intermediate coupling[3]) which was thought to be the most suitable to represent the Auger transtion in the atom of interest.

To conclude this section we propose to have a look to at least one measured spectrum: this will give the reader some ideas about what an Auger spectrum from isolated atoms seems like. In literature many Auger spectra from inert gases and monoatomic vapors of several elements can be found, i. e. Zn, Ag, Cd, K, Ge, Hg. As an example Fig.(2.2) shows the $M_{4,5}N_{4,5}N_{4,5}$ spectra from Cd vapors [28] measured using electron impact excitation. In these transitions the initial core hole has been produced in the $3d_{\frac{3}{2}}$ and $3d_{\frac{5}{2}}$ ($M_{4,5}$) shells, while the two final holes are in the $4d_{\frac{3}{2}}$ and $4d_{\frac{5}{2}}$ ($N_{4,5}$) levels. Points represent the experimental data after a procedure of background subtraction, while the solid line is the calculated Auger profile obtained summing all the calculated Lorentian curves also reported in the figure. In the attempt to avoid drowning in a too much detailed description of calculation, here we only say that the reported Auger line shapes were evaluated using an expression similar to Eq.(2.2) but summed over the contributions of all the possible final states. The double vacancy final state configuration ($4d^{-2}$) of the $M_{4,5}N_{4,5}N_{4,5}$ Auger transitions gives rise in the intermediate coupling scheme to the levels $^1S_0$, $^1D_2$, $^1G_4$, $^3P_0$, $^3P_1$, $^3P_2$ and $^3F_4$, $^3F_3$,

[3]In this kind of coupling scheme [27] each state of the used basis set is completely identified using as labels the S, L, J and M_j quantum numbers. As it is quite known these describe respectively the total atom quantum numbers relative to the spin, orbital angular momentum, total angular momentum operators and its projection on the system quantum axis. The intermediate coupling scheme is used in all that cases where the two main interactions present in the total Hamiltonian of a many electron atom (the electrostatic and the spin-orbit energies) may be of any relative order of magnitude, or else in all that cases where we do not want to neglect any one of these two kind of interactions. In this scheme the Coulomb operator is completely diagonal, while the spin-orbit interaction is diagonal with respect to J and M_j. Within this coupling scheme each state is indicated by $^{2S+1}L_J$, where J and S were written as the corresponding numeric values, while L is given in terms of the spectroscopic notation, i. e. $L = 0$ is indicated by S, $L = 1$ by P, $L = 2$ by D and so on. For example the $^1S_0$ term corresponds to a state characterized by $S = 0$, $L = 0$ and $J = 0$.

$^3F_2$. The total Auger intensities were calculated as a sum of delta functions, one for each of these final two holes multiplet term corresponding to a possible way to place two holes in the $N_{4,5}$ shells in intermediate coupling scheme. In summation each delta function is centered to an energy of the final state which was calculated in intermediate coupling scheme also taking into account Configuration Interaction (CI) between the final state configurations $4s^{-2}$, $4p^{-2}$, $4s^{-1}4d^{-1}$, $4d^{-2}$, $5s^{-2}$, $4s^{-1}5s^{-1}$ and $4d^{-1}5s^{-1}$. The weights of delta functions, or else the intensities of the several lines, were evaluated using an expression very similar to Eq.(2.7).

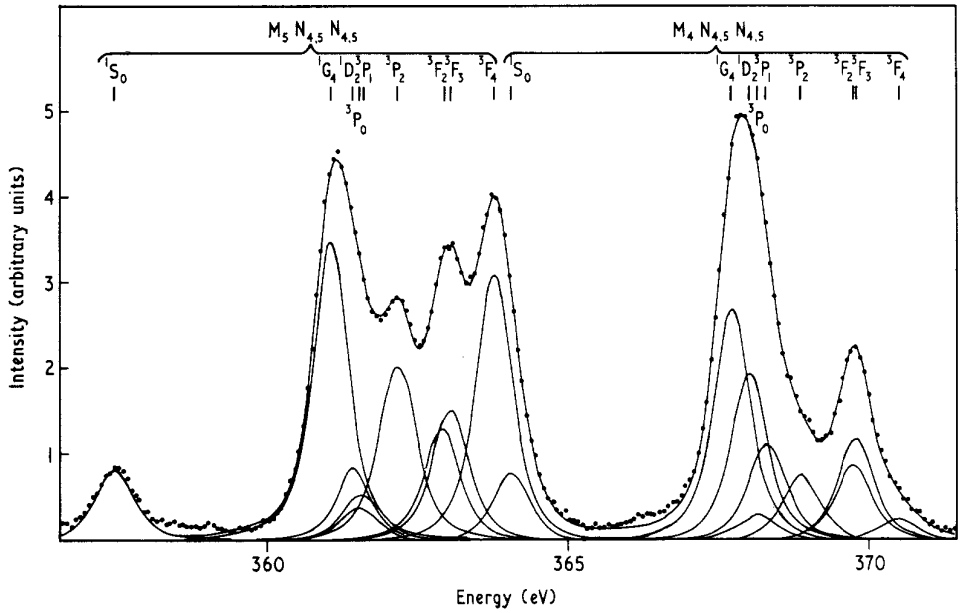

Figure 2.2. *The $M_{4,5}N_{4,5}N_{4,5}$ Auger spectra from cadmium vapor [28] excited by 2 KeV electrons after constant background subtraction and dispersion correction. The experimental result is described by the points. Solid lines instead represent the components whose sum make up the calculated Auger profile also shown in the figure. In particular each component corresponds to one of all the possible multiplet final states with two holes in the $N_{4,5}$ shells in intermediate coupling scheme.*

By methods similar to this one, a good agreement with the experiment in general can be achieved. Depending upon the particular considered element, several complications may arise because of relativistic and spin-orbit effects which become relevant for atoms with high atomic numbers, Z. For $Z > 40$ the most correct way to proceed is to use Eq.(2.4) for the interaction producing the Auger decay of interest and CI relativistic wave functions for the initial and final states. The use of the so-called Breit interaction [29, 30, 31] can be a good approximation for atoms with $Z < 70$ instead of the Möller potential. Besides this for heavy atoms also the finite size of the nucleus may influence calculations because in these cases

it is no more negligible as compared to the K shell dimension. The possible presence of Coster-Kronig and super Coster-Kronig transitions superimposing the parent diagrammatic lines further complicates the analysis and the decoupling of the several lines appearing in an Auger spectrum. Today the values obtained for the energies of the Auger transitions from isolated atoms are reliable to a good level of confidence, while a less satisfactory agreement has been obtained between theory and experiment for the Auger intensities, especially as far as Coster-Kronig transitions are concerned.

2.3 The Auger Decay in Solids: the Core-Valence-Valence Transitions

The core levels of an atom embedded in a solid remain quite the same as in the isolated case, while instead the outer shells are strongly perturbed as it is demonstrated by the appearance of bands. For this reason if the considered Auger transition involves only electrons coming from the inner shells, its spectrum will differ, from the one gained in the isolated atom case, only in the presence of:

1. a background due to secondary electrons;
2. characteristic energy losses for the Auger electrons;
3. shake up satellites provoked by single particle or plasmons excitations;
4. rigid shift of peaks produced by initial and final state effects. In particular the former ones are mainly due to the fact that the atom feels a different electrostatic potential because of its embedding in the crystal lattice and this gives rise to a “chemical shift”. Final state effects instead are mainly produced by the increased solid polarization around the final two holes state respect to a single hole one.

All these effects are present also in transitions involving the creation of final holes in the valence band, but in this case the corresponding spectra represent a real mine of information about chemical bounds and especially electronic correlations.

In this section we will focus on a particular kind of Auger transitions from solids: the Core-Valence-Valence ones (CVV). This type of processes starts with the creation of an initial core hole produced in an inner shell of a lattice atom and ends with a final state characterized by two holes in the valence band. The first attempt to find a theoretical explanation

to the measured CVV line shapes was made by Lander [32] in 1953. In his work he proposed a model which implicitly neglects the effects of electronic correlations. The Auger profile in fact was evaluated as proportional to:

$$P_{if}(\omega) \propto \sum_{f} |M_{if}|^2 A(\omega) \tag{2.9}$$

where M_{if} is the Auger matrix element calculated between the initial and final states of the process as before, while $A(\omega)$ is a two holes density of states evaluated in an independent particle picture as the convolution of one particle density of states. As one expects from Eq.(2.9) and from the way $A(\omega)$ is defined, the shapes of the Auger spectra that can be obtained by using this method can only be band-like, or else they correspond to broadened and quite structureless peaks. This finding was in contrast with some results showed by the first experiments on Auger CVV line shapes which started to be intensively performed on several materials a few decades later. In particular in 1973 Powell [33] measured the CVV Auger spectra from Ag and Al discovering a problem which puzzled scientists until a solution came by the Cini-Sawatzky (CS) theory [34, 35, 36]. While the measured CVV spectrum from Al metal displayed a band-like line shape in accordance with Lander's theory predictions, the one from Ag showed an atomic-like pattern, or else it was dominated by several resolved sharp peaks recalling to the mind the Auger spectra from isolated atoms. In the following years it was shown that CVV Auger spectra from transition metals as Cu [37], In [38], Zn [39], Cd [39, 40] and Ni [40], have an atomic-like line shape, while the same kind of spectra from metals like Li [41] or semiconductors like Si [42] displays a band-like Auger line shape. In the next section it will be demonstrated that these two apparently contrasting behaviours have a common root in the same unified theory for CVV Auger processes from closed band materials and their evident differences are due only to different magnitude of electronic correlations in the considered cases.

2.3.1 The Cini-Sawatzky "Basic" Model for Closed Band Materials

The first of these models to appear was that one of Cini [34, 35], which is based on an Anderson-like [43] approach, i.e. the atom in which the Auger transition is taking place is regarded as an isolated impurity atom embedded in a solid.

The assumptions at the basis of this approach were: a single not degenerate valence band which is initially completely filled and the validity of the "sudden approximation", that is,

no interaction between the departing Auger electron and the ionized solid was included. Relaxation effects and spin-orbit interaction were neglected. Within this picture the total Hamiltonian of the unperturbed system in the hole representation can be written as [35, 44]:

$$H = H_a + H_s + H_{int} + H_f, \tag{2.10}$$

where H_s is the sum of all the one-electron contributions describing the band structure of the solid, while H_{int} collects all the atom-crystal hopping terms. H_f describes the free particle continuum above the vacuum level:

$$H_f = \sum_{k\sigma} \frac{\hbar^2 k^2}{2m} c_{k\sigma} c^+_{k\sigma}. \tag{2.11}$$

Supposing that the initial core hole was created with spin up[4] the atomic contribution in Eq.(2.10) contains a spin-up deep hole term for the primary hole and the hole-hole repulsion Hamiltonian H_r:

$$H_a = \varepsilon_{dh} c^+_{dh\uparrow} c_{dh\uparrow} + \varepsilon_l \sum_{m,\sigma} c^+_{m\sigma} c_{m\sigma} + H_r. \tag{2.12}$$

Here $c^+_{m\sigma}$ ($c_{m\sigma}$) is the creation (annihilation) operator for a hole with spin σ and magnetic quantum number m. H_r instead is the Coulomb repulsion term representing the interaction between the two final holes. The first fundamental difference between Cini's and Sawatzky's approaches comes from the choice they made for H_r:

$$\begin{aligned} H_r^{(Cini)} &= \frac{1}{2} \sum_{\sigma,\sigma'} \sum_{m_1,m_2,m_3,m_4} U_{m_1 0, m_2 0, m_3 0, m_4 0} c^+_{m_1 0\sigma} c^+_{m_2 0\sigma'} c_{m_4 0\sigma'} c_{m_3 0\sigma}, \\ H_r^{(Saw)} &= \frac{1}{2} \sum_{i} \sum_{\sigma,\sigma'} \sum_{m_1,m_2,m_3,m_4} U_{m_1 i, m_2 i, m_3 i, m_4 i} c^+_{m_1 i\sigma} c^+_{m_2 i\sigma'} c_{m_4 i\sigma'} c_{m_3 i\sigma} \end{aligned} \tag{2.13}$$

with

$$U_{m_1 j, m_2 j, m_3 j, m_4 j} = \langle \varphi_{m_1 j\sigma}(1) \varphi_{m_2 j\sigma'}(2) | \frac{1}{r_{12}} | \varphi_{m_4 j\sigma'}(1) \varphi_{m_3 j\sigma}(2) \rangle \quad (j = 0,i). \tag{2.14}$$

[4]The opposite hypothesis leads to a treatment which is completely similar to the one presented in this section except for a sign change in the spin projection of the initial deep hole.

While the latter author considered the two final holes as interacting also when they delocalize in the solid hopping together on different lattice sites (as it is shown by the presence of a summation on the lattice sites i in $H_r^{(Saw)}$ of Eq.(2.13)), Cini used a very localized expression for the hole-hole Coulomb interaction ($H_r^{(Cini)}$), assuming that only the short range part of the Coulomb interaction will be of interest for the considered problem, because the two final holes are expected to effectively interact only when they stayed on the same site (indicated by the fixed label 0 in Eq.(2.13)) where they were created.

It can be anticipated that the different form chosen by Sawatzky for H_{int} has as only consequence for the closed band case a further broadening factor in the calculated final Auger line shape.

The ground state $|\Psi\rangle$ of H is characterized by empty continuum states and completely filled deep hole, valence shell and band states, so the initial state of the CVV Auger transition of interest can be written as $|i\rangle = c^+_{dh\uparrow}|\Psi\rangle$. Starting from this point the system will undergo a CVV Auger transtion under the influence of the time independent perturbation :

$$H' = \sum_{\overrightarrow{k}} \sum_{m,m'} \sum_{\sigma,\sigma'} A_{mm'}(\overrightarrow{k}) c^+_{m\sigma} c^+_{m'\sigma'} c_{dh\sigma'} c_{k\sigma} + h.c., \tag{2.15}$$

where $h.c.$ stands for the Hermitian conjugate and:

$$A_{mm'}(\overrightarrow{k}) = \langle \varphi_{dh}(1)\varphi_{\overrightarrow{k}}(2)|\frac{1}{r_{12}}|\varphi_m(1)\varphi_{m'}(2)\rangle \tag{2.16}$$

is the Auger matrix element. In Eq.(2.16) φ_{dh} and
$varphi_{\overrightarrow{k}}$ represent respectively the deep hole and the free electron single particle wave functions, while φ_m and $\varphi_{m'}$ are the ones of the two final holes.

Neglecting inter-atomic transitions because of their very small Auger matrix elements, the effect of H' is to lead the system to the allowed final state $|00\rangle$, which represents a state characterized by two holes localized on the atomic lattice site where the Auger transition started to take place. Obviously this can not be an H eigenstate because of the possibility of hole delocalization through hopping. This is the reason why $|00\rangle$ has to be projected on a set of two holes states $\{|ln\sigma\rangle\} = \{c^+_{n\sigma}c^+_{l\uparrow}|\Psi\rangle\}$, which are localized on the valence orbitals of the same atom labeled as 0.
By applying the Fermi Golden Rule the Auger spectrum can be decomposed in an atomic and a solid state problem, it will be in fact proportional to:

$$S(\omega) \propto \sum_{lnpq} A^*_{ln}(\overrightarrow{k}) A_{pq}(\overrightarrow{k}) D_{lnpq\sigma}(\omega), \tag{2.17}$$

where summation is made over all the possible allowed two holes final states written in terms of the $\{|ln\sigma\rangle\}$ basis set.

The atomic part of Eq.(2.17) is represented by the Auger matrix elements $A_{pq}(\overrightarrow{k})$ and their hermitian conjugates. This happens because often the valence orbital is only slightly perturbed by the solid and so it can be assumed to be independent from the Auger electron energy and taken from atomic calculations. Otherwise in case of an energy dependence of the Auger matrix elements, its effect on the Auger line shapes is usually negligible because they vary very slowly within an energy interval comparable with the band width. The solid state part of Eq.(2.17) is instead represented by the two holes Local Density Of States (2hLDOS), $D_{lnpq\sigma}(\omega)$, which is given by superposition integrals projecting on a localized holes configuration and describing the two final holes in the valence band:

$$D_{lnpq\sigma}(\omega) = \langle pq\sigma|\delta(\hbar\omega - H_r - H_0)|ln\sigma\rangle \tag{2.18}$$

here H_0 is the sum of all the one body terms contained in $H - H_f$. Before going on with the treatment, it has to be underlined that the presence of a local density of states rather than the band density of states appearing in Lander's theory is one of the characteristics which are completely new in this approach and which makes us able to explain the role of Auger spectroscopy as a local probe for valence states.

There are two limit cases:

1. **Atomic limit** ($H_{int} = 0$ and $H_s = 0$): the Hamiltonian is diagonal in the LS-representation and the spectrum consists of unbroadened multiplet terms.

2. **Non-interacting limit** ($H_r \rightarrow 0$): in the time space the two holes density of states matrix $D^{(0)}_{lnpq\sigma}(t)$ factors as:

$$\begin{aligned} D^{(0)}_{lnpq\downarrow}(t) &= \rho_{lp}(t)\rho_{nq}(t); \\ D^{(0)}_{lnpq\uparrow}(t) &= \rho_{pl}(t)\rho_{qn}(t) - \rho_{lq}(t)\rho_{np}(t), \end{aligned} \tag{2.19}$$

and so, passing to the ω space by Fourier transforming these expressions, $D^{(0)}_{lnpq\sigma}(\omega)$ reduces to simple convolutions of single hole density of states. In this way one recovers the Lander's theory.

In all the possible **intermediate cases** instead the interacting 2hLDOS can be obtained by the real part of the corresponding interacting two holes Green's function:

$$G_{00}(\omega) = i\langle 00|\frac{1}{\omega - H + i\delta}|00\rangle \tag{2.20}$$

which can be gained by projecting the following Dyson-like equation on the complete set (expressed in terms of the $\{|nl\sigma\rangle\}$ basis set) made up of $|00\rangle$ and all the possible states which can be reached from $|00\rangle$ setting free by hopping one or both the localized holes:

$$\frac{1}{\omega - H + i\delta} = \frac{1}{\omega - H_0 + i\delta} + \frac{1}{\omega - H_0 + i\delta} H_r \frac{1}{\omega - H + i\delta}, \tag{2.21}$$

In the previous equation $H = H_0 + H_r$ is the total Hamiltonian of the system (see Eq.(2.10)) which has been decomposed again as the sum of a one-body part, $H_0 = H - H_f$, and the repulsion one H_r. By this procedure one obtains a set of coupled equations for $G(\omega)$ which can also be written in the form of a matrix equation. Passing to the Russell-Saunders coupling scheme, the explicit expression for $G_{00}(\omega)$ of Eq.(2.20) is:

$$G_{00}(\omega) = \sum_{LS} \frac{G^{(0)}_{LS}(\omega)}{1 - U_{LS} G^{(0)}_{LS}(\omega)} \tag{2.22}$$

If the solid does not perturb significantly the spherical simmetry of the atom the G matrix is diagonal in the LS-coupling scheme and the diagonal elements of the transformed matrices G obeys to uncoupled equations. This way we may drop the L,M,S quantum indices and obtain:

$$G_{00}(\omega) = \frac{G^{(0)}_{00}(\omega)}{1 - U G^{(0)}_{00}(\omega)} \Longrightarrow G(\omega) = \frac{G^{(0)}(\omega)}{1 - U G^{(0)}(\omega)} \tag{2.23}$$

with:

$$G^{(0)}(\omega) = i\langle 00|\frac{1}{\omega - H_0 + i\delta}|00\rangle. \tag{2.24}$$

Finally the wanted interacting 2hLDOS will be given by:

$$D(\omega) = \frac{1}{\pi} Re[G(\omega)] = \frac{D^{(0)}(\omega)}{[1 - UI^{(0)}(\omega)]^2 + \pi^2 U^2 D^{(0)}(\omega)^2}, \tag{2.25}$$

where $I^{(0)}(\omega)$ is nothing else than the Hilbert transform of the two holes non interacting density of states $D^{(0)}(\omega)$:

$$I^{(0)}(\omega) = \int_{-\infty}^{\infty} d\omega' \frac{D^{(0)}(\omega')}{\omega - \omega'}. \tag{2.26}$$

The great merit of Eq.(2.25) is to draw attention to the tailoring action of the hole-hole Coulomb interaction on the CVV Auger spectra of the particular material of interest. As it is evident from this expression in fact U acts not only on the Auger kinetic energy determining where we expect to be centered the corresponding structures but also on the line shape itself. Eq.(2.25) covers the whole range between weak and strong interactions resuming in a unique expression both the band-like and the atomic-like behaviors of the Auger spectra. Besides this, it provides a new feature of this kind of transitions corresponding to a completely quantum phenomenon: the so-called two holes resonances. They appears in the spectrum as sharp peaks corresponding to the poles of $G(\omega)$ outside the bands. Physically these resonances are due to the formation of a two hole bound state because of the complete filling of the valence band which prevents the final holes from delocalizing. In this way, just because of repulsion, the holes remain trapped giving rise to a bound state.
To better understand this result, let us consider the case of a rectangular single particle LDOS of width α:

$$\rho(\omega) = \frac{\theta(\alpha - |\omega|)}{2\alpha}. \tag{2.27}$$

The main ingredients to evaluate $D(\omega)$ by using Eq.(2.25) are the self-convolution of $\rho(\omega)$ and its Hilbert transform which yield respectively the triangular shaped result:

$$D^{(0)}(\omega) = \theta(2\alpha - \omega)\left(\frac{1}{2\alpha} - \frac{|\omega|}{4\alpha^2}\right) \tag{2.28}$$

and

$$I^{(0)}(\omega) = \frac{1}{2\alpha} log\left|\frac{\omega + 2\alpha}{\omega - 2\alpha}\right| + \frac{\omega}{4\alpha^2} log\left|\frac{\omega^2 - 4\alpha^2}{\omega^2}\right|. \tag{2.29}$$

Fig.(2.3) displays an example of the changes in $D(\omega)$ interpreted as a function of the dimensionless parameter $\gamma = U/\alpha$, allowing to illustrate the results and the working of Eq.(2.25) we described previously. The undistorted triangular-shaped DOS in panel (a) corresponds to the case $U = 0$. As U increases ($0 \leq \gamma \leq (ln2)^{-1} \sim 1.44$) so the line shape progressively distorts with the maximum becoming sharper and shifting to higher binding energies (panel (b)). A further increase in U makes the overlap between $D(\omega)$ and $D^{(0)}(\omega)$ start to die and a localized split-off state develops with energy $\omega > U$ (panel (c)). Finally for $\gamma \gg 1$ the split-off state becomes an atomic state and the solid induced features vanish (panel (d)).

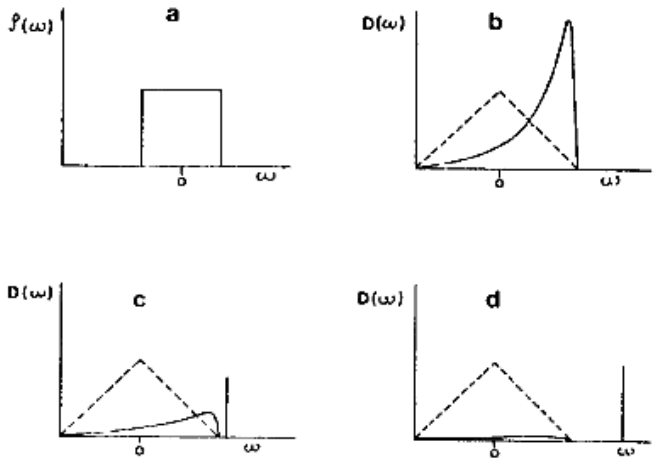

Figure 2.3. *This figure shows the effect of interaction [35] on the final 2hLDOS $D(\omega)$ for a CVV Auger process evaluated by using Eq.(2.25). Panel a) reports a model one electron density of states which the starting point for the $D(\omega)$ calculation. The obtained interacting 2hLDOS is displayed instead in panels b), c) and d) respectively for $\gamma = U/\alpha = 1, 1.8$ and 3, where α is the band width.*

As we anticipated before the other model by Sawatzky [36] fundamentally differs from Cini's one in the choice he made for the hole-hole Coulomb interaction expression. The particular form adopted for $H_r^{(Saw)}$ (see Eq.(2.13)) indicates that Sawatzky based his approach on the Hubbard's model[5] [45]. Starting from the same initial assumptions as Cini

[5]The Hubbard model is a model of interacting particles in a lattice, with only two terms in the Hamiltonian:

with regard to an initially filled band and the "sudden approximation", he solved exactly the Hubbard Hamiltonian in terms of Green's function.

This model recovers the same phenomenology for the Auger line shape found by Cini's theory as far as the band-like, atomic-like and two holes resonances are concerned but in this case these changes in the line shape were analyzed as a function of the dimensionless ratio $U^H/2\alpha$ instead of U/α. Here α represents again the one-particle band-width while U^H stems from:

$$H_r^{(Saw)} = U^H \sum_i n_{i\uparrow} n_{i\downarrow}, \tag{2.30}$$

where $n_{i\uparrow}$ ($n_{i\downarrow}$) is the number operator counting the spin up (down) holes on the $i-th$ lattice site.
Sawatzky's approach provides in fact that the solution for large U^H ($U^H \gg 2\alpha$) consisted of $N(N-1)$ band states and N bound states lying outside the band, where N is the total number of atoms. On the other hand, for $U^H \sim 0$, the line shape would be simply the self-convolution of the single-particle LDOS recovering Lander's result.

It is quite evident that the general conclusions reached by Cini and Sawatzky about progressive distortion of the density of states followed by the splitting-off of discrete states are the same. Their criteria for the appearance of quasiatomic Auger spectra look slightly different because of the different models used and hence the different definitions of the Coulomb repulsion. In a later note [46] Cini compared the two mathematical approaches and showed they were formally similar. However it should be noted that Cini's original treatment involved only one-electron density of states, while Sawatzky's one included also details of the band dispersion. Thus the bound states found by Cini were in the form of δ functions (see Fig.2.3) while Sawatzky's solution gave to the bound states a finite width.

2.3.2 The Off-Site Interaction and Other Extensions

During the years following the ones that saw the birth of the CS model, the comparison between theory and experiment started to be performed in an extensive way on a variety of

a kinetic term allowing for tunneling ('hopping') of particles between sites of the lattice and a potential term consisting of an on-site interaction. This sets up a competition between the hopping integral and the on-site repulsion. The main difference with the Anderson approach consists in taking into account the possibility of interaction between two particles also when they hop together delocalizing on different lattice sites.

systems. The first studies of this kind focused their attention on the check of the criterion U/W which would allow the prediction of band-like and atomic-like spectra. Many of these experimental works showed a striking good agreement between theory and measured data, such as for example in the case of the L_3VV and $N_{6,7}VV$ transitions respectively from metallic Ag and Au studied by Powell [47]. The systematic works made by Weightman and coworkers [48, 49, 50] resulted to be particularly noteworthy because they studied CVV Auger spectra from expressly created alloys so as to vary the band width and study its effects on the Auger line shape.

A great quantity of experiments showed that the CS theory for closed bands materials is useful and fundamentally correct, also if some works threw light on some limitations of the model, which are essentially due to the characteristics of the considered system. As an example the study on the CVV Auger spectrum from Si, made by Feibelman et al. [42], confirmed the expected band-like character in the Auger spectrum but showed also the importance of the Auger matrix elements variations as a function of the Auger kinetic energy. The energy dependence of the Auger matrix elements can be easily introduced in the CS theory but the model will not give the same the correct results, because of the overlap of orbitals belonging to nearest neighbor atoms. To take correctly into account this kind of correction a more involved theory is needed like the one in [51].

The awareness of the existence of limitations immediately brought as a consequence to the flourishing of several corrections and extensions to the "basic model" to better adapt it to the particular studied system. Cini, firstly alone in 1978 [52] and then together with D'Andrea in 1983 [53], studied how the coupling of Auger holes and plasmons can affect the Auger line shape. They showed in fact that if one describes the plasmon dynamics by one effective mode, representing long-wavelength bulk plasmons in the dispersionless limit, then the model can be exactly solved in terms of a continued fraction technique. Their treatment demonstrated that the hole-plasmon coupling can produce not only plasmon satellites, but also important changes in the line shape. For weak coupling the only effect of plasmons will be a slightly asymmetric deformation of the peaks with a tail on the same side of the one due to energy losses. If the coupling instead is strong enough respect to the single-electron level width, the plasmons-coupling will sharpen the peak compared to the unperturbed one. This narrowing is due to the fact that plasmons can only screen a localized hole and tend to favor localization. Eventually for very strong coupling the hole may become self-trapped and a localized state recalling a small polaron develops.

Other important extensions to the basic form of the CS theory came from the introduction

of spin-orbit coupling and the effects of degenerate bands. Both these two aspects were included in two works made by Cini and Verdozzi in 1991 [54] and in 1994 [55] where they showed the need to take into account also the so-called off-site Coulomb interaction for a more realistic description of CVV Auger spectra. Within these approaches the line shape was evaluated by using the Eq.(2.22) written in the LSJ picture and where this time $G^{(0)}(\omega)$ was evaluated in the j-j coupling scheme including also the spin-orbit coupling term in H_0. The total intensity of the whole spectrum and the on-site correlation energy for two $5d$ holes localized in a $^1G_4$ state on one Au atom have been used as free parameters to be determined by a procedure of best fit in the work on the $N_{6,7}O_{4,5}O_{4,5}$ Auger line shape of metallic Au [54]. For the paper on the $M_{4,5}N_{4,5}N_{4,5}$ Auger line shape of metallic silver [55] instead the free parameters adopted were again the on-site correlation energy (but this time for two $4d$ holes localized in a $^1G_4$ state on one Ag atom) and the one describing the effective coupling between valence holes and long-wavelength plasmons, because in this work they included also the dynamical screening effects by introducing the plasmon coupling we previously described. Notwithstanding these differences, both these two papers clearly showed that the CS theory applied to the CVV Auger profile of Au and Ag was unable to give a simultaneous agreement between theory and experiment for both the shape and the position of the spectrum on the kinetic energy scale. In particular they found an excellent agreement with the shape of the spectrum for $U(^1G_4)$ values that positioned the spectrum at 1.2 eV and 2.2 eV higher than experiment respectively for Au and Ag. As an example Fig.(2.4) displays the comparison between the experimental and calculated $N_{6,7}O_{4,5}O_{4,5}$ Auger line shapes from metallic Au as they are reported in [54]. It is evident from this figure (in particular from panels (a) and (b)) that the curves that best reproduce the shape of the experimental patterns (dots) are the ones obtained for $U(^1G_4) = 3.4$ eV (dashed lines): this value need to be shifted of further 1.2 eV (solid lines) to match the experimental position of the spectrum. This failure of the CS model to describe correctly both the spectral profile and its energy position was then attributed to the neglect of interatomic ("off-site") correlation effects. Because of less efficient on-site screening in fact the two final holes of the Auger transition can still interact when they are some distance apart so, in terms of the CS theory, what is required is an extension of the theory to include the radial dependence of the Coulomb interaction term, $U_{LSJ}(r)$ (where r is the distance between the two final holes). A mathematical first order treatment of this effect can be found in [56, 57, 58], while the exact solution of the problem of two holes on a lattice with an arbitrary interaction is described in [59]. This work in particular shows that the main effect of a long-range interaction is to favour the development of bound states,

while the presence of short-range ones mostly produce a shift in the calculated spectrum. Here we only say that a $U(r,LSJ)$ interaction sensitive to nearest neighbor distances could explain the observed shift. If we indicate in fact with U_0 and U_n the hole-hole Coulomb interactions when the holes are respectively both on site or when one of them is found on an adjacent site, then we would expect to observe a profile described by the standard CS theory but with an effective U given by $U_{eff} = U_0 - U_n$ and the whole spectrum shifted to lower kinetic energies by U_n. The assumption of a constant shift, U_n, to represent the effects of several adjacent hole configurations is obviously a simplification: some inhomogeneous broadening effects are expected if one includes the distance dependence in the interaction. The two studied materials displayed different values of the off-site interaction also if they are both metals and it would be reasonable to assume that this will lead to a similar value of the two holes interaction in Ag and Au. This is not the case because Au and Ag have different valence band width W, so the corresponding Auger spectra are different in character because of the different ratios U/W. According to the U/W ratio, in Ag the two hole states will be more localized in character than in Au and thus they will experience on average a greater off-site contribution.

This result in a larger shift in Ag than in Au as observed. Another key quantity in this approach is the ratio u/W, where u represents the off-site interaction for the two metals: its magnitude allows a first order treatment for Au but suggests the need of higher order treatment of the off-site interaction for Ag.

A better agreement between theory and experiment can be obtained in many cases also taking into account the several broadening factors described by Cini and D'Andrea [60] which may occur in a CVV Auger spectrum. The width of quasi-atomic peaks in Auger spectra from several transition metals is mainly due to d hole lifetime effects with some contribution arising from dispersion and phonon broadening. These mechanism are respectively due to the finite life time of holes in the valence band[6], the possibility of delocalization of the two final holes in the perfect periodic lattice[7] and finally to phonon shake up following the sudden creation of a hole. Together with these well known broadening factors, in their work Cini and D'Andrea described a new process which is the resonant decay of two holes bound state. Deepening too much the description of this mechanism is well beyond the scope of

[6]This happens because of Auger and other processes which are due to Coulomb interaction with the conduction electrons.

[7]This broadening mechanism is implicitly yet included in the Sawatzky approach, so in this case it needs no to be considered as a further broadening factor.

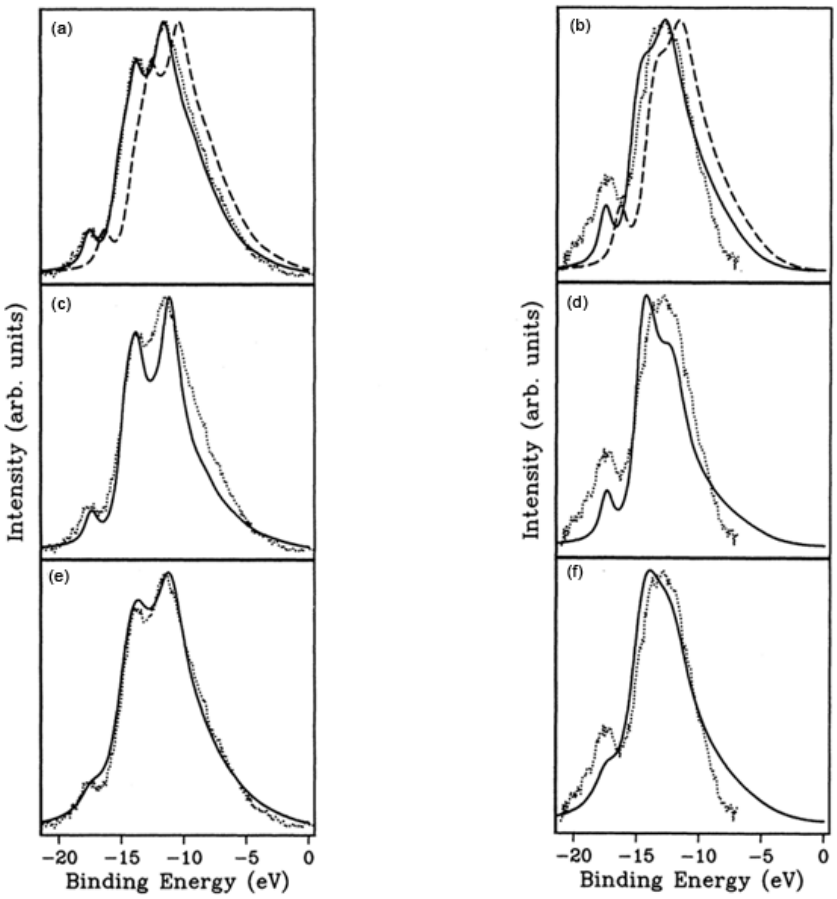

Figure 2.4. *The left and right columns display the comparison between the experimental (dots) and the calculated line shape (solid and dashed lines) respectively for the $N_6O_{4,5}O_{4,5}$ and $N_7O_{4,5}O_{4,5}$ Auger transition in metallic Au [54] which are plotted as a function of the binding energies. In panels (a) and (b) the dashed line represents the theoretical profile calculated for $U(^1G_4) = 3.4$ eV, while the solid line is obtained by shifting the dashed line to higher binding energies by 1.2 eV. Panels (c) and (d) instead show the profiles calculated for $U(^1G_4) = 4.6$ eV, which are represented by a solid line. In panels (e) and (f) at last the solid line represents the theoretical profiles displayed respectively in (c) and (d) by increasing the FWHM.*

this section, here we only say that because of the scattering of the d hole(s) into the d band continuum, this process provides that a localized two-holes resonance can decay into the d band by emitting a many body excitation of energy of the order of U. This electronic process is present only in Auger spectra and not in photoemission ones because it needs of a localized bound state to take place. The importance of these broadening factors strongly depends on the relative importance of d hole lifetime broadening. In Ag and Cd for example this resonant mechanism yields a significant contribution.

2.3.3 CVV Spectra from Unfilled Bands: an Open Problem

The CS model and its several extensions we just described give reliable predictions for Auger spectra from materials characterized by filled or almost filled valence bands. The presence of empty states in the valence band leads to the need of a completely new theory not only because it allows the possibility of intra-band polarization and shake-up events but especially because it provokes many other complications which strongly contribute to keep the modeling of CVV Auger line shapes from open band materials a still open problem at the state of the art today.
There are three fundamental difficulties caused by the presence of empty states within the sample valence band which are completely new respect to the closed band case:

1. The lifetime of the core hole is long enough to polarize the valence electrons which belong to the open band attracting screening charges on the ionized atom. When the Auger decay happens the charge distribution is perturbed by this process and this makes the effect of the deep core hole to be explicitly considered during the spectra calculation. In this case the Auger line shape evaluation has to be described in terms of a three body Green's function (which are the two valence holes and the deep electron filling the initial hole) instead of a two body one.

2. Taking into account only the possibility that the two holes interact when they stay on the same lattice site where they were created favours this site respect to the others. This makes the Hartree Fock ground state energy of an atomic level of given spin belonging to the considered system lacking in the shift Un which is due to the interaction effect,where n is the expectation value for the hole number of opposite spin[8]. This difficulty can be overcome by introducing the U repulsion on all the lattice sites as in the

[8]For the closed band case this problem does not exist because the expectation value of n is zero.

original Sawatzky approach.

3. For small U values the perturbative calculation of the Green's functions is a quite trivial task to be accomplished for, but the cases attracting greater interest are characterized instead by strong U values. To make expansions possible in these cases, one firstly has to find a small parameter which is representative of the system and has a physical meaning for the problem at hand.

In Ref. [61], Cini described an extension of his method, whereby he was able to overcome these difficulties for transition metals such as Ni and Pd. These materials have rather narrow valence bands laying mostly under the Fermi level, i.e. almost completely filled[9]. This suggests to use n_h (the ground state average number of holes at site 0, $n_h = \langle c_{0\sigma} c^+_{0\sigma} \rangle$ with $\sigma = \uparrow , \downarrow$) as a small parameter in terms of whom expansions can be made.
The assumption of a small hole density plays a fundamental role at several stages of the theory. Besides providing an approximate solution, it helps in formulating the model justifying the use of the two-step approach for the Auger process in order to be able to separate the deep hole creation from its subsequent decay. This assumption is justified this time (for long enough life times of the initial core-hole) on the grounds that for low unfilling the initial core hole has a little phase space available to leave the system in an excited state[10]. Also if there are many experimental evidences of the presence of high energy satellites [65, 66] in the photoemission spectra of transition metals (which are due to valence holes trapped at the deep hole site), the two step approach can be invoked again because the weight of these two hole states decreases with decreasing n_h. The shake down satellites we are missing are very weak in the low density case. Another simplifying aspect for the theory produced by a low hole density is the fact that it allows the use of an Anderson like Hamiltonian as in the closed band case (see Eq.(2.13)):

$$H = H_{TB} + U n_{0\uparrow} n_{0\downarrow}. \tag{2.31}$$

In the previous expression H_{TB} is a non interacting tight binding model term, while $U n_{0\uparrow} n_{0\downarrow}$ represents the correlation term with $n_{0\sigma} = c^+_{0\sigma} c_{0\sigma}$ ($\sigma = \uparrow , \downarrow$), where $c^+_{0\sigma}$ ($c_{0\sigma}$) creates (kills) a hole with spin σ on the lattice site 0.

[9] They are characterized by a hole mean number per valence state $n_h \ll 1$

[10] For long lived initial core hole the Gunnarsson and Schönhammer criteria [13] for the validity of the two-step model want the presence of the deep core hole to do not introduce extra bound states in the single-particle spectrum.

In his works Cini neglected also complications arising from crystal field effects and orbital degeneracy, granting this way the decoupling of two holes states characterized by different L momenta and hole-hole repulsion. We stress here that this can be a reasonable approximation for open band materials only in the low-density case: in an exact theory the scattering of several holes at a time (even in absence of crystal field effects) and orbital degeneracy have to be explicitly included.

Under these simplifying hypotesis the Auger spectrum can be related to a three-body Green's function, $\widetilde{T}(t)$, describing the propagation of two valence holes and a core electron in the final state. The low hole band filling ($n_h \ll 1$) allows the use of the Galitzkii's Low Density Approximation[11] (LDA) [67], where n_h plays the role of the small physical quantity in terms of which expansions have to be made, while the U interaction is treated at all orders, permitting the study of strongly correlated cases. Within this approximation, selecting only that class of Feynman diagrams which dominates the perturbation series for $n_h \ll 1$, it can be shown [61] that the three body Green's function we are interested in factors as:

$$\widetilde{T}(t) = G(t)g(t) + O(n_h^2), \tag{2.32}$$

where $g(t)$ is the Green's function accounting for the deep electron while $G(t)$ describes the two final valence holes in absence of the initial core hole. This means that, only for low unfilling, the spectrum can be modeled in the energy space as the simple convolution between a two and a single body Green's function, where $g(\omega)$ plays the role of an asymmetric line shape which allows to take into account shake up effects also in $\widetilde{T}(\omega)$.

As we said previously, considering the interaction between the two final holes as localized on the same site of the Auger decay makes this one a privileged site because it perturbs the charge density in its neighbourhood. To avoid the use of a more complex mathematics needed to extend the Sawatzky model to the open bands case and to gain the same the expected level shift due to the interaction effect, Cini noticed that, defining the self-energy $\Sigma(\omega)$ by means of the following Dyson's equation giving the dressed single particle Green's function $g(\omega)$ in terms of its bare counterpart $g^{(0)}(\omega)$ [61]:

[11] In the case of a low hole density, Galitzkii's approach consists of selecting those graphs in all orders of perturbation theory that do not involve propagation of more than one electron at a time and treating all interactions in the ladder approximation.

$$g(\omega) = \frac{g^{(0)}(\omega)}{1 - g^{(0)}(\omega)\Sigma(\omega)}, \tag{2.33}$$

the imaginary part of $\Sigma(\omega)$ roughly represents a level shift, while its real part is positive (negative) under (above) the Fermi level. The first self-energy contribution is given by:

$$\Sigma^{(1)}(\omega) = -iU\langle n\rangle, \tag{2.34}$$

so he chose to reabsorb this level shift into the definition of the one body energy level and seek for a self-energy with vanishing first order contribution. It has to be kept in mind that this trick does not eliminate the factitious privileged condition of site 0 inside the lattice, which is due to the model Hamiltonian adopted, but it can be shown that the error made by using this approximation has an higher order than a linear dependence from n_h.
Following Galitzkii's well known LDA and summing all the ladder terms shown in Fig.(2.5.c) (the graph 3c would contribute to the self-consistent LDA but is unimportant if $n_h \ll 1$) the self-energy results to be:

$$\Sigma_{LDA}(\omega) = iU\langle n\rangle + \int_{-\infty}^{+\infty} \frac{d\omega'}{2\pi} g^{(0)}(\omega')T(\omega + \omega'). \tag{2.35}$$

Here the first term has been added to compensate for the average level shift as discussed before, while the T matrix represents a sort of effective (ladder) interaction containing contributions to infinite order in U which is given by:

$$T(\omega) = \frac{iU}{1 + iUG^{(0)}(\omega)}. \tag{2.36}$$

In the previous expression $G^{(0)}(\omega)$ is nothing else than the two-holes non-interacting propagator which can be gained by simply autoconvolving $g^{(0)}(\omega)$:

$$G^{(0)}(\omega) = \int_{-\infty}^{+\infty} \frac{d\omega'}{2\pi} g^{(0)}(\omega')g^{(0)}(\omega - \omega'). \tag{2.37}$$

Finally the interacting $G(\omega)$ in the ladder approximation can be evaluated through [62]:

$$G(\omega) = \frac{G_D^{(0)}(\omega)}{1 + iUG_D^{(0)}(\omega)}, \tag{2.38}$$

with:

$$G_D^{(0)}(\omega) = \int_{-\infty}^{+\infty} \frac{d\omega'}{2\pi} g(\omega')g(\omega - \omega'). \tag{2.39}$$

As it clearly appears from Eq.(2.38), we gain again an expression for the interacting two-holes Green's function which displays the same functional dependence as in the CS theory for closed bands. It was expected at the time that in order to improve the above theory one should insert in Eq.(2.39), in place of g, its self-consistent version (Self-Consistent Low-Density Approximation).

$$T(\omega) = \frac{iU}{1 + iUG^{(0)}(\omega)}. \tag{2.40}$$

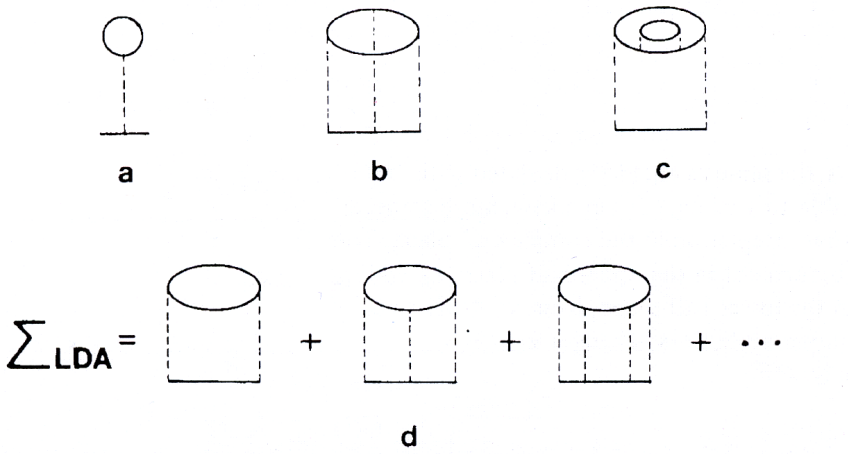

Figure 2.5. *Diagrams (a), (b) and (c) represent the various contributions to the self-energy $\Sigma(\omega)$ in the LDA [61]. $\Sigma_{LDA}(\omega)$ is the sum of of the ladder diagrams (panel d) that dominate the series at each order of perturbation theory.*

In their works made at the end of the 80's [62, 63, 64], Cini and Verdozzi discovered that it is not so. They introduced a new method, the so-called Bare Ladder Approximation (BLA), in which, quite the other way, g is replaced by its bare form $g^{(0)}$.

The results obtained by exact model calculations conducted on finite clusters (made up of 27 and 125 atoms) were compared [62] with the ones gained by using three different approaches, all deep-rooted in the formalism developed a few lines ago:

- The so-called Low Density Ladder Approach (LDLA): the two holes Green's function can be gained by following the whole procedure traced before from Eq.(2.33)

to Eq.(2.39) or else by using Eq.(2.38) to evaluate the interacting two body propagator, $G(\omega)$, where $G_D^{(0)}(\omega)$ is the simple autoconvolution of the LDA single particle propagators,$g(\omega)$.

- Second order expansion: in a series of papers Treglia and coworkers [68, 69]proposed as a general solution which has to be valid for any n_h the one obtained by expanding to second order in U the effective interaction matrix $T(\omega)$ of Eq.(2.40) and breaking off to second order also the expression for Σ_{LDA}.

- The last considered approach is the Bare Ladder Approximation: it simply consists in following the same procedure adopted for the LDLA but making use in Eq.(2.38) of the bare non interacting two particles propagator, $G^{(0)}(\omega)$, instead of $G_D^{(0)}(\omega)$.

Fig.(2.6) shows the results obtained comparing the several $G(\omega)$ calculated by these three approaches as applied to a non magnetic sample for different values of the parameters n_h and U. As expected in all the reported cases the Treglia approximation fails to give a good description of the line shape. The series truncation they made was a clear oversimplification. Besides this another strong limitation of this approach is due to the fact that the second order approximation to $T(\omega)$ cannot have singularities outside the band continuum.
Both the LDLA and the BLA are expected instead to be exact in the low density limit, but the panels of Fig.(2.6) show that LDLA does not give a good reproduction of the $G(\omega)$ pattern especially at increasing U and n_h[12]. This failure was not expected and cannot be due to the low density approximation because it still gives good single particle spectra for the same range of U values as it is shown in [62]. Those results on one body propagators show that Galitzkii's LDA provides a good description of dressed holes in a wide range of physical situations and it is more accurate than the second order approximation up to at least $n_h = 0.25$. The disagreement with exact two particle propagators must come from vertex corrections to hole-hole scattering that were neglected in the LDLA. Within this approximation in fact we have systematically applied the criterion of selecting the dominant diagrams at each order of perturbation theory, which is reasonable but can be granted only asymptotically, because we cannot say *a priori* what will be the effect of the neglected terms at finite n_h.

[12]For not very small n_h values an approximation better than LDA is represented by its self-consistent version (SFC-LDA, SelF-Consistent- LDA)[70]. This approximation differs from LDA in the fact it is based on the iteration of the procedure leading to $g(t)$ when starting from $g^{(0)}(t)$. Although this procedure is not very useful for not small n_h, because in this range the model itself loses validity, today SFC-LDA is thought as a better approximation than LDA also for small n_h [71].

In the BLA instead we assume that the effect of vertex corrections to the ladder approximation is such that the two holes tend to interact as bare holes, essentially because the size of their screening clouds is larger than the range of the hole-hole repulsion. The accordance between the BLA results and the exact patterns reported in Fig.(2.6) shows this way that this approximation resolves the said difficulty of the LDLA in a wide range of parameters, simply basing on the idea that the holes observed in Auger electron spectroscopy are essentially bare. This behaviour may be understood since the interaction is so short ranged that the holes are allowed to interact only at site 0. On the other hand, the site 0 can only accommodate two bare holes, and not two holes plus their polarization clouds. Thus the description of undressed holes is accurate unless U and n_h became so large that the charge density at site 0 is strongly perturbed. The good agreement between the experimental and the calculated photoemission and Auger spectra from metallic Pd, confirm the success and the advantages in the use of BLA under certain conditions of validity. BLA revealed to be accurate also for single particle correlated spectra allowing for example to understand for the first time the three structures present in the photoemission spectrum from valence band of Pd and to establish they are due to correlation effects (in fact they are not provided by a not correlated theory).

As far as the Auger spectra are concerned, it has to be stressed that the BLA patterns resulted to be extremely sensitive to hole concentration and also the case $n_h = 0.1$ may produce strong changes on the line shape if U is comparable with the band width. Because of a lesser electron number the spectrum area diminishes, while the two hole resonance broadens and loses intensity, shifting towards the band-residuum of the spectrum. Comparing this case with the results obtained for closed band materials, one can notice that higher U values are needed to gain an atomic-like spectrum. This is not a surprising finding because an open band displays the possibility of screening the effect of repulsion at least partially.

Several experimental data confirmed at least qualitatively the results foreseen by the BLA. In particular Andrews and coworkers [72] measured the CVV Auger spectra from pure metallic Ni and in the alloys Ni50% Zn50%, Ni20% Zn80% and Ni50% Al50%. They found that along this series n_h diminishes and the corresponding Auger line shape progressively distorts. In metallic Ni the two hole resonance results to be wider than what is typically found for other metals characterized by closed bands.

Another fundamental feature of the BLA comes from the fact that Eq.(2.38) is nothing else than a Dyson equation in which the U matrix is an instantaneous self-energy. Therefore

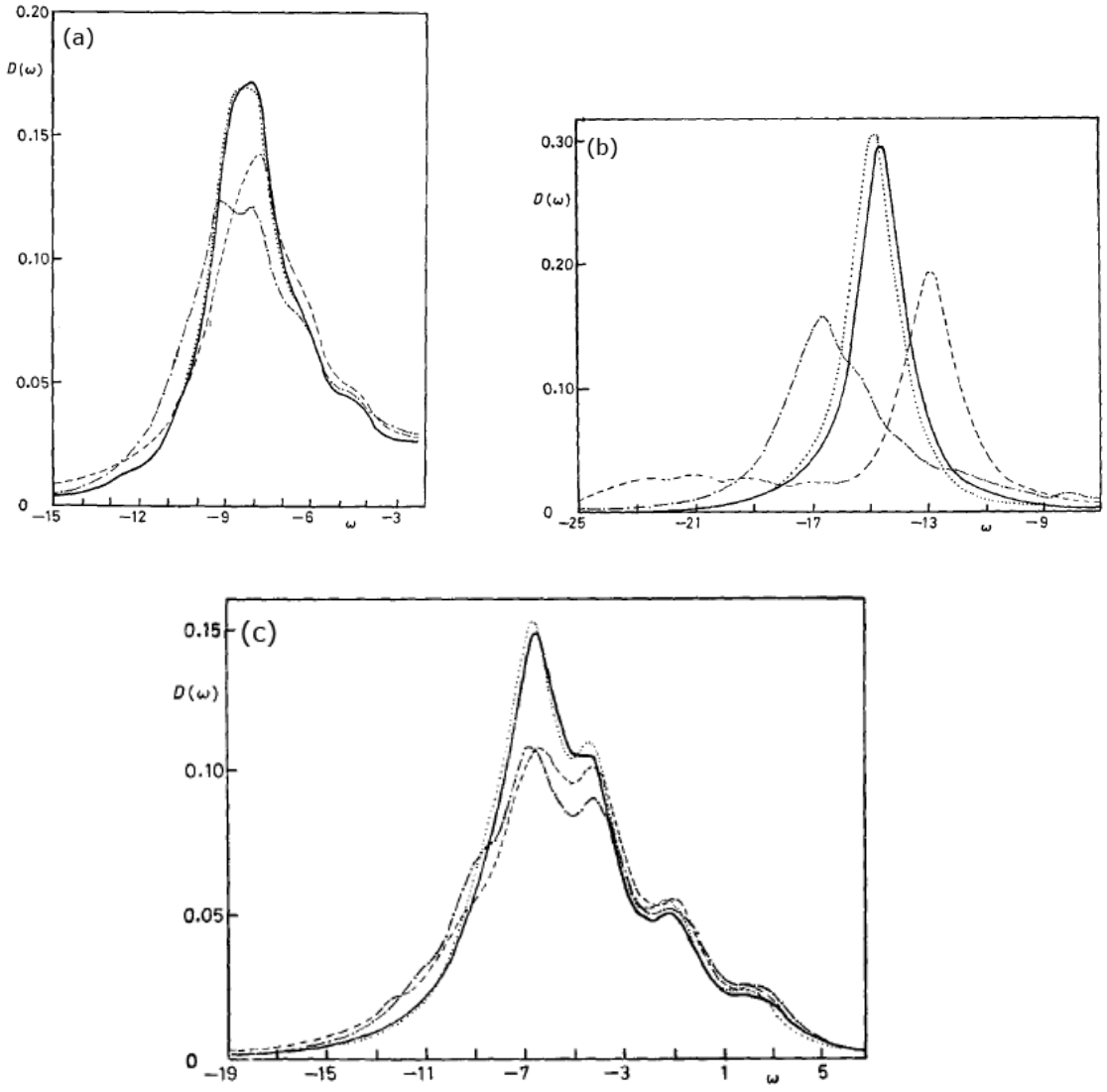

Figure 2.6. These figures display the interacting two holes LDOS for a non magnetic sample as a function of the binding energies. In each panel the exact result is represented by the continuous line, while the LDLA, the Treglia approximation and the BLA patterns are respectively reported as the dashed, dash-dotted and dotted lines. In particular the curves in panels (a), (b) and (c) have been obtained respectively for $n_h = 0.1$ and $U = 7$, $n_h = 0.1$ and $U = 15$, $n_h = 0.25$ and $U = 5$. Both the exact results shown in panels (a) and (b) have been evaluated for a 125 cluster atom, while the exact one in panel (c) refers to calculations on a 27 cluster atom.

it grants the Herglotz[13] property which is a a basic requirement for a sensible approximation,

[13]The density of states is granted to be non-negative. It is quite a common drawback of perturbation approaches that potentially powerful diagram summations become untenable because they fails to guarantee this zero-order requirement of positive probability.

yet it is not easily obtained by diagrammatic approaches.

The theory we just described is valid for low hole density per valence state n_h and reproduces at least qualitatively the Auger spectra of interest: as an example the BLA has been useful to interpret the line shape of Graphite [73]. This way we are left with the problem of describing CVV Auger spectra from all that open band materials which are characterized by not particularly small n_h. Metals with wide valence band and low U values may still be well described without the need of adding any further complication in the theory because an essentially uncorrelated spectrum is expected in accordance with the U/W criterium. This is confirmed for example by the CVV Auger spectra from Li [41], Al [74] and Be [75] which are well described by using simply convolutions of the single particle LDOS, only with slight modifications due to the need of including polarization effects induced by the core hole for the case of Be, or the inclusion of Coulomb effects treated as a perturbation for the case of Al.

The question about the way to face the problem of CVV Auger spectra from tight bands with values of n_h and U not very small remains unsolved. There are cases where the ratio U/W is still small such as for example Fe and Co and the broad peak of their Auger spectra tempts to speak of band-like patterns, but it has to kept in mind that in these materials the holes concentration results to be dangerously high so as to invalidate the used model.

The failure of the BLA model for the description of the CVV Auger spectra of Ti and Sc [76] gave birth in the 80's to the so-called U$<$0 phenomenon [77]. To model these spectra Sawatzky and coworkers [77] in fact proposed again the use of the CS model which seemed to work also in that case but only admitting the possibility of $U < 0$. The maximum of the Auger line shape obtained by the CS theory resulted to be shifted for these materials by the interaction towards lower binding energies, which is the contrary of what typically happens for closed band solids. Till today there is not a known mechanism able to produce an attractive U in the eV range, this means that for almost empty bands one must formulate a new theory which is not a simple extrapolation of the closed band approach. An hint suggesting the direction to pursue came at the beginning of the $90's$ from Sarma [78], who firstly recognized in the CVV line shape of Ti a sort of linear combination of one-electron density of states and its convolution. This suggested to Cini and Drchal [79, 80] that the real responsible of this kind of exotic behavior was the failure of the two-step approximation. They started from a one step expression for the Auger current:

$$J(\varepsilon_k) = \int_0^\infty dt_1 \int_0^\infty dt_2 f(t_1,t_2) exp[i\varepsilon_k(t_1 - t_2)], \tag{2.41}$$

where:

$$\begin{aligned} f(t_1,t_2) &= \sum_{m,m'} \langle\psi|e^{i(H_{rel}+i\Gamma)}|m\rangle\langle m|H_A^+ e^{iH_{unrel}(t_1-t_2)} H_A|m'\rangle\langle m'|e^{-i(H_{rel}-i\Gamma)}|\psi\rangle, \\ H_{unrel} &= \sum_{k,\alpha} \varepsilon(k) n_{k,\alpha} + U \sum_i \sum_{\alpha\neq\beta} n_{i,\alpha} n_{i,\beta}, \\ H_{rel} &= H_{unrel} + H_{ch} = H_{unrel} - \widetilde{W} \sum_\alpha n_{0,\alpha}. \end{aligned} \tag{2.42}$$

In the last three equations H_{rel} and H_{unrel} correspond, with obvious notation, respectively to the relaxed and unrelaxed Hamiltonians leading the system to the "relaxed" and "unrelaxed" ground state, $|\phi\rangle$ and $|\psi\rangle$. These states differ one from the other only in the presence of the H_{ch} term, which represents the interaction between the conduction electrons and the core-hole. The first addend in H_{unrel} represents the Bloch electrons with α as a spin-orbital band index ($\alpha = 1,...,d$), while the second one stems from the electron-electron interaction acting on all sites and treated in the Hubbard form. H_A is the perturbation inducing the Auger transition, while Γ is an operator which produces virtual Auger transitions. The sum on m and m', appearing in the first of Eqs.(2.42), run over a complete set of valence states. At this stage, to further simplify the model, the authors proposed that the complete set summation aforementioned could be largely exhausted by summing over just two orthogonal states, namely, $|\psi\rangle$ and $|\phi\rangle$.

Within this scheme also the Auger spectrum can be reduced to a sum of an unrelaxed and a relaxed contribution [80], where the first one arises from $|m\rangle = |m'\rangle = |\psi\rangle$ and can be expressed in terms of the two hole Green's function $G(\omega)$ appearing also in the CS model. The relaxed contribution instead arises from $|m\rangle = |m'\rangle = |\phi\rangle$.

It can be shown [79, 80] that this part can be written in terms of a three body Green's function, calculated on the unrelaxed ground state $|\psi\rangle$, if one approximate the screening cloud by a single electron moving from the Fermi surface to the empty local states of the Auger site. For small or vanishing hole densities the scheme proposed by Cini and Drchal recovered the previously successful BLA results, where the spectrum essentially reflects the shape of the two hole local density of states. In the middle and in particular at the beginning of the early transition metals series, the screening of the core-hole by valence

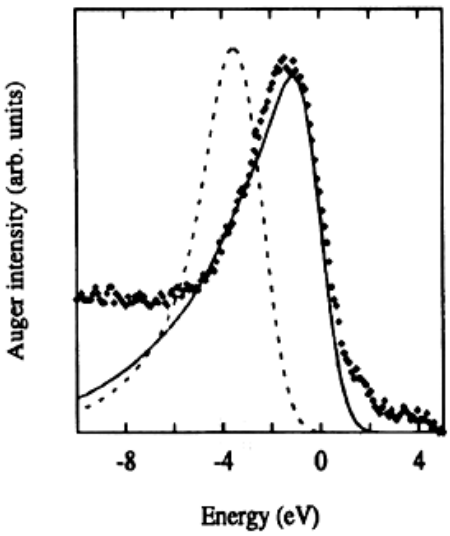

Figure 2.7. Comparison [80] between the experimental $L_2M_{45}M_{45}$ Auger line shape of Ti (points) and the calculated patterns obtained by applying the relaxed (solid line) and the unrelaxed theory (dashed line). Both the theoretical curves use U = 1.68 eV, W = 7.14 eV and n_h = 0.254. The calculated patterns were broadened by means of a convolution with a Gaussian characterized by σ = 0.7 eV.

electrons becomes progressively important and its signature appears in the line shape in the form of a combination of one-hole and two-hole one-electron features. This model correctly reproduces the $L_2M_{45}M_{45}$ Auger line shape of Ti as it is shown in Fig.(2.7) by using a normal U, without having to postulate an attractive hole-hole interaction that would be hard to explain.

Before ending this chapter, we give here only the flavour[14] of the so-called Core Ladder Approximation (CLA), which is the method still standing at the frontier of what it is known for open band CVV Auger transitions. The need of such a method comes from the difficulties involved in the calculation of a three body Green's function, which is an essential ingredient for the theory described a few lines ago. To overcome this problem Marini and Cini proposed [81] this simple approach in the spirit of the BLA, which allowed to extend the analysis to several transition metals, giving at least a qualitative understanding of their spectra. It has to be kept in mind that also this approach represents only an approximation but it is able to capture the essential physics of a formidable problem which otherwise would require an excessive computational effort. This theory starts from the ground of the Drchal and Cini's theory or else it is based on the use of the one-step model for describing the CVV Auger decay and the bare ladder approximation for selecting the relevant diagrams making up the final three body Green's function. Such an approximation should have essentially the same physical meaning as in the BLA and we expect it should work properly in a wide range

[14] A complete and exhaustive description is deferred to [81, 82, 83] because it is far from the scope of this thesis work.

of U and hole fillings, n_h. The need of calculating a three body Green's function further complicates the solution of the problem making difficult the evaluation of the diagrams summation. This problem can be overcome recurring to the CLA. It can be shown in fact that, using some two bodies Green's function sum rules [81], the three body one reduces to the form of a convolution product in the ω space of single and two particles Green's functions, still representing all kinds of ladder diagrams which can be evaluated at all orders. The price to pay for this simplification is the introduction, through the used sum rules, of infinite summations over the complete set of spin orbitals, γ. The CLA consists properly in limiting the γ summation to local states γ_l. Physically we expect in fact that only the sites which are closest to the Auger site give an important contribution to the summations, so one can actually work with a limited set to express the local single particle Green's functions elements. Larger sets will lead to more precise results at the cost of more computation. Comparison with exact cluster calculations [81] showed that the CLA is very accurate in the easy cases (high filling and/or small interaction). However many transition metals are in the range of fillings and U where the CLA approach is useful and the approximation remains reasonable, Herglotz and qualitatively good even for $U/W = 1$. This holds true for both the one body features and the two holes-one electron contributions resulting from the full three body's Green's function. CLA treats the screening electron and the Auger holes on equal footing, carries on a partial summation of the perturbation series to infinite order and becomes exact both at weak and at strong coupling (in the sense that it becomes equivalent to a full Ladder approximation). A particularly interesting feature is that this approach grants the Herglotz property. The authors in fact proved that there exist a model Hamiltonian for which the Core Ladder series gives the exact answer.

Today there is the complete lack of a general practical recipe to evaluate a correlated three body propagator and the fact that CLA gives a reliable one qualifies this approach as an appealing starting point to model in particular Auger CVV and APECS line shapes from transition metals, where much of the intensity comes from core holes that are screened when the Auger decay occurs. Some of these spectral features are amenable to the one-body Green's function, but the rest requires a three-body propagator. A Ladder Approximation could be justified in many cases and could describe bound states, but it cannot be carried to infinite order. This happens because there is no way to represent the general term as an iteration of a simple pattern, as it happens with two bodies. This is the reason why the CLA, being born as an extension of this model, represents a reliable candidate to describe that kind of spectra. In Chapter four a new method to calculate a correlated three body's Green's function will be

proposed as applied to the modeling of Coster-Kronig preceded Auger transitions.

3

The Gutzwiller Approximation

The task of this chapter is to provide an introduction to the fundamentals of the Gutzwiller's Approximation (GA) in order to give to the reader all the instruments he may need to undertake the reading of Chapter 4, where it will be used to model Auger spectra from incompletely filled valence band materials (see Sec.4.4).

Gutzwiller firstly composed this theory in 1965 as a variational time independent approach aiming to find a solution to the Hubbard model, but in the following decades many attempts had been done to extend this approach to the study of magnetic systems and to include a time dependence. This chapter will describe the main steps of this formalism since its start to its latest developments. The first part of it will be devoted to the description of the static version of GA, while the second one will be focused on the introduction of the time dependence and the way it can be used to gain a correlated two-particles response function.

3.1 The Time Independent Case: the Static Approach

As it has been said a few lines ago, the Gutzwiller Approximation [84] is a variational approach whose aim is to find a solution for the Hubbard model at zero temperature ($T = 0$), which describes a system of fermions on a lattice with narrow bands:

$$H = \sum_{ij} \sum_{\sigma} t_{ij} c^{+}_{i\sigma} c_{j\sigma} + U \sum_{i} n_{i\uparrow} n_{i\downarrow}. \tag{3.1}$$

The first term of the previous equation is the kinetic energy representing the possibility of hopping between the $j-th$ and $i-th$ lattice sites. The second term instead is simply the

Coulomb repulsion. $c^{+}_{i\sigma}$ ($c_{j\sigma}$) creates (destroys) electrons with spin σ in the $i-th$ ($j-th$) lattice site, while $n_{i\uparrow}$ ($n_{i\downarrow}$) counts the spin up (down) electrons on site i.

Some of the fundamental parameters which are needed to build up the theory are:

- L = Number of lattice sites.
- $N_{\uparrow}$ ($N_{\downarrow}$) = Number of spin up (down) electrons.
- D = Number of doubly occupied sites.
- $|\psi_0\rangle$ = Ground state for the non interacting system ($U=0$).
- $n_{\uparrow}=\frac{N_{\uparrow}}{L}$ = Density of spin up electrons.
- $n_{\downarrow}=\frac{N_{\downarrow}}{L}$ = Density of spin down electrons.
- $d=\frac{D}{L}$ = Density of doubly occupied lattice sites.

Gutzwiller's idea to gain the ground state for the correlated system, $|\psi\rangle$, is to calculate the Hamiltonian functional (in presence of interaction U) on a trial wave function and then minimize it. The trial correlated state is obtained from $|\psi_0\rangle$ as [84]:

$$|\psi\rangle = \Pi_i[1-(1-g)n_{i\uparrow}n_{i\downarrow}]|\psi_0\rangle, \tag{3.2}$$

where $g\in(0,1)$ is the variational parameter. The uncorrelated case ($|\psi\rangle=|\psi_0\rangle$) corresponds to $g=1$; $g=0$ gives $|\psi\rangle\neq 0$ only in absence of doubly occupied states that is only if $D=0$, which can be easily seen writing $|\psi\rangle$ as:

$$|\psi\rangle = g^{D}|\psi_0\rangle. \tag{3.3}$$

This can be done because:

$$\begin{aligned} g^{D_i} &= e^{D_i log(g)} = 1 + D_i\left[log(g)+\frac{log(g)^2}{2!}+...\right] \\ &= 1+D_i[e^{log(g)}-1] = 1+D_i[g-1], \end{aligned} \tag{3.4}$$

where:

$$D_i = n_{i\uparrow} n_{i\downarrow},\ D = \sum_i D_i \ \text{and}\ D_i^2 = D_i. \tag{3.5}$$

Once the trial wave function has been defined, the Gutzwiller's approach reduces (in contrast to the several Green's-function methods) the problem to the evaluation of the norm $\langle\psi|\psi\rangle$ and the matrix elements making up $\langle\psi|H|\psi\rangle$, in order to minimize then the energy functional $E = \frac{\langle\psi|H|\psi\rangle}{\langle\psi|\psi\rangle}$.
In the next section I shall show how the author achieved the result. One essentially needs to evaluate the $\langle\psi|\psi\rangle$ and $\langle\psi|H|\psi\rangle$. A key role to gain an explicit expression for the needed matrix elements is played by some approximations made by Gutzwiller about the phase relations between different spin configurations [84]. He claimed in fact that the motion of the spin up electrons was essentially independent of the dynamics of the spin down particles (and vice versa). Therefore these particles could just as well be assumed to be infinitely heavy, that is they act only as an obstruction for the spin up particles. As a result it turned out that under these assumptions the problem reduced to one of mere combinatorics [84, 85, 86, 87]. Indeed, after minimization with respect to the variational parameter g, Gutzwiller [84] obtained an extremely simple result for the ground-state energy, namely [87]:

$$\frac{E}{L} = q_\uparrow(d,n_\uparrow,n_\downarrow)\bar{\varepsilon}_\uparrow + q_\downarrow(d,n_\uparrow,n_\downarrow)\bar{\varepsilon}_\downarrow + Ud, \tag{3.6}$$

which still has to be minimized respect to d. Here q_σ are the discontinuities in the single-particle occupation number $\langle c_{k\sigma}^+ c_{k\sigma}\rangle$ at the Fermi surface. They are given by [87]:

$$q_\sigma = \frac{\{[(n_\sigma - d)(1 - n_\sigma - n_{-\sigma} + d)]^{1/2} + [(n_{-\sigma} - d)d]^{1/2}\}^2}{n_\sigma(1 - n_\sigma)}. \tag{3.7}$$

Furthermore,

$$\bar{\varepsilon}_\sigma = \frac{1}{L}\langle\psi_0|\sum_{ij} t_{ij} c_{i\sigma}^+ c_{j\sigma}|\psi_0\rangle = \sum_{|k|<k_{F,\sigma}} \varepsilon(k) < 0 \tag{3.8}$$

is the average energy of the σ spins in the uncorrelated state, while $k_{F,\sigma}$ is the corresponding Fermi momentum (only if $n_\uparrow = n_\downarrow$ one has $k_{F,\uparrow} = k_{F,\downarrow}$). One can easily see that always $q \sim 1$ ($q = 1$ only if $U = 0$) as one should expect for a non interacting system. So, while treating the interaction term exactly, the Gutzwiller approach concentrates on

an approximation of the kinetic energy term, calculating its reduction due to the decrease of doubly occupied sites (and therefore also of empty sites), which makes hopping energetically unfavorable.

3.1.1 Properties of the Solution

Using Eq.(3.6) Gutzwiller [84] discussed the possibility of ferromagnetism in his model, concluding that in three dimensions the ground state was never ferromagnetic.
Arguing from a different point of view, Brinkman and Rice [88] realized that the Gutzwiller's result predicted a metal-insulator transition. For a half-filled band ($n = 1$) and $n_\uparrow = n_\downarrow$, they found that ($q_\uparrow = q_\downarrow = q$ and $\overline{\varepsilon}_\uparrow = \overline{\varepsilon}_\downarrow \equiv \overline{\varepsilon}_0/2$) $q = 8d(1-2d)$; besides this, minimizing the ground-state energy, they obtained:

$$d = \frac{1}{4}\left(1 - \frac{U}{U_c}\right), \quad q = 1 - \left(\frac{U}{U_c}\right)^2 \quad \text{and} \quad \frac{E}{L} = -|\overline{\varepsilon}_0|\left(1 - \frac{U}{U_c}\right)^2, \tag{3.9}$$

where $U_c = 8|\overline{\varepsilon}_0|$. This implies that at a finite critical interaction U_c the number of doubly occupied sites vanishes, such that every lattice point is singly occupied, i.e., that the particles are localized. At this point $q = 0$ (reduction of the kinetic energy to zero) and, as $d = 0$, the ground-state energy E vanishes, indicating the metal-insulator transition. Clearly, very close to the transition, Eq.(3.9) cannot be correct. It is well known from perturbation theory [89] that for $U/|\overline{\varepsilon}_0|$ or $U/t \gg 1$ (where t is the hopping parameter), when the spins are localized and antiferromagnetically ordered, the ground-state energy is proportional to t^2/U. In contrast, the above result implies the formation of a paramagnetic, localized ground state. It has recently been shown that for $d = 1$ Gutzwiller's ansatz represented by Eq.(3.2) does yield in fact a ground-state energy $E = -\alpha t^2/U$, when no approximations in the calculation of the matrix elements are made [90]. To allow for the possibility of antiferromagnetism Ogawa et al. [86] and Takano and Uchinami [92] extended Gutzwiller's analysis. Introducing alternating lattices, they found that before localization sets in ($d = 0$), a transition to an antiferromagnetic state was indeed energetically favorable. The results slightly differ, because different approximations were used, but the overall feature is that for $U/U_c < 0.41$ [92] (or $U/U_c < 0.35$ [86]) the system is paramagnetic, being described by Gutzwiller's earlier results, while for an interaction strength larger than these critical values antiferromagnetism appears. A state with a vanishing number of doubly occupied sites is thus never reached at finite U, in agreement with the Green's function results [93, 94].

As a by-product, however, the work of Ogawa et al. (1975) clarified the physics contained in GA. While starting from Gutzwiller's idea of constructing a trial wave function, they applied a much more transparent formalism to the problem. Especially, they showed that it was one particular approximation in their formulation which exactly yielded Gutzwiller's results. This approximation concerns the dependence of the energy expectation values on the spin configurations of the wave function. While spin configurations with the same number of doubly occupied sites all have the same expectation value for the interaction term, their expectation value for the kinetic energy will generally be different (in some configurations the hopping is more advantageous than in others). Ogawa et al. [86] showed that neglecting the configuration dependence of the expectation values was equivalent to all assumptions made by Gutzwiller [84] and leads to an identical result. So, while the interaction term is treated exactly, the kinetic energy is approximated in a way which includes all possible hopping processes but neglects the environment where this hopping takes place.

In this context it is interesting to compare GA's results with those of Green's-function methods which use Hartree-Fock (HF) decoupling approximations. While the Green's-function method [93, 94] predicts a transition to an antiferromagnetic state for $U = 0$ in the ground state for SC and BCC lattices, in the Gutzwiller approach a finite correlation is necessary [86, 92, 95]. The ground-state energies in the two approximations for very small correlation are given by:

$$\left(\frac{E}{L}\right)_{Gutzw} = -|\bar{\varepsilon}_0| + \frac{U}{4} - \frac{U^2}{64|\bar{\varepsilon}_0|} \quad \text{and} \quad \left(\frac{E}{L}\right)_{HF} = -|\bar{\varepsilon}_0| + \frac{U}{4} - O\big(e^{-|\bar{\varepsilon}_0|/U}\big), \tag{3.10}$$

i.e., the Gutzwiller solution has a much lower energy. Also, the single-particle occupation numbers differ significantly: in the GutzwillIer case the momentum distribution $\langle n_k \rangle$ has a discontinuity $q < 1$ for $U > 0$ at the Fermi energy. This is characteristic for an interacting Fermi system [99, 100] for which a perturbation expansion in terms of the interaction can be used [101]. These differences appear to be due to the fact that the HF method concentrates only on the antiferromagnetic phase and hence only on the anomalous Hartree-Fock averages of the interaction term, exactly as in the BCS case. Thereby spin fluctuations, which are important in the Hubbard model, do not seem to be included sufficiently.

3.1.2 The Slave-Boson Method

In 1986 Kotliar and Ruckenstein [102] introduced a new point of view for the GA which allowed for a unified treatment of ferromagnetism, antiferromagnetism, and metal-insulator

transitions in a mean-field theory. This agrees with Hartree-Fock theory in the weak-coupling case, while for strong coupling it incorporates the qualitative physics expected from the few available exact results.

Qualitatively the KR (Kotliar and Ruckenstein) approach is based on the idea that, in a strongly correlated system, an electron is accompanied in the process of hopping by a "back-flow" of spin and density excitations of the medium [1]. Formally, this qualitative idea can be realized by the application of the slave-boson method [103, 104, 105, 106], that is, rewriting the original Hamiltonian in terms of the original fermions and a set of four projection operators, whose role is to keep track of the environment by measuring the occupation numbers in each of the four possible states available for hopping.

To be explicit, we first concentrate on the Hubbard model which is expected to capture the main features of the physics of lattice fermions in a narrow energy band. The corresponding Hamiltonian which includes a nearest-neighbor hopping, t_{ij}, and an on-site repulsion between electrons of different spins, U, is given again by Eq.(3.1).
At this point we enlarge the Fock space at each site to contain, in addition to the original fermions, a set of four bosons represented by the creation (annihilation) operators e_i^+ (e_i), $s_{i\sigma}^+$ ($s_{i\sigma}$), d_i^+ (d_i). In particular these operators stem for:

- e_i^+ (e_i) = creation (annihilation) operator for a boson in an empty lattice site $i \Rightarrow$ it describes empty states;
- $s_{i\sigma}^+$ ($s_{i\sigma}$) = creation (annihilation) operator for a boson with spin σ in a lattice site i ($\sigma = \pm 1$) $\Rightarrow$ it describes singly occupied states;
- d_i^+ (d_i) = creation (annihilation) operator for a couple of spin up and down electrons in a lattice site $i \Rightarrow$ it describes doubly occupied states;

This enlarged space contains unphysical states which can be eliminated by imposing the following set of constraints [102]:

$$\sum_\sigma s_{i\sigma}^+ s_{i\sigma} + e_i^+ e_i + d_i^+ d_i = 1 \tag{3.11}$$

$$c_{i\sigma}^+ c_{i\sigma} = s_{i\sigma}^+ s_{i\sigma} + d_i^+ d_i \quad \text{with } \sigma = \pm 1. \tag{3.12}$$

[1] In a quasiparticle picture this shows up as a renormalization of the hopping amplitude and simply leads to a change of the effective mass.

When restricted by Eqs.(3.11) and (3.12) the number operators corresponding to the Bose fields e_i,$s_{i\sigma}$ and d_i act respectively as projection operators onto the empty, singly occupied (with spin up) and doubly occupied electronic states at each site. Equation (3.11) can then be interpreted as a completeness relation and reflects the fact that no more and no less than one of the four possible states must be occupied at each site; the second constraint equates the two ways of counting the fermion occupancy of a given spin. It is not too hard to check that in the physical subspace defined by Eqs.(3.11) and (3.12) the Hamiltonian:

$$\widetilde{H} = \sum_{ij}\sum_{\sigma} t_{ij}\widetilde{c}^{+}_{i\sigma}\widetilde{c}_{j\sigma}z^{+}_{i\sigma}z_{j\sigma} + U\sum_{i} d_i d_i \tag{3.13}$$

$$z_{i\sigma} = e^{+}_{i}s_{i\sigma} + s^{+}_{i,-\sigma}d_i, \tag{3.14}$$

has the same matrix elements as those calculated for Eq.(3.1) in the original Hilbert space. It is worth to note that the $c^{+}_{i\sigma}$ ($c_{i\sigma}$) operator appearing in Eq.(3.1) creates "physical" electrons and it is found as $\widetilde{c}^{+}_{i\sigma}z^{+}_{i\sigma}$ ($\widetilde{c}_{j\sigma}z_{j\sigma}$) in Eq.(3.13), where $\widetilde{c}^{+}_{i\sigma}$ ($\widetilde{c}_{j\sigma}$) represents a pseudo-fermion operator.

To calculate observable quantities we write down the partition function Z of the system as a functional integral over coherent states of Fermi and Bose fields [105, 106]. The constraints represented by the Eqs.(3.11) and (3.12) are taken into account by introducing three proper Lagrange multipliers per site, $\lambda^{(1)}_{i}$ and $\lambda^{(2)}_{i\sigma}$ ($\sigma = \pm 1$). The partition function then is used to build up the free-energy functional, $f = -k_B T ln Z/L$, which has to be minimized respect to d.

In the atomic limit ($t_{ij} = 0$) the functional integral Z can be calculated exactly and leads to the known results. For $t_{ij} \neq 0$ instead the simplest approach to calculate Z is the so-called "saddle-point approximation" [112] in which all Bose fields and Lagrange multipliers are taken to be independent of space and time. Unfortunately, the resulting saddle-point equations lead to the incorrect result in the noninteracting limit (which occurs either for $U = 0$ or in the case of fully polarized spins). This is because in this approximation the constraints are only satisfied on the average, and not explicitly at each site of the lattice.
To overcome this problem Kotliar and Ruckenstein [102] made use of the fact that the procedure described above is not unique; there are many different Hamiltonians, $\widetilde{H}$, with different properties in the enlarged Hilbert space. It is worth to note that the operator appearing in Eq.(3.13) leads to the same spectrum as Eq.(3.1) when restricted to the physical subspace defined by Eqs.(3.11) and (3.12). Clearly this arbitrariness presents no difficulty as long

as the constraints are handled exactly. However, any approximation which relaxes the constraints is sensitive to the precise choice of $\widetilde{H}$. In any practical calculation this ambiguity can be used to our advantage, and the form of $\widetilde{H}$ can be determined by requiring that the approximation scheme leads to physically sensible results in known limiting cases. In particular, in this case we replace $z_{i\sigma}$ in Eq.(3.14) by another operator, $\widetilde{z}_{i\sigma}$[2][102]:

$$\widetilde{z}_{i\sigma} = (1 - d_i^+ d_i - s_{i\sigma}^+ s_{i\sigma})^{-1/2} z_{i\sigma} (1 - e_i^+ e_i - s_{i,-\sigma}^+ s_{i,-\sigma})^{-1/2}, \tag{3.15}$$

which has the same eigenvalues and eigenvectors as $z_{i\sigma}$ in the physical subspace but also leads to the correct $U = 0$ limit in the saddle-point approximation.

This was the start of a new viewpoint but important mathematical points are fixed by Arrigoni and Strinati [107], who presents the KR approach in a slightly different way, leading however to the same conclusions.

In their paper Kotliar and Ruckenstein [102] show that the saddle point approximation reproduces the same results as GA, but this time they are no more restricted only to the paramagnetic case.

Another important improvement to the original theory came from the works firstly of Metzner and Vollhardt [108] in 1989 and then of Gebbhard [109] in 1990. They studied a systematic formalism for the variational evaluation of ground-state properties of Hubbard-type models in finite dimensions d. In particular Gebbhard's formalism started from generalized Gutzwiller correlated wave functions, which were then studied in a systematic $(1/d)$ expansion around the limit of high dimensions ($d \to \infty$) and estabilished that the Gutzwiller approximation become exact in $d \to \infty$ for translationally invariant wave functions. This means that the Gutzwiller approximation is the exact solution for a GW variational problem for the case $d = \infty$. This type of approximation is no longer exact for more complicated (e.g., antiferromagnetic) wave functions. Gebbhard found also that performing a $(1/d)$ expansion for the Gutzwiller wave function, the lowest orders in $(1/d)$ are sufficient to reproduce at least qualitatively all numerical findings in $d = 2{,}3$. The limit of $d = \infty$ systems revealed this way to be a very fruitful starting point for the study of finite dimensional systems.

[2] $q_\sigma = \langle \widetilde{z}_{i\sigma}^+ \widetilde{z}_{i\sigma} \rangle$

3.2 TDGA: the Dynamical Mean-Field Theory

The irksome mathematical formalism is a major disadvantage of the KR method and in fact there was no application of their approach to broken-symmetry states due to technical difficulties. Besides this the KR choice for the $\widetilde{z}$ hopping factor does not lead to controlled sum rules [110].

In 2001 Seibold and Lorenzana [111] laid the foundations of the time dependent version of the GA for the Hubbard model. In their work they overcame the above mentioned difficulties within the functional integral formalism and introduced an alternative scheme to compute fluctuation corrections around the GA to dynamical and static correlation functions and the ground state energy. The method can be viewed as a Time-Dependent GA (TDGA) in the same way as the Random Phase Approximation (RPA) method on top of a HF solution (HF + RPA) can be viewed as time-dependent HF approximation in the limit of small amplitude oscillations [112]. For this reason they labeled the method as GA + RPA.

The ground state energy of the one-band Hubbard model gained by using this method is in excellent agreement with exact results up to moderate coupling in one dimension (1d) and for all couplings in a 2d system. This approach allowed Seibold and Lorenzana to calculate also dynamical correlation functions, which resulted to be substantially better than HF + RPA ones and obey well behaved sum rules.

They considered the one-band Hubbard Hamiltonian of Eq.(3.1). Their starting point was then an energy functional $E[\rho,D]$ of the GA type [102]. Here ρ is the density matrix of an associated Slater Determinant $|SD\rangle$, i.e. $\rho_{i\sigma,j\sigma'} = \langle SD|c^+_{i\sigma}c_{j\sigma'}|SD\rangle$ and D is a vector of the GA double occupancy parameters, D_i, at site i. In order to consider arbitrary fluctuations the charge and spin distribution of ρ and the distribution of D should be completely unrestricted. For simplicity they considered only solutions where the associated SD is an eigenstate of the z component of the total spin operator ($\rho_{i\sigma,j\sigma'} = \delta_{\sigma,\sigma'}\rho_{ij\sigma}$). $E[\rho,D]$ can be obtained by exploiting the equivalence between the KR saddle point solution and the GA [102], which is given by [111]:

$$E[\rho,D] = \sum_{ij}\sum_{\sigma} t_{ij}\rho_{ij\sigma}z^+_{i\sigma}z_{j\sigma} + U\sum_i D_i, \tag{3.16}$$

with

$$z_{i\sigma} = \frac{\sqrt{(1-\rho_{ii}+D_i)(\rho_{ii\sigma}-D_i)}+\sqrt{D_i(\rho_{ii,-\sigma}-D_i)}}{\sqrt{\rho_{ii\sigma}(1-\rho_{ii\sigma})}} \tag{3.17}$$

and $\rho_{ii} = \sum_\sigma \rho_{ii\sigma}$. The stationary solution $\rho^{(0)}$, $D^{(0)}$ is determined by minimizing the energy functional with respect to ρ and D. The variation with respect to the density matrix has to be constrained to the subspace of Slater Determinants by imposing the projector condition $\rho^2 = \rho$ [112]. Within this subspace they considered small time-dependent amplitude fluctuations of the density matrix $\rho(t)$. To this end a weak time-dependent field was added to Eq.(3.16) of the form $F(t) = \sum_{i\sigma,j\sigma'}(f_{i\sigma,j\sigma'}e^{-i\omega t}c^+_{i\sigma}c_{j\sigma'} + h.c.)$. This produces small amplitudes oscillations $\delta\rho(t)$ around the stationary density, i.e., $\delta\rho(t) = \rho(t) - \rho^{(0)}$. They assumed that at each instant of time the double occupancy parameter is at the minimum of the energy functional compatible with the corresponding $\rho(t)$; i.e., the double occupancy parameters $\{D\}$ adjust antiadiabatically to the time evolution of the density matrix. This is reasonable since the double occupancy involves processes which are generally high in energy and hence fast.

The formal complication of their approach, as compared to the standard RPA has its origin in the proper adjustment of D to the time evolution of $\rho(t)$, i.e., the determination of $\delta D(t)$. This step is achieved by expanding the energy functional Eq.(3.16) up to second order in $\delta\rho$ and δD around the saddle point:

$$E[\rho,D] = E_0 + \overline{h}_0^+\delta\overline{\rho} + \frac{1}{2}\delta\overline{\rho}^+ L_0\delta\overline{\rho} + \delta\overline{D}S_0\delta\overline{\rho} + \frac{1}{2}\delta\overline{D}^T K_0\delta\overline{D} \tag{3.18}$$

where the bar indicates that we are treating a matrix as a column vector and the subindex 0 indicates evaluation in the stationary state. To write Eq.(3.18) we defined [111]:

$$\begin{aligned} h_{ji\sigma} &= \frac{\partial E}{\partial\rho_{ij\sigma}}; \quad L_{ij\sigma,kl\sigma'} = \frac{\partial^2 E}{\partial\rho^*_{ij\sigma}\partial\rho_{kl\sigma'}}; \\ S_{k,ij\sigma} &= \frac{\partial^2 E}{\partial D_k\partial\rho_{ij\sigma}}; \quad K_{k,l} = \frac{\partial^2 E}{\partial D_k\partial D_l}; \end{aligned} \tag{3.19}$$

By applying the condition of antiadiabaticity $\partial E/\partial\delta D = 0$ to Eq.(3.18), a linear relation between $\delta\rho$ and δD can be obtained. In fact [111]:

$$\frac{\partial E}{\partial D} = S_0\delta\rho + K_0\delta D = 0 \tag{3.20}$$

$$\Rightarrow \delta D = -K_0^{-1}S_0\delta\rho \tag{3.21}$$

Using this expression δD can be eliminated from Eq.(3.18), finally yielding to an expansion of the energy as a functional of $\delta\rho$ alone $\widetilde{E}[\rho] = E[\rho,D(\rho)]$,

$$\widetilde{E}[\rho] = E_0 + \overline{h}_0^+ \delta\overline{\rho} + \frac{1}{2}\delta\overline{\rho}^+ (L_0 - S_0^+ K_0^{-1} S_0)\delta\overline{\rho}. \tag{3.22}$$

This can be regarded as the expansion of an effective interacting energy functional in which the interaction potential between particles is density dependent. This kind of functional often appears in the context of nuclear physics and there exists the Ehrenreich-Cohen method [113], which allows to compute the RPA fluctuations induced by this type of interaction.

Seibold and Lorenzana [111] applied this formalism to the half-filled Hubbard model in the antiferromagnetic Néel state [115]. In particular they evaluated the density-density correlation function, the optical properties and the double occupancy and compared them to the exact result and other approximations for a 1d system.

As it can be seen from Fig.(3.1) the static quantities they calculated, like GA ground state energy and double occupancy, resulted to be in excellent agreement with exact results in one dimension up to moderate coupling and in two dimensions for all couplings. They found a substantial improvement over traditional GA and HF + RPA treatments. Also the dynamical correlation functions resulted to be substantially better than HF + RPA ones and to be well behaved with respect to important sum rules.

The better performance of GA + RPA with respect to conventional HF + RPA theory was supported by another important work of Seibold, Becca and Lorenzana [114] in 2003, where they calculated the charge-charge and current-current dynamical correlation functions in one and two dimensions.

An example of the comparison between the results given by this approach with the ones of the HF + RPA method is reported in Fig.(3.2), which reveals that GA + RPA provides a better description of both the low and the high-energy excitations than the HF + RPA, even at larger values of U/t.

3.2.1 An Alternative Approach for Two-Particles Response Function

In Chapter 2 we saw that for materials with incompletely filled valence band the dynamical two-particles response function and the formation of anti-bound states[3] are still not well

[3]Here and henceforth we will refer to the two holes resonance described in Chapt.2 as anti-bound state.

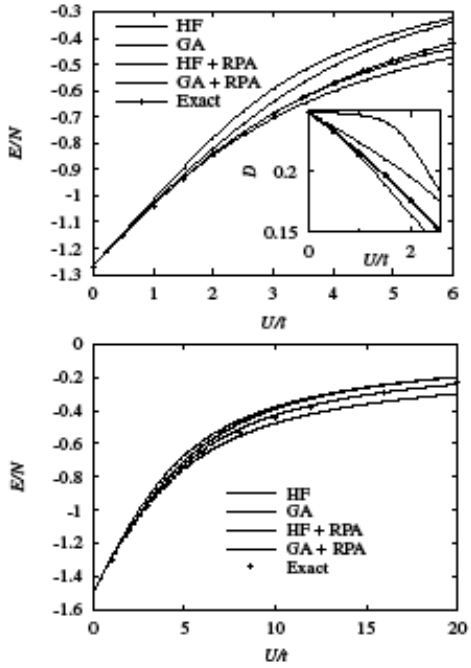

Figure 3.1. *Comparison of the exact ground state energy with the various approximate methods discussed in [111] for the half-filled Hubbard model in 1d (upper panel) and 2d (lower panel). Exact results in the upper panel are for an infinite 1d system after Ref. [116], whereas approximate results are for a 32-site lattice. (Finite size errors are estimated to be of the order of line width.) Exact [117] and approximate results in the lower panel are for a* 4×4 *cluster. The inset show the corresponding curves for the 1d double occupancy (exact and GA* $+$ *RPA are almost undistinguishable).*

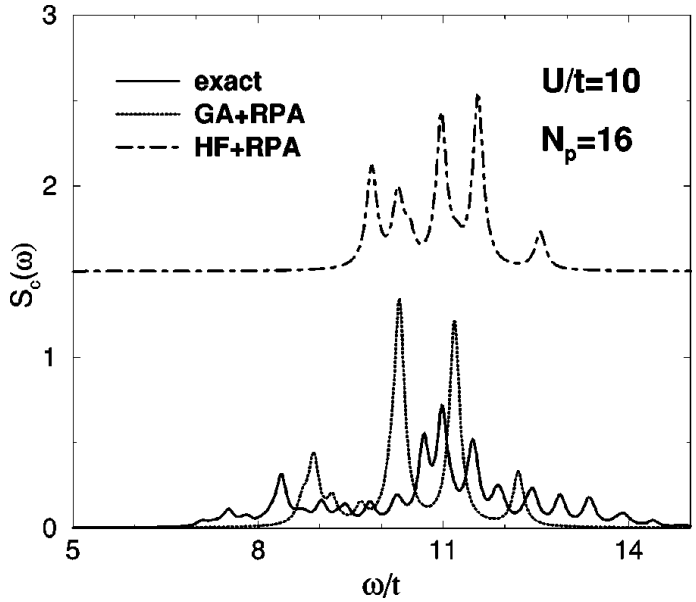

Figure 3.2. *Charge correlation function* $S_c(\omega)$ *[114] for the half-filled* 4×4 *Hubbard model (*$\sim$*16 particles) in the case of* $U/t = 10$*, where* t *stands for the hopping parameter.*

understood. Cini [61] explained the Ni XPS satellite and put forth a first approximation to the Auger spectra within the low-density approximation; later, as discussed above, Cini and coworkers [82, 118] found that for small fillings the best approximation for the spectral function corresponds to a generalization of the original CS theory, namely summing a ladder series with bare Green's functions. For moderate fillings and large interactions, this bare ladder approximation (BLA) breaks down and no reliable theory is available.

In Ref. [61] several effects are expected to affect the two-particle spectra in the case of partially filled bands. First, strong correlation produces band narrowing which should help to split-off anti-bound states from the two-particle continuum. Second, the spectral weight of the anti-bound state should depend on doping since the probability to find an empty site where to create an anti-bound pair is concentration dependent. Third, the other holes present in the system are expected to screen the effective interaction among the added holes which may lead to a renormalization of the position of the anti-bound state with respect to the continuum.

From what we said so far about the TDGA, we expect that this approach can be a good candidate to build up a theory of anti-bound states for the Hubbard model which incorporates all these effects. Seibold and collaborators [119] computed in fact the pairing fluctuations within the TDGA, reproducing the effects discussed above while sharing the numerical simplicity with the CS theory. Interestingly they found that the effect of a finite density is to anti-screen the Hubbard U interaction, i.e. the effective interaction is larger than the bare one. Besides this the comparison of their results with the ones gained by exact diagonalization shows that the TDGA is reliable even at high densities where the BLA breaks down.

Their starting point was again the Hubbard Hamiltonian [119]:

$$H = \sum_{ij\sigma} (t_{ij} - \mu\delta_{ij}) c^{+}_{i\sigma} c_{j\sigma} + U \sum_{i} n_{i\uparrow} n_{i\downarrow}, \tag{3.23}$$

where $c^{+}_{i\sigma}$ creates a fermion with spin σ at site i, $n_{i\sigma} = c^{+}_{i\sigma} c_{i\sigma}$, U is the Coulomb on-site repulsion and μ is the chemical potential.

Seibold and coworkers [119] wanted to evaluate the two particles correlated response functions:

$$P_{ij}(\omega) = \frac{1}{i} \int_{-\infty}^{\infty} dt e^{i\omega t} \langle T c_{i\uparrow}(t) c_{i\downarrow}(t) c^{+}_{j\downarrow} c^{+}_{j\uparrow} \rangle, \tag{3.24}$$

whose imaginary part yields the two particles insertion (removal) spectra for $\omega > 0$ ($\omega < 0$).

To this end they choose as trial wave function:

$$|\psi\rangle = g^D|\Phi\rangle, \tag{3.25}$$

where $|\Phi\rangle$ represents this time a Bogoljubov vacuum[4] [112, 120] and g^D partially projects out from it doubly occupied states.
The single particle density matrix is defined as $\rho_{i\sigma,j\sigma'} = \langle\Phi|c^+_{j\sigma'}c_{i\sigma}|\Phi\rangle$ and the pair matrix $k_{i\sigma,j\sigma'} = \langle\Phi|c_{j\sigma'}c_{i\sigma}|\Phi\rangle$ which satisfies the constraints [121]:

$$\rho^2 - \rho = kk^*, \quad [\rho,k] = 0. \tag{3.26}$$

To perform GA, we need to build up the energy functional $E = \frac{\langle\psi|H|\psi\rangle}{\langle\psi|\psi\rangle}$ as a first step. This is more easily done by rotating at each site the fermion annihilation and creation operators to a basis where anomalous expectation values vanish [122]. Then one derives the GA with one of the known techniques [102, 109] (see also Sect.3.1.2) and finally for a non magnetic state one finds:

$$E[\rho,k,D] = \sum_{ij\sigma} t_{ij}z_iz_j\rho_{i\sigma,j\sigma} + U\sum_i D_i, \tag{3.27}$$

with the hopping renormalization factors:

$$z_i = \frac{\sqrt{\frac{1}{2} - D_i + J_{iz}}(\sqrt{D_i - J_{iz} - J_i} + \sqrt{D_i - J_{iz} + J_i})}{\sqrt{\frac{1}{4} - J_i^2}}. \tag{3.28}$$

Here we defined:

$$\begin{aligned} &J_{ix} = \frac{k_{i\uparrow,i\downarrow} + k^*_{i\uparrow,i\downarrow}}{2}; \quad J_{iy} = i\frac{k_{i\uparrow,i\downarrow} - k^*_{i\uparrow,i\downarrow}}{2}; \\ &J_{iz} = i\frac{\rho_{i\uparrow,i\uparrow} + \rho^*_{i\downarrow,i\downarrow} - 1}{2}; \quad J_i = |J_i|; \quad D_i = \langle\psi|n_{i\uparrow}n_{i\downarrow}|\psi\rangle \end{aligned} \tag{3.29}$$

[4] A Bogoljubov vacuum is a way to represent the BCS ground state by means of a fermion quasi-particles vacuum.

The ground state is found by minimizing Eq.(3.27) with constraints given by Eq.(3.26), leading to the static ρ^0, k^0, J^0 and D^0. In particular Seibold et al. [119] concentrated on a paramagnetic normal metal, thus $k^0 = J^0_x = J^0_y = 0$.
To compute the response function they add a weak time dependent pairing field $F(t) = \sum_i (f_i e^{-i\omega t} c_{i\downarrow} c_{i\uparrow} + h.c.)$ to Eq.(3.23), whose effect is to produce small time dependent deviations in the particle density, $\delta\rho(t) = \rho(t) - \rho^0$. In addition, since F does not conserve the particle number it induces pairing correlations k, which they computed in linear response.

Expanding the energy up to second order in $\delta\rho$ and k one finds:

$$\delta E = \sum_{k\sigma} (\varepsilon_{k,\sigma} - \mu)\delta\rho_{k\sigma,k\sigma} + V \sum_i (J^2_{ix} + J^2_{iy}). \tag{3.30}$$

Here $\varepsilon_k = z_0^2 e_k + \Sigma_G$ denotes the GA dispersion relation (e_k is the bare one), Σ_G coincides with the Lagrange parameters of the slave-boson method [102] and is given by $\Sigma_G = z_0 z_0' \overline{e}$, with $\overline{e} = \sum_{i\sigma} t_{ij} \rho^0_{i\sigma,j\sigma'} z_0$ is the hopping renormalization factor at the saddle point and z_0' is its density derivative. Our notation emphasizes the fact that Σ_G can be interpreted as a local GA self-energy. Finally they evaluated the pair correlation function by using the usual ladder expression:

$$P(\mathbf{q},\omega) = \frac{P^0(\mathbf{q},\omega)}{1 - V P^0(\mathbf{q},\omega)}, \tag{3.31}$$

with an effective on-site particle-particle interaction V, which is defined as [119]:

$$V = \frac{U - 2\Sigma_G}{1 - n}, \tag{3.32}$$

where n denotes the particle concentration.

The explicit expression for $P^0(\mathbf{q},\omega)$, appearing in Eq.(3.31), is:

$$P^0(\mathbf{q},\omega) = \frac{1}{L} \sum_{\mathbf{k}} \frac{1 - f(\varepsilon_{\mathbf{k}}) - f(\varepsilon_{\mathbf{k+q}})}{\omega - \varepsilon_{\mathbf{k}} - \varepsilon_{\mathbf{k+q}} + 2\mu + i\eta_{\mathbf{k},\mathbf{k+q}}}, \tag{3.33}$$

where L is again the number of lattice sites, $f(\varepsilon_{\mathbf{k}})$ is the Fermi distribution function and $\eta_{\mathbf{k},\mathbf{k}'} = 0^+ sign(\varepsilon_{\mathbf{k}} + \varepsilon_{\mathbf{k}'} - 2\mu)$.

Eqs.(3.31) - (3.33) represent the main result gained by Seibold and coworkers [119]. These expressions show that their approach leads to the same formal ladder structure as in

the CS theory [34, 35, 36] but with the HF self-energy ($\Sigma_{HF} = Un/2$, with $z_0 = 1$) replaced by the GA one and the Hubbard repulsion U replaced by an effective interaction V. Notice that Eq(3.32) is valid in the BLA, provided one replaces $\Sigma_G \to \Sigma_{HF}$, leading to $V = U$.

The local response is obtained as proportional to the imaginary part of [119]:

$$P_{ii}(\omega) = \frac{1}{L}\sum_{\mathbf{q}} P(\mathbf{q},\omega). \tag{3.34}$$

The problem within the BLA is not so much the energy of the anti-bound state but rather the energy of the particle continuum, which is given by the HF eigenvalues. This affects the anti-bound state because, as the continuum approaches the energy U, the anti-bound pair becomes less localized in the relative coordinate and eventually disappears.

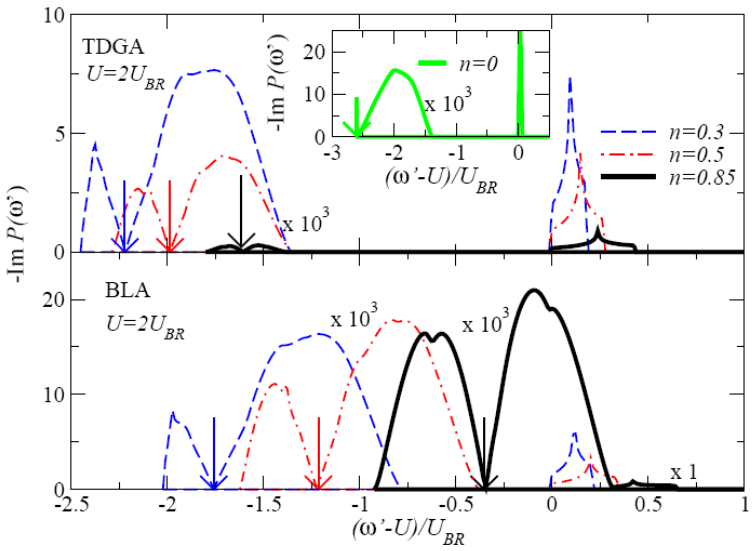

Figure 3.3. *Local spectral function for different fillings [119] in TDGA and BLA. Results are for the Hubbard model on a square lattice with nearest-neighbor hopping ($U_{BR} = 128t/\pi^2$). The vertical arrows indicate the position of 2μ, separating the addition part $\omega' > 2\mu$ from the removal part $\omega' < 2\mu$. The intensity of two-particle scattering states have been multiplied by 10^3. Inset: the $n = 0$ case which coincides in the two approximations.*

Fig.3.3 compares the local two-particles spectral function for an infinite two-dimensional system and $n < 1$, within TDGA and BLA. The inset shows the $n = 0$ case where TDGA and BLA coincide. Differences occur at finite concentrations (main panel) where the line shapes are dominated by the anti-bound state at $\omega' \sim U$ (as in CS), which is significantly stronger in the TDGA. The intensity of the continuum at low energies has been multiplied

by 10^3 to make the line shape visible. As anticipated the two-particles continuum is far from the anti-bound state in GA, whereas it quickly approaches it in the BLA. The anti-bound state can propagate and forms a band as in the Sawatzky approach; this is the reason for the width of the high-energy feature, other broadening mechanisms are discussed in Ref. [60]. The pair correlation function satisfies the sum rules:

$$S = -\frac{1}{\pi}\int_{2\mu}^{\infty} d\omega' ImP_{ii}(\omega') = 1 - n + \langle n_{i\uparrow} n_{i\downarrow}\rangle. \tag{3.35}$$

This can be used to evaluate ladder corrections to the GA or HF double occupancy. The BLA introduces a strong correction to the HF double occupancy which is in accordance to GA for small fillings and then deviates.

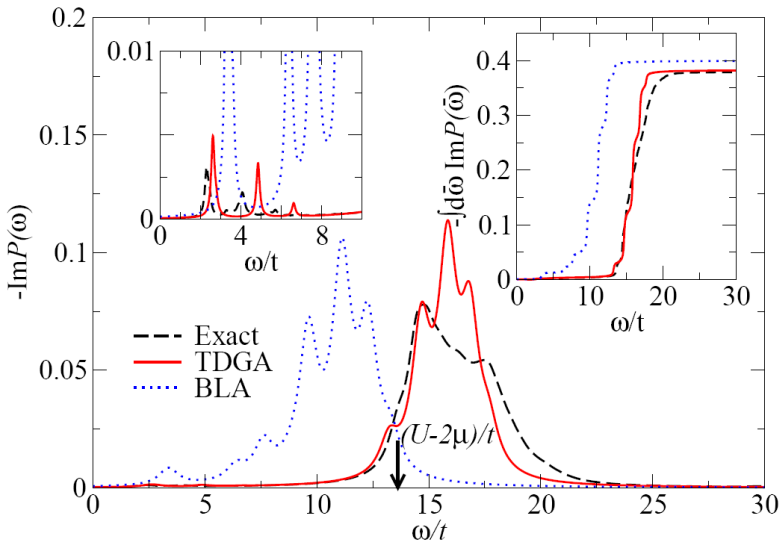

Figure 3.4. *Imaginary part of the pair correlation function for the Hubbard model [119] with $U/t = 15$ and 12 particles on a 4×4 square lattice obtained by exact diagonalization, TDGA and BLA. The origin of the energy axis is at 2μ. The left inset enlarges the region of low energy band excitations, while the right inset shows the frequency evolution of the integrated spectra. The broadening of the delta peaks is $0.5t$ in the main panel and the right inset, and $0.1t$ in the left inset.*

In order to validate their results, Seibold and coworkers [119] computed also the exact two-particles addition spectra for 10 particles on a 4×4 lattice with only nearest-neighbor hopping t and $U/t = 15$, by using exact diagonalization. Fig.3.4 shows a comparison between the present theory and BLA.

Despite the large value of the Hubbard repulsion, TDGA yields excellent agreement with

exact diagonalization concerning the location, width and intensity of the high-energy anti-bound states. On the other hand, BLA predicts that these excitations have a much lower energy when referenced to 2μ and no clear separation with the band states is visible (see upper-left inset). For the system under consideration, there are three band-like two-particles energies which are very well reproduced by TDGA in contrast with BLA. The upper-right inset demonstrates that the double occupancy after Eq. (3.35) is accurate within TDGA, whereas BLA overestimates as it is expected. The good performance of TDGA is not restricted to this particular value of U but persists to even larger (and of course lower) on-site repulsions. The simplicity of the method elaborated by Seibold and coworkers suggests its application to the computation of Auger spectra on top of realistic Gutzwiller calculations. The first attempt towards this direction will be described in Sec.4.4.

4

Results

The aim of this chapter, which represents the original core of this thesis work, is to pave the way towards an understanding of CVV Auger spectra from open band materials by means of the several models we developed. This offers also a precious chance to deepen our knowledge about the mechanisms which are at the basis of the way strongly correlated systems respond to a very strong and local probe such as Auger spectroscopy.

The several sections here presented will be arranged in an order of increasing originality and complexity of the proposed models, which are all deep rooted on the common ground of electronic correlations, the underlying *fil rouge* of this thesis work.

The journey starts within the secure waters of quite closed band materials: the first section in fact will be devoted to the description of the results gained by applying the Cini-Sawatzky theory (CS) theory to explain the AR-APECS (Angular Resolved - Auger PhotoElectron Coincidence Spectroscopy) spectra from metallic Copper, while the second one will be focused on an *ab-initio* approach to evaluate the on-site hole-hole Coulomb interactions. This represents an essential step towards a prediction of the measured Auger spectra without making use of experimentally determined parameters. The reader's attention then will be turned to the problem of CVV Auger spectra from open band materials. To start with, I shall present the results of a new approach to the Graphite and carbon nanotubes spectra, which is based on the use of the BLA (see Sec.2.3.3) density of states. Subsequently we will apply both the BLA and the Time Dependent GA (TDGA, see Sec.3.2) to the CVV Auger spectra from CuO_2 planes of high T_c superconductors. The comparison between the results provided by these two methods will allow us to trace the path for a new approach aimed to model this kind of spectra in the attempt of going beyond the limit of the BLA. Finally the last section will

be devoted to the description of a new theory able to model Coster-Kronig preceded Auger line shapes in solids. The double value of this approach stems from the fact it both gives a recipe for calculating a correlated three holes Green's function and it represents the first theory able to model these kind of contributions to the Auger spectra, allowing to decouple them from the corresponding parent diagrammatic lines.

4.1 The M_3VV Spectrum from Cu(111): a Survey by AR-APECS Technique and Model Calculations

As it has been anticipated a few lines ago, this section will be centered on the study of the $M_3M_{4,5}M_{4,5}$ Auger spectrum from metallic Copper [123], that is a transition due to the non radiative decay of a $3p_{3/2}$ core hole which leads the target atom to a two holes final state in the $3d$ valence band. This has been achieved both by using modeling and experimental techniques. In particular the measured data were acquired by means of AR-APECS [16], a coincidence spectroscopic technique whose spectra are produced only by those Auger electrons which are revealed simultaneously with the primary photoelectron coming from the creation of the first core hole (which starts the Auger decay).

4.1.1 The Experiment

The experiment was performed by the group of Prof. G. Stefani at the beamline ALOISA of the synchrotron ELETTRA (Trieste). A detailed description of the measuring apparatus is far from the scope of this section and a section on Ref. [124] is devoted to it.

The sample was a single crystal of Cu(111) cleaned using the usual procedure of cycles of sputtering and annealing. Its chemical cleanness and the absence of lattice defects were verified by photoemission, Reflection of High Energy Electron Diffraction (RHEED) and PhotoElectron Diffraction (PED) measurements.

Monochromatic p-polarized radiation of energy $h\nu = 241$ eV impinged on the sample at a grazing incident angle of about 6^o, where the surface normal lied in the plane determined by the photon beam direction and its polarization vector ε.

Fig.(4.1) shows a schematic representation of the analysers disposition inside the ALOISA experimental chamber. As it can be seen from the figure, among the seven hemispherical analysers contained in the experimental chamber, two of them are mounted 18^o apart on an array termed bimodal frame, which has the possibility of rotate around the photon beam axis

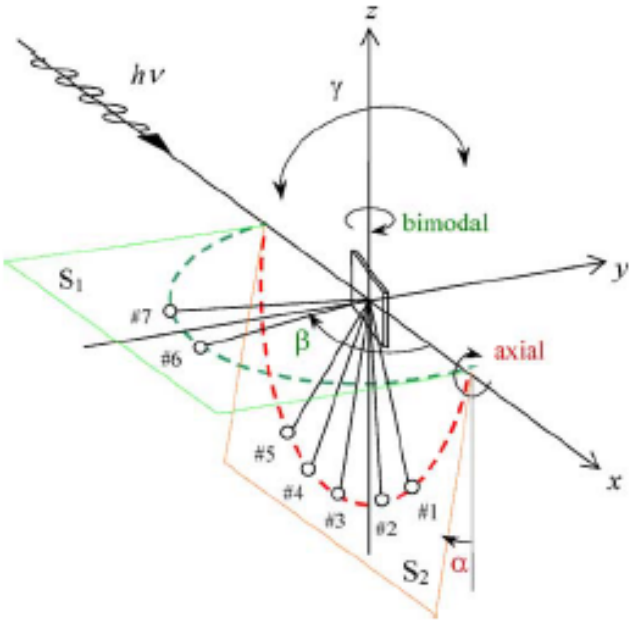

Figure 4.1. *Schematic representation of the experimental chamber of the beamline ALOISA at the synchrotron ELETTRA (Trieste). The seven electron analysers making up the measuring apparatus are placed on two frames having different motion degrees of freedom. The two analysers embedded in the bimodal frame in fact can rotate around a direction which is orthogonal to the x-axis, or else around the direction of the impinging primary beam. The remaining five analysers, which are placed instead on the so-called axial frame, are able to rotate around the x-direction independently from the experimental chamber.*

and around an axis normal to it. The other five analysers (18^o apart) are positioned on a plane (axial frame) containing the photon beam axis and rotating around it.

To perform the coincidence measurements the bimodal analysers (with an energy resolution of 2.16 eV) were tuned to a fixed kinetic energy of $E_k = 157.8$ eV, which corresponds to the high kinetic energy side of the $3p$ photoemission peak. This energy was chosen in order to avoid the detection of photoelectrons coming from the ionization of the $3p_{1/2}$ shell. The axial analysers (with an energy resolution of 0.9 eV) sampled instead the energy range of the Auger spectrum.

For the experiment two configurations were used and in the following they will be referred to as condition AN and AA. In the former geometry one electron of the pair was aligned (A) with the polarization vector, ε, while the other one (the Auger electron) was collected at more than 40^o from the surface normal, so it was not aligned (N) with ε. In the latter condition instead both axial and bimodal frames were mostly close to the surface normal (at angles mainly $\leq 20^o$) and thus most of them can be assumed to be aligned (A) with ε. In Fig.(4.2) the comparison between the M_3VV experimental coincidence Auger spectra measured for the configuration AN (open triangles) and AA (open circles) is shown [123]: from this graph

it is clear that the patterns relative to the two different geometries differ one from the other for the relative intensity ratio of the two main peaks of the spectra which are due to the final two holes terms ^1G (the principal peak) and ^3F (the peak on the high kinetic energy side of the main one).

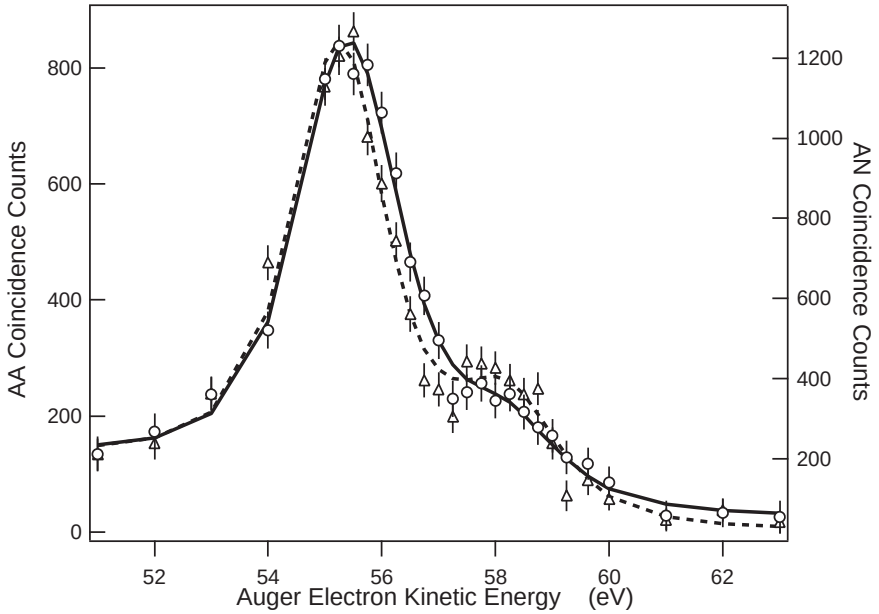

Figure 4.2. *Comparison between the M_3VV coincidence Auger spectra of Cu(111) [123] measured in configuration AA (open circles and solid line) and AN (open trianglesand dashed line). The solid and dashed lines are only guides to the eye.*

4.1.2 The Model

To explain the trend shown by the experimental data reported in Fig.(4.2), the Cini theory for the closed band case [34, 35] was used but with a slight modification represented by the introduction of the off-site interaction (see Sec.2.3.2) and the spin-orbit coupling also for the two holes in the final state [123]. It has been possible to introduce solid state effects thanks to the use of off-diagonal one hole local density of states (1hLDOS) matrix elements, which were calculated within Density Functional Theory (DFT).

The studied Auger transition leads the target atom to a final state with two holes in the $3d$ shell. To take into proper account spin-orbit interaction, the intermediate coupling scheme was adopted, thus $\{^1S_0,^1D_2,^1G_4,^3F_4,^3F_3,^3F_2,^3P_2,^3P_1,^3P_0\}$ represents the two holes basis set upon which the several operators present in the calculation has to be projected. The

spin-orbit coupling parameter, $\zeta_{3d} = \frac{\hbar^2}{2m_e c^2 a_0^3}\langle\varphi_{3d}(r)|\frac{1}{r}\frac{dU}{dr}|\varphi_{3d}(r)\rangle$, was taken from a DFT calculation on atomic Copper [125].

As it has been described in full details in Sec.2.3.1, in the CS basic model the correlated two holes local density of states (2hLDOS) can be obtained within the two step approach from a two holes Green's function:

$$G(\alpha_1,\alpha_2,\alpha_3,\alpha_4;\omega) = \langle\Phi|c_{d,\alpha_4}c_{d,\alpha_3}\frac{1}{\omega-\widehat{H}+i\delta}c^+_{d,\alpha_1}c^+_{d,\alpha_1}|\Phi\rangle, \tag{4.1}$$

where $|\Phi\rangle$ is the ground state of the neutral target atom and c_{d,α_i} (c^+_{d,α_i}) represents the annihilation (creation) operator for a hole in the d shell with quantum numbers all specified in α_i. $\widehat{H}$ [1] is the Hamiltonian of the system, which can be split as the sum of a non interacting and an interacting part:

$$\widehat{H} = \widehat{H}_0 + \widehat{H}_{int}. \tag{4.2}$$

Here $\widehat{H}_0$ is given by the sum of single-particle operators, while instead $\widehat{H}_{int}$ recollects all the interaction term present in $\widehat{H}$, that are the hole-hole interaction, $\widehat{H}_r$ and the spin-orbit coupling, $\widehat{H}_{so}$, $\widehat{H}_{int} = \widehat{H}_r + \widehat{H}_{so}$.

To gain the Auger spectrum we will follow basically the same procedure outlined in Sec.2.3.1 for the CS theory, but with two main differences: a matrix approach which is essential to take into account solid state effects, and the inclusion of the spin-orbit coupling interaction for the two final valence holes. This term will modify the interaction Hamiltonian present in the Dyson like equation which is used to evaluate the interacting two holes Green's function. In the following this procedure will be described in more details.
Starting from the DFT 1hLDOS matrix, the non-interacting 2hLDOS matrix, $\widehat{D}^{(0)}(\omega)$, has been built by simply convolving the 1hLDOS. Then also the Hilbert transform matrix of the two holes non interacting density of states, $\widehat{I}^{(0)}(\omega)$ was evaluated, so as to make up the non interacting two holes Green's function matrix:

$$\widehat{G}^{(0)}(\omega) = \widehat{D}^{(0)}(\omega) - i\pi\widehat{D}^{(0)}(\omega) \tag{4.3}$$

[1] All through this chapter the symbol "$\widehat{\ }$" will be used to mean that the stressed quantity is an operator and the corresponding equations where it appears are valid independently from the particular chosen basis set of states.

The correlated two holes Green's function can be obtained by using the following Dyson equation:

$$\widehat{G}(\omega) = \widehat{G}^{(0)}(\omega) + \widehat{G}^{(0)}(\omega)\widehat{H}_{int}\widehat{G}(\omega), \tag{4.4}$$

which is very similar to the one that can be gained by Eq.(2.21) except for the presence of $\widehat{H}_{int}$ instead of the simpler $\widehat{H}_r$. The interacting 2hLDOS we are interested in can be then easily calculated as the imaginary part of $\widehat{G}(\omega)$, which can be evaluated by inverting Eq.(4.4):

$$\widehat{D}(\omega) = -\frac{1}{\pi} Im[\widehat{G}(\omega)]. \tag{4.5}$$

The total spectrum at last will be proportional to [123]:

$$S(\omega) = \Sigma_{XY\sigma} A_X^* D_{XY\sigma}(\omega) A_Y \tag{4.6}$$

where X and Y contain the quantum numbers identifying a particular two holes multiplet term and $D_{XY\sigma}$ represents the correlated two-hole local density of states matrix elements calculated on the states X and Y. A_Y and A_Y^* are respectively the Auger matrix elements and their hermitian conjugates for an Auger transition from the deep initial core hole state to the final two hole multiplet term Y. Before going on I wish to remind the reader that Eq.(4.6) is valid within the two step approach. In actual calculations we neglected the dependence of the Auger matrix elements on the kinetic energy and direction of the emitted Auger electron. The amplitudes A_Y appearing in Eq.(4.6) were obtained by using the PHAGEN code (PHAses GENerator) to calculate both bound state and excited radial wave functions. This code is based on a self consistent procedure within the single configuration Dirac-Fock scheme, where Breit's interaction is included only as a first-order perturbative correction. Excited state radial wave functions are calculated using the muffin tin approximation for the potential and adding an exchange-correlation part calculated within the LDA scheme. Multiple scattering effects have been neglected, i.e. only the direct waves (those which directly reach the detector) have been considered. At the low kinetic energies of the outgoing electron considered here, such effects could influence the diffraction patterns, but we neglected them in the calculation of the energy spectrum.

4.1.3 The Screening Energy

Among the several ingredients which are needed to calculate the Auger spectrum, the two holes correlation energies were taken from [126]. They were calculated using the Slater integrals from [166] and they take into account also the exchange integrals present for the triplet multiplet final state terms. Besides this it has to be considered that the effective Coulomb interaction felt by the two final holes is diminished by a screening energy, Δ, due to initial and final state effects. The former are due mainly to the fact that the photoelectron and the Auger electron come from different electrostatic potentials, while instead the final state effects are produced by the screening of the other passive electrons.

Finding a rigorous way to evaluate this screening energy is a problem still open at the state of the art today. Some attempts have been done in this direction by several groups of research [149, 129]. Unfortunately at the standard level of DFT the accuracy reached by all these approaches is still far from satisfactory. One cannot disentangle the various effects in the measured spectra. For these reasons the procedure described in [54, 55] was adopted to obtain a theoretical line shape that better reproduces the experimental patterns. The Auger profile was calculated by fitting the screening energy Δ to get the line shape which best reproduces the experimental one, without caring about its absolute position. The remaining energy shift was attributed to the off-site interaction χ (see Sec.2.3.2), that is the energy that has to be subtracted from the Coulomb interaction U together with the screening energy Δ to reach the effective hole-hole interaction. χ is due to the fact that also when they are some distance apart, the two final holes can still interact because of an incomplete screening. The best value found in this way for the screening energy is 20 eV. By using this Δ value however our calculated spectrum results to be still shifted of about 3 eV towards higher kinetic energies respect to the experimental one. Recalling to the mind the works of Cini and Verdozzi [54, 55] we are tempted to attribute all this shift to the off-site interaction, χ. This cannot be done directly because a further shift of 0.5 eV has to be considered, whose origin has an experimental nature. Panel (a) of Fig.(4.3) shows the comparison between the coincidence spectrum (open triangles in the left side of Fig.(4.3)) and the one which has been measured not in coincidence (dashed line). From this figure one sees in fact that the kinetic energy position of the intensity maximum for the coincidence pattern (open triangles in the left side of Fig.(4.3)) is shifted respect to the one measured not in coincidence (dashed line) by 0.5 ± 0.2 eV. To understand this behaviour it is worth noticing that for the coincidence experiment the photoelectron analysers were set to collect electrons with a kinetic energy 1.3

eV higher than the maximum of the $3p_{3/2}$ photoemission peak.

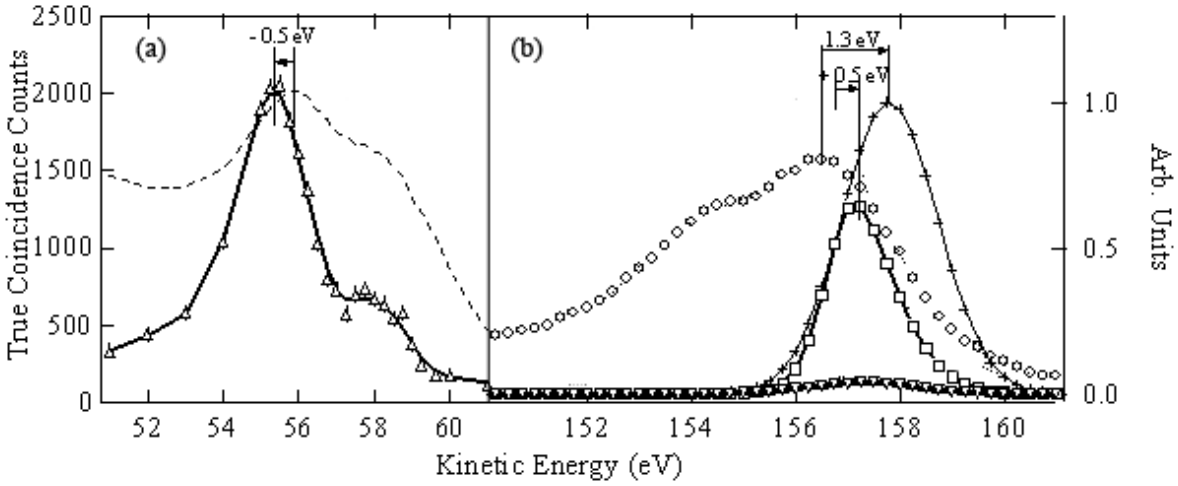

Figure 4.3. *Panel (a): total coincidence spectrum (open triangles) with the best fit obtained by the deconvolution of multiplet terms (thick solid line). The comparison with the Auger spectrum (dashed line), not measured with a coincidence technique and which has been simultaneously acquired, outlines a shift of about 0.5 eV between the energy position of the maxima of the two spectra. Panel (b): photoemission spectrum (open circles) superimposed to its best fit which has been obtained by using two Voigt components and an integral background (dotted lines). By convolving each one of the two Voigt peaks with the analyser transmission curve (crossed symbols and line), one obtains the patterns representing the accepted $3p_{1/2}$ photoelectrons (open triangles and line) and the $3p_{3/2}$ photoelectrons (open squares and line).*

In panel (b) of Fig.(4.3) the photoemission spectrum is shown as open circles, superimposed to the best fit which has been obtained by using two peaks, one for each of the two spin-orbit splitted components (dotted lines) of the $3p$ shell. Crossed symbols and solid line represent instead a gaussian with a FWHM of 2.16 eV (the bimodal analyser energy resolution), centred at an energy 1.3 eV higher than the photoemission spectrum maximum, which represents the energy window collected by the photoelectron analyser. Multiplying such gaussian with the lorentzian curve which represents the photoelectron energy distribution as obtained by the fitting procedure, one gets what may be called the "accepted" $3p_{1/2}$ photoelectrons (open triangles and solid line in panel (b) of Fig.(4.3)) and the "accepted" $3p_{3/2}$ photoelectrons (open squares and solid line in the right side of Fig.(4.3)). It results that the accepted $3p_{3/2}$ photoelectrons are inside a curve that is centred at +0.5 eV from the $3p_{3/2}$ spin-orbit term and with a FWHM of 1.5 eV. Since energy is conserved collectively by the electron pair, if higher energy photoelectrons are selected, Auger electrons originating from the same core ionization must have a lower energy than the diagrammatic value, so this

explains why the coincidence Auger spectrum is shifted of -0.5 eV with respect to the not in coincidence one (panel (a) of Fig.(4.3)). The reasonableness of these arguments is strengthened by a work of Jensen and coworkers [130] where it was observed a linear dispersion of the coincidence photoline as a function of the Auger electron energy.

Taking into account this further shift of the coincidence measured spectrum, the total shift of the theoretical spectrum towards higher kinetic energies can be estimated as 2.5 eV and now it can be fully attributed to the off-site interaction that has to be subtracted to the Coulomb interaction U together with the screening energy Δ to gain the effective hole-hole interaction. The off-site shift is very similar to the one estimated for Ag [55]. This is not surprising because Ag and Cu have a quite similar U/W ratio[2] (where W is the d band width) and the two wave functions are similar in both cases.

4.1.4 Discussion

Fig.(4.4) displays the calculated $M_3M_{4,5}M_{4,5}$ Auger line shape from metallic Copper [123] as obtained by following the procedure described in the previous subsection. The two reported patterns have been gained by making use in Eq.(4.6) of angle-resolved Auger matrix elements for the Auger electron detected at 0^o (open circles and solid line) and 40^o (open triangles and dashed line) from the sample surface normal, so as to reproduce at least for this electron the two different geometrical configurations adopted to perform the experiment. These two configurations correspond in fact to the geometries in which the Auger electron is respectively aligned (A) and not-aligned (N) with the light polarization vector, ε.
The theoretical patterns shown in Fig.(4.4) were convoluted with a lorentzian curve characterized by a FWHM of about 1.8 eV. This value has been achieved accounting for several broadening mechanisms (except for the experimental one) that may occur in a CVV Auger decay, such as for example lifetime and phonon broadening or the one due to dispersion (see Sec.2.3.2). The magnitude and exact values of all these contributions for the case of Copper are reported in Table 4.1. Considering also the experimental broadening leads to a calculated line shape which results to be too much broadened respect to the measured one, because in this case we have to convolve the theoretical pattern with a lorentzian curve having a FWHM of about 2.2 eV. Again we explain this finding as due to the tuning of the bimodal analysers at an energy higher than the $3p_{3/2}$ photoelectron line. We are revealing only the high kinetic

[2]They are respectively $(U/W)_{Ag} \sim 1.3$ and $(U/W)_{Cu} \sim 1.14$

energy tail of the core-hole photoemission; this means that we are selecting only fast photoelectrons. In this way we are artificially reducing the rate, as if the core-hole photoemission peak were narrower than the Cu $3p_{3/2}$ natural width.

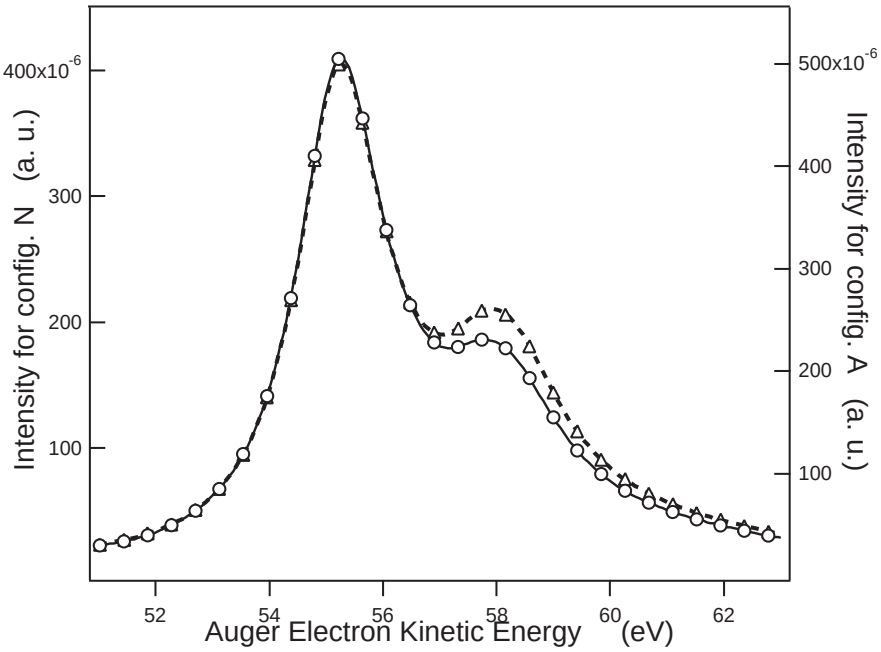

Figure 4.4. *Comparison between the calculated M_3VV Auger line shape of Cu(111) [123] obtained using angle-resolved Auger matrix elements for the Auger electron detected at 0^o (open circles and solid line) and 40^o (open triangles and dashed line) from the sample surface normal. Arbitrary units are employed.*

Type of broadening	Value [eV]	Reference
Lifetime broadening	$\Gamma(M_3)$=1.6	[131]
Experimental broadening	Γ_{exp} = 0.9	
Dispersion	Γ_{disp} = 0.15	[60]
Phonon broadening	Γ_{ph} = 0.14	[60]

Table 4.1. *Magnitude of the several factors contributing to broaden the theoretical Auger line shape. The origin and physical meaning of these mechanisms are described in details in [60].*

Another overestimated broadening contribution is the dispersive one: AR-APECS in fact is a surface sensitive technique and the energy range of the measured Auger electrons is near the minimum in the universal electronic mean free path curve. This means that the Auger

electrons revealed in this experiment come directly from the sample surface or from the first layers next to it, so that we have not the possibility to perceive the effects of the lattice "perfect" periodicity, or else of the periodic identical copies of the considered target atom. The main responsible for the increasing of the calculated line shape is however the narrowing mechanism relative to the natural lifetime width of the core-hole peak previously described: this fact clearly appears by simply comparing the order of magnitude of the several contributions to the total broadening.

By comparing the calculated spectra reported in Fig.(4.4) to the corresponding experimental ones of Fig.(4.2), it clearly appears that the theoretical patterns reproduce quite well the same trend as the AR-APECS measured data, that is the relative intensity ratio of the two main peaks depends on the emission angles of the involved electrons. In particular also the calculated spectra show a suppression of the ^3F triplet contribution in favor of the $^1G_4$ singlet one, when passing from the aligned to the not aligned configuration, although the calculation was done in a two-step model and only the alignment of the Auger electron was considered.

It has to be underlined that, notwithstanding this agreement between the trends shown by experimental and calculated spectra as far as the triplet suppression is concerned, the $^1G/^3F$ intensity ratio gained by model calculations is different from the measured one for the two chosen geometrical configurations even if we would use the correct broadening factor. Here I report a qualitative explanation for this behavior, following an argument suggested by Ref. [132]. A more quantitative explanation requires to apply a multiple scattering technique to the CS theory; we hope to develop this in a forthcoming paper.

As a first step we treat the emission from the atomic state and the following diffraction by the crystal as two independent processes. Within this approach the photoelectron and the Auger electron diffraction (PED and AED) patterns are generated once the atomic wave function of the ejected electron, the so-called "source wave", is diffracted by the crystal lattice. Regarding the role played by diffraction, forward scattering is dominant in determining the angular distribution of high energy electrons (> 300 eV), while at lower energies large angle scattering is also important and diffraction effects will influence the amplitude of the pattern while leaving almost unaffected the symmetry dictated by the atomic source wavefunction. Thus, as a starting point to discuss the shape of the energy spectra previously presented, one can consider which partial waves are allowed for the continuum electrons and evaluate their relative relevance at the various angles upon which photo and Auger electrons have been detected. The core hole polarization determines anisotropy of the observed angular

distribution, which is accounted for by the introduction of a polar quantization axis (the light polarization). In case of linear polarization, the core hole ion can only be aligned along this direction (equal populations for $\pm m_l$, where m_l is the magnetic quantum number for projection along the quantization axis). Thus the polarization vector of the impinging light, which is the quantization axis, leaves a fingerprint on the core-hole quantum numbers. These last ones influence the photoelectron and Auger electron quantum numbers through the dipole and the Auger transition selection rules (for more details see [132]) allowing only some values of l and m_l for these two emitted electrons. For an isolated (i.e., spherically symmetric) atom these permitted values for the photoelectrons and the Auger electron quantum numbers correspond to different spherical harmonics characterized by different angular distributions, thus modifying the angle of detection it is possible to enhance or suppress contributions from determined sublevels.

However, when analyzing electron emission from solids, diffraction effects must be taken into account: electrons coming from the decay of different multiplet terms may give rise to different diffraction patterns since they have slightly different energies and different partial wave expansions. To deepen the understanding of this behavior the group of prof. Stefani [132] did simulations of diffraction based on the Multiple Scattering Calculation of Diffraction (MSCD)[3], neglecting such multichannel dependence of diffraction and considering only the dependence on the quantum numbers of the scattered electrons. The results of these simulations for some specific azimuthal angles are shown in Fig.(4.5.a) (photoelectron), and Fig.(4.5.b) and Fig.(4.5.c) (Auger electron).

From Fig.(4.5) we can observe that each magnetic sub level contributes to the total intensity with different relative weight at the different scattering angles [the $m_A = \pm 3$ contributions are not included in Fig.(4.5.b) and Fig. (4.5.c) and in the following discussion, since are thought to be much less intense than the others]. Therefore in an AR-APECS experiment the electron analysers, set at specific detection angles, will prevalently detect electrons characterized by particular quantum numbers rather than by others. On the other hand selecting particular orbital and magnetic quantum numbers of the two emitted electrons results in selecting different contributions for the two holes states whose combinations originate the

[3]The MSCD code simulates the electron diffraction patterns from a solid on the base of the Rehr-Albers separable representation of spherical propagators. Calculations are performed using a muffin tin potential. The cluster size was of about 300 atoms, with a Debye temperature of 350 K [132]. The potential, the phase shifts and the radial matrices needed for the calculations have been obtained within the MSCD package. For the Auger MVV, the calculation has been performed by simulating an f-like wave, originating from a d-level (quantum number $l_i = 2$[4]) with only the $l_A = 3$ as the final channel.

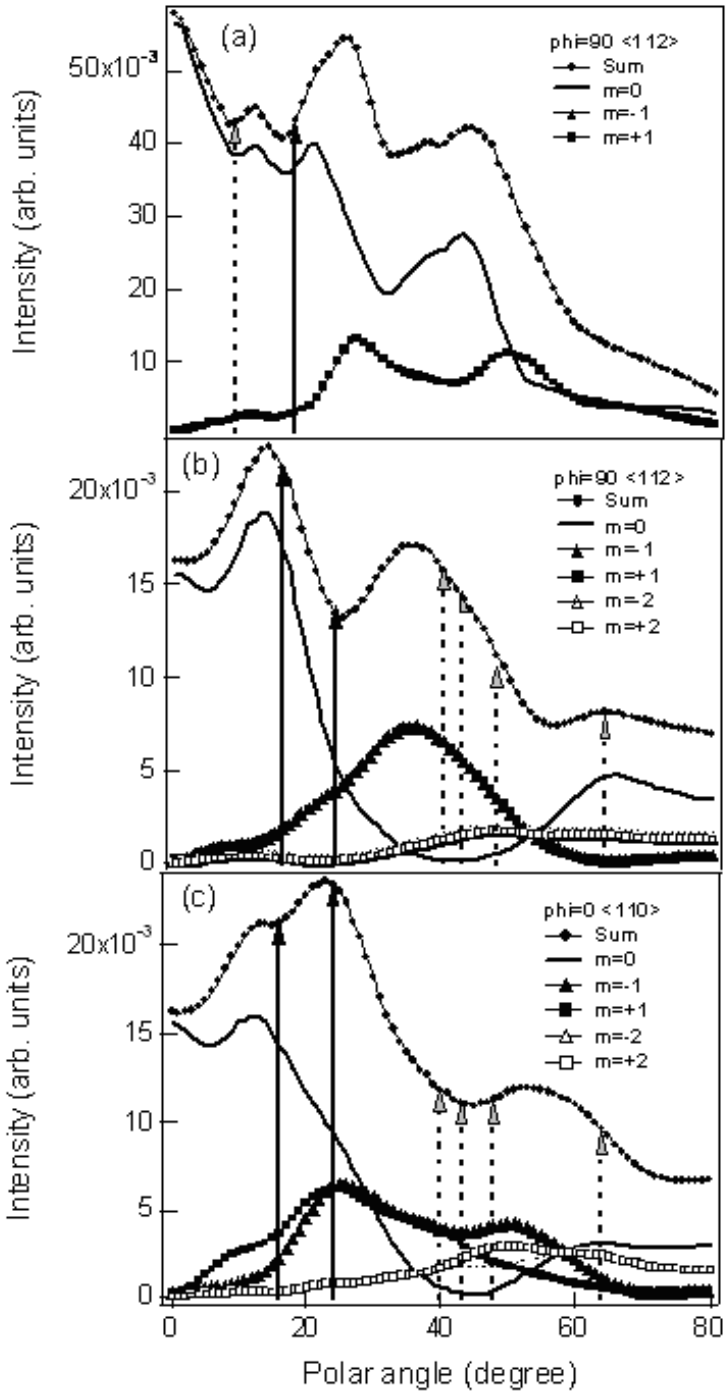

Figure 4.5. *Electron diffraction pattern simulations with an MSCD code [132]. Photoelectron pattern is shown in (a) at an angle corresponding to the* $\langle 112 \rangle$ *azimuthal direction. Auger electron pattern are shown in (b) and (c), along the* $\langle 112 \rangle$ *and* $\langle 110 \rangle$ *azimuthal directions, respectively. The total intensity (solid circles and line) and the partial intensities for a wave with* $m_l = 0$ *(solid line),* $m_l = -1$ *(solid triangles),* $m_l = 1$ *(solid squares),* $m_l = -2$ *(open triangles) and* $m_l = 2$ *(open squares) are plotted as a function of the polar emission. Solid (dashed) arrows indicate the position of the analyser in configuration AA (AN).*

multiplet structure of the Auger spectrum. In other words a magnetic quantum number selectivity can be achieved through selecting experimental conditions. For example, from Fig. (4.5) it is evident that near the normal to the surface the $m_l = 0$ contribution is dominant for both photoelectrons and Auger electrons. Solid (dashed) arrows in the figure indicate the position of the analysers in configuration AA (AN). Thus configuration AA, in which both photoelectrons and Auger electrons are detected closer to the normal, is expected to enhance the contribution $m_l = 0$ for both the photoelectron and the Auger electrons, and consequently to favour the $m_{l_1} = m_{l_2}$ condition for the two holes final state. In such a case, taking into account that the orbital moments l_1 and l_2 are the same since the two holes are both in a d-level, the intensity of the ^3F multiplet term results to be zero, because the presence of two holes in the same level with all the same quantum numbers is forbidden by the Pauli exclusion principle. The simulations of Fig.(4.5) also indicate that contributions from other m_l sub-levels are not zero at the detection angles of configuration AA. This means that also in configuration AA we are not revealing only the $m_l = 0$ contribution, but we are detecting electrons characterized by a mixtures of states given by all the allowed magnetic quantum numbers m_l among which the $m_l = 0$ component is dominant. Therefore the ^3F term does not vanish completely but its intensity has to be reduced, leading to a ratio $^1G/^3F$ greater in configuration AA than in other geometrical conditions where the $m_l = 0$ contribution is lesser important. The curves of fig.(4.5) also show that the $m_l \geq 1$ contributions are exactly zero at the normal to the surface for both the photoelectron and the Auger electron, and become dominant at larger angles, where the $m_A = 0$ is less important. In the geometrical condition of configuration AN the bimodal analysers were positioned close to the surface normal, while the axial analysers were at angles $\geq 40^o$ from it. Thus, according to the results of Fig.(4.5), in this experimental set-up we were revealing essentially electrons characterized by $m_{l_{ph}} = 0$ and $m_A \geq 1$, taking however into account that also in this case the total diffraction pattern would actually be an admixture of the different contributions with their own relative weights. Opposite to configuration AA, we therefore expect that in configuration AN the ^3F contribution is not depressed (since $m_{l_1} \neq m_{l_2}$ and the ^3F term does not vanish), leading to a $^1G/^3F$ ratio higher in configuration AN than in configuration AA. This is indeed the qualitative result one observes by comparing the two experimental patterns shown in Fig.(4.2). Such changes in the coincidence spectra indicates that due to the different spatial orientations of the five-fold degenerate d orbitals and the three-fold degenerate p orbitals involved in the process, different contributions from the magnetic sublevels can be observed for particular geometrical conditions.

Recollecting together all the findings of this study about the M_3VV Auger line shape from Cu(111), we can say that the theory here developed within the framework of the two step approach and the CS theory is able to explain the trend shown by the measured AR-APECS patterns as it can be seen from Fig.(4.4). Novelties of the developed theory are the introduction of solid state effects and spin-orbit coupling between the two final valence holes. The theoretical spectra were calculated by using only two fitting parameters which are the screening energy and the off site hole-hole interaction. The obtained value for the latter is similar to the one found for Ag [55], while the on-site hole-hole Coulomb interaction agrees well with other values found in literature [126, 133].

The clear differences between the experimental patterns however are not completely explained by the proposed theory and perhaps they may be due to the capability of the AR-APECS technique of selecting final spin-state terms thanks to the particular choice of the experimental geometry. Besides the selection rules of the involved transitions and the filtering role of the electron diffraction from the solid, the directions of detection of the photo and Auger electrons relative to the system quantization axis (fixed by the light polarization vector) act on the partial wave of the emitted electrons in such a way to enhance or suppress some of the two final spin-state terms with respect to the others. Much more work however has to be done in order to gain a complete understanding of these effects on the measured line shape: the arguments proposed to explain the differences between the exact values of the measured and calculated $^1G/^3F$ intensity ratio in fact are as plausible as heuristic and qualitative. To make them concrete and quantitative, with the aim of verifying the suspected spin-selective qualities of the AR-APECS technique, there is the need of a calculation made within the CS theory embedded in a multiple scattering approach as a first step towards a more realistic one-step formulation.

4.2 An *ab-initio* Method for CVV Auger Spectra from Closed-Shell Systems

The path towards a sound understanding of CVV Auger spectra from open band materials passes necessarily through the solution of the problem represented by the determination of Coulomb interactions without making use of experimental hints. Many attempts, based on DFT (Density Functional Theory) calculations, have been done in this direction since the nineties. The basic idea of these approaches was to include explicitly on-site Hubbard terms

to the LDA (Low Density Approximation), and prompted an extension to nearest neighbor interactions. As an example these are infact the principles which inspired in 1991 Anisimov and coworkers [135, 136] who proposed the so called "LDA+U" approach. Till today however experimental findings still play a fundamental role also with these theories, though without a direct determination of Coulomb interactions by means of a procedure based on fitting the spectra. Since the true Density Functional is unknown, one cannot deduce in fact the proper treatment from first principles and some experimentation is in order to get confidence with the method and choose the most appropriate version.

In this section we resume the Auger line shape problem, in a fully ab-initio treatment [137, 138], with application to Cu and Zn spectra as test cases. This is interesting for its own sake for Auger spectroscopy people, and there is an obvious interest in upgrading the theory of electron spectroscopy to a fully first-principles status. However, this work acquires a more general interest since Auger spectroscopy is ideally equipped to look at the short-range interaction, and hence can give clues about the best way to implement a LDA+U strategy.

4.2.1 Methods

Model Hamiltonian and the CS solution

We describe the system in the hole picture using a Hubbard-like Hamiltonian [45]:

$$\widehat{H} = \widehat{H}_0 + \widehat{H}_{int} \tag{4.7}$$

with:

$$\begin{aligned} \widehat{H}_0 &= \varepsilon_c c_c^\dagger c_c + \sum_{\nu_i} \varepsilon_{\nu_i} c_{\nu_i}^\dagger c_{\nu_i}, \\ \widehat{H}_{int} &= \frac{1}{2} \sum_{\nu_1,\nu_2,\nu_3,\nu_4} U_{\nu_1\nu_2\nu_3\nu_4} c_{\nu_1}^\dagger c_{\nu_2}^\dagger c_{\nu_4} c_{\nu_3}. \end{aligned} \tag{4.8}$$

Here c_c ($c_c^\dagger$) and c_{ν_i} ($c_{\nu_i}^\dagger$) represent the annihilation (creation) operators respectively for a core hole c and for a hole in a single particle valence band state labeled by ν_i. H_0 describes in this way the core hole and the valence band hole energies. Only correlation effects between the two final holes in the valence band are considered as it is shown in H_{int}.

Our approach then consists in making use of a two-step model to represent the Auger process: the initial ionization and the following Auger decay of the core hole are treated as two

independent events (see Chapt.2), that is the Auger transition we are interested in follows a fully-relaxed ionization of a core shell. A further simplification comes from restricting our attention to systems with filled valence bands. In this case in fact the two final holes are created in a no-hole vacuum and one is left with a two-body problem.
With these initial assumptions a solution to this problem can be achieved by using again the matrix Eq.(4.4), which can be written also as:

$$\widehat{G}(\omega) = \widehat{G}^{(0)}(\omega)\big[1 - \widehat{H}_{int}\widehat{G}^{(0)}(\omega)\big]^{-1}. \tag{4.9}$$

$\widehat{G}^{(0)}(\omega)$ is again the non-interacting two holes Green's function. The imaginary part of $\widehat{G}(\omega)$ gives the density of final states in presence of correlation, $\widehat{D}(\omega)$. The total spectrum is proportional to:

$$S(\omega) = \Sigma_{X,Y,\sigma} A^*_X D_{XY\sigma}(\omega) A_Y, \tag{4.10}$$

where X and Y contain all the required quantum numbers identifying a particular two hole multiplet term. $D_{XY\sigma}$ represents the correlated two-hole local density of states (2hLDOS) matrix elements calculated on the states X and Y. A_Y and A^*_Y are respectively the Auger matrix elements and their hermitian conjugates for an Auger transition from the deep initial core hole state to the final two holes multiplet term Y.
We are interested in modeling the $L_{23}VV$ Auger spectra from Copper and Zinc metals as a test-bed for our approach. To this end in both cases the corresponding non interacting $3d$ 1hLDOSs have been obtained by performing a DFT calculation. Both for Zn and Cu Eq.(4.9) has been evaluated in two different cases to probe the importance of solid state and spin-orbit effects. The interacting two holes Green's function, $G(\omega)$ has been calculated in fact using both diagonal and off-diagonal[5] 1hLDOS matrix elements and explicitly including or not the spin-orbit coupling operator in $\widehat{H}_{int}$. This means that Eq.(4.9) has been solved for $\widehat{H}_{int} = \widehat{H}_{coul}$ (see Eq.(4.8)) and for $\widehat{H}_{int} = \widehat{H}_{coul} + \widehat{H}_{so}$, where $\widehat{H}_{so} = \xi(r)\overline{L} \cdot \overline{S}$ and $\xi(r) = \frac{1}{2m_{el}^2c^2}\frac{1}{r}\frac{dV}{dr}$[139]. To perform calculations the spin-orbit coupling parameter ζ_{3d} [140], $\zeta_{3d} = \frac{\hbar^2}{2m_e c^2 a_0^3}\langle\varphi_{3d}(r)|\frac{1}{r}\frac{\partial U}{\partial r}|\varphi_{3d}(r)\rangle$, has been taken from literature values [141] evaluated by a DFT free-atom calculation. The intermediate coupling scheme resulted to be the most convenient basis to represent the two holes final states for the case where spin-orbit coupling

[5]Off-diagonal matrix elements in $\widehat{G}(\omega)$ are present for the $3d$ band of Copper and Zinc if one uses the complex spherical harmonics basis set

was explicitly included in H_{int}. The final multiplet terms this way are completely identified using as labels the L, S, J and M_J quantum numbers. The Russell-Saunders coupling scheme instead has been adopted for the case with no spin-orbit coupling. Whatever was the adopted form of $\widehat{H}_{int}$, we followed in all cases exactly the same procedure to gain the Auger current, which consists in evaluating the interacting two holes density of states from the imaginary part of the corresponding Green's function gained by Eq.(4.9), once it has been projected on a suitable basis set. The Auger spectrum is obtained by Eq.(4.10), where the used Auger matrix elements have been taken from literature [133], neglecting any energy dependence. This represents a good approximation because we expect that for Cu and Zn and for the transitions of interest the Auger matrix elements do not greatly vary with the Auger electron energies.

The comparison between these two approaches as applied to the cases of Zinc and Copper will be shown in Fig.(4.7) in Sec.4.2.2, while the following paragraph will be devoted to the description of the *ab initio* method we found to evaluate the last fundamental ingredient needed to calculate an Auger spectrum: the Coulomb interaction matrix.

Ab initio hole-hole interaction in the framework of DFT

The presence of Coulomb interaction between the two final holes of an Auger transition plays a fundamental role in determining both the energy position and the shape of an Auger line as it is apparent from Eq.(4.9). As far as the line shape is concerned, particular importance has the ratio between the Coulomb interaction U and the valence band width W (see Sec.2.3.1). Varying the ratio U/W we can cover in fact all the possible intermediate line shapes of an Auger process between the two limiting cases of a completely *atomic-like* and *band-like* spectrum. Increasing U at fixed W, that is increasing the ratio U/W, the band-like part of the line shape progressively loses spectral weight and the spectrum becomes dominated by the so-called two-hole resonance of the Cini model [34, 35].

The method we adopt to evaluate ab initio the Coulomb interactions is basically the one first proposed in Ref. [134]. One computes total energies for the system with N, $N-1$ and $N-2$ electrons by DFT calculations with constrained occupations for $N-q$ electrons, with q small (typically, up to 0.05), so that periodic systems can be treated in rather small supercells. From Janak's theorem [142] we know that:

$$\frac{\partial E}{\partial n_i} = \varepsilon_i(n_i), \tag{4.11}$$

where E represents the total energy of the system, while ε_i and n_i describe respectively the energy of the single particle orbital i and its occupation number. Subtracting an amount of charge q_i from this orbital for the case of a system made up of N electrons, Eq.(4.11) gives:

$$\begin{aligned} E_{fin} - E_{in} &= \int_N^{N-q_i} dE = E(N-q_i) - E(N) \\ &= -\int_0^{q_i} \varepsilon_i(1-q_i)dq_i, \end{aligned} \tag{4.12}$$

where in this work we use for ε_i the Kohn-Sham (KS) eigenvalue of level i.

To write the previous equations we made use of: $n_i = 1 - q_i$.

We make now the assumption that the explicit expression of Eq.(4.12) can be well reproduced by a power expansion in q_i truncated to third order [137, 138]:

$$E(N-q_i) = E(N) + A_i q_i + B_i q_i^2 + C_i q_i^3, \tag{4.13}$$

with coefficients A_i, B_i and $C_i \geq 0$. In the following we will assume that this can be extended to finite values of q_i. To be valid Eq.(4.13) needs that:

$$\varepsilon_i(1-q_i) = -[A_i + 2B_i q_i + 3C_i q_i^2]. \tag{4.14}$$

From XPS (X-ray Photoemission Spectroscopy) experiments we know also that:

$$\hbar\omega - E_{kin} = E_{N-1} - E_N = \varepsilon_i^{XPS}, \tag{4.15}$$

where ε_i^{XPS} is the binding energy of an electron which has been removed from the single particle orbital i because of the absorption of impinging photons with energy $\hbar\omega$. The assumption contained in Eq.(4.13) allows to write this energy also as:

$$E(N-1) - E(N) = A_i + B_i + C_i, \tag{4.16}$$

which can be expressed in terms of ε_i as:

$$\varepsilon_i^{XPS} = -\varepsilon_i(1-q_i)\big|_{q_i=0} + B_i + C_i. \tag{4.17}$$

The coefficients A_i, B_i and C_i (where i labels the core and valence level involved in the transition) are in this framework all what is needed to compute the Auger electron energies. They can be evaluated in two equivalent ways, whichever is most convenient: by taking the first, the second and the third derivatives of the total energy $E(N-q_i)$ for $q_i \longrightarrow 0$; by using Janak's theorem [142] and computing the KS eigenvalue of level i and its first and second derivatives.

As it can be seen from Eq.(4.17) the term $B_i + C_i$ acts like a correction to the (-) KS eigenvalue, ε_i, of level i accounting for dynamical relaxation effects.

In the following we describe the procedure allowing us to calculate the screening interaction U for CVV transitions in terms of A_i, B_i and C_i parameters.
Let us consider for the moment the case of spherically symmetric holes (non-spherical contributions, giving rise to multiplet splitting, will then be added). Such spherical interaction, U_{sph}, can be determined, similarly to the interaction energy for two holes in a valence level, as:

$$U_{sph} = [E(N-2) - E(N)] - 2[E(N-1) - E(N)] = 2B_v + 6C_v, \tag{4.18}$$

where for the last identity we made use of Eq.(4.13).

To complete the U calculation, non-spherical contributions, which give rise to multiplet splitting, are then added to U_{sph}. For Cu and Zn, as well as other materials, these terms are well reproduced by atomic Coulomb integrals usually written as $a_2F^2 + a_4F^4$ [143] - as demonstrated in [133] (notice that the spherical Coulomb interaction F^0 is embedded into U_{sph}).

The problem of U evaluation translates this way to the calculation of the A_i, B_i and C_i coefficients. This task for the case of localized states poses no additional difficulty. Care instead must be taken when determining those corresponding to the delocalized valence shells of bulk materials. To this end we propose the following methodology. For the case of valence bands ($\Longrightarrow i = v$) A_v is a continuous function of the quantum number v and, by taking advantage from Janak's theorem, it is simply the band energy. To estimate B_v and C_v, we neglect A_v dependence on v and assume that a single value can be taken across the valence band acting as a rigid shift of the latter. We expect this to be a good approximation as long as the valence band is sufficiently narrow. Still under this simplification, the direct evaluation of B_v and C_v would ask for constraining the occupations for fairly delocalized states, which is a practicable but uneasy task. As an alternative, we suggest a simpler approach based on the

working hypothesis that the environment contribution to the screening of the positive charge q_i in Eq.(4.13) does not depend strongly on the spacial distribution of the latter. Practically, we take the neutral isolated atom as a reference configuration, and evaluate the corresponding coefficients B_i^a and C_i^a . The two quantities $\Delta B = B_i - B_i^a$ and $\Delta C = C_i - C_i^a$ can be easily computed for core levels. We found that such bulk-atom corrections are almost independent on the core level, supporting the above hypothesis, and enabling us to use them to estimate the expansion factors in the valence as:

$$B_\nu = B_\nu^a + \Delta B, \tag{4.19}$$

$$C_\nu = C_\nu^a + \Delta C. \tag{4.20}$$

Summarizing, one has:

$$U = 2B_\nu^a + 6C_\nu^a + 2\Delta B + 6\Delta C + a_2F^2 + a_4F^4. \tag{4.21}$$

It is customary to write $U = F - R$, where $F = F^0 + a_2F^2 + a_4F^4$, and R is the "relaxation energy" [144]. This can be further decomposed into an atomic and an extra-atomic contribution [126], $R = R_a + R_e$. R_a stems from a static relaxation energy, which takes into account the effect of the relaxation of the other passive electrons toward the first created valence hole. R_e is instead an additional extra-atomic relaxation energy arising from electronic relaxation toward the valence band hole from the surrounding lattice. From Eq.(4.21), one identifies $R_a = F^0 - 2B_\nu^a - 6C_\nu^a$ and $R_e = -2\Delta B - 6\Delta C$. It is worth to note that our approach computes as a unique term $F^0 - R_a$, so that it is not possible to separate the two contributions.

Computational details

The results that will be presented in the following sections have been obtained by DFT calculations with the Perdew-Burke-Ernzerhof [145] generalized gradient approximation for the exchange and correlation functional. We used an all-electron augmented-planewave code to perform the simulations with constrained core occupations. Periodically repeated supercells at the experimental lattice constants were adopted to describe the solids. One atom was ionized in a four-atoms and an eight-atoms unit cell for Cu and Zn, respectively. In both cases the ionized atom has no ionized nearest neighbours. Test calculations were also performed

by ionizing all atoms in the cell: this resulted in almost identical A values, while B was generally overestimated by about 1 eV.

The spin-orbit splitting in core states has been taken into account by adding the corresponding energy shift, as quoted by NIST for free atoms [141], to the values of A_c we computed. Spin-orbit interaction in the valence shell has been also considered and the results gained for the corresponding Auger spectrum will be discussed, together with the used parameters, in the following section.

As for the coefficients A, B and C in Eq.(4.13), the values obtained from a second order expansion of the eigenvalues proved to be more numerically stable with respect to convergence parameters than those from a third order expansion of the total energy. Therefore, we made use of Janak's theorem and evaluated A, B and C by fitting the DFT eigenvalues for $N - q$ electrons, with q from 0 to 0.05 at intervals of 0.01. Fulfillment of Janak's theorem was numerically verified to high accuracy in a few selected cases.

4.2.2 Discussion

Table 4.2 collects our results for the A, B and C coefficients [see Eqs.(4.13) and (4.19-4.20)], to be used for the determination of the $L_{23}M_{45}M_{45}$ line shape of Cu and Zn. As for the M_{45} values, for our estimate of the average XPS energy we indicate by $A_{M_{45}}$ the weighted average of the KS eigenvalue of the $3d$ band (with opposite sign). The values of $B_{M_{45}}$ and $C_{M_{45}}$ are instead obtained according to Eqs.(4.19-4.20), as explained above. To this purpose, we determined the bulk-atom correction, ΔB, as the average of the difference $B_i - B_i^a$ across the $1s$-$3p$ core levels (analogous for ΔC). The results gained in this way are shown in Table 4.2. As anticipated, such values are almost independent on the core level, justifying our hypothesis that the environment contribution to the screening properties only mildly depends on the spacial distribution of the perturbation charge.

Both ΔB and ΔC are negative, $\Delta B = -4.85(-4.23)$ eV and $\Delta C = -0.81(-0.35)$ eV for Cu (Zn), since the interaction amongst the two holes is more effectively screened in the solid. Table 4.2 also reports the comparison between the XPS excitation energies, evaluated by virtue of Eq. (4.17), and the corresponding experimental values. Notice that bare KS excitations energies can be 30 eV off the experimental value, but the addition of B and C accounts properly for the missing relaxation energy: evaluated core excitation energies fall within 1 eV of experimental values.

Fig.(4.6) shows our results for the $3d$ components of the 1hDOS, $d(\omega)$, for Cu and Zn

	Level	A^a	B^a	C^a	A	B	C	E^{XPS}	Exp.
Cu	L_2	930.17	27.74	1.25	928.40	22.84	0.43	951.67	952.0
	L_3	909.81	27.74	1.25	908.04	22.84	0.43	931.31	932.2
	M_{45}	5.04	5.72	0.91	2.86	0.87	0.10	3.84	3.1
Zn	L_2	1019.40	30.44	1.08	1016.98	26.17	0.82	1043.97	1044.0
	L_3	995.69	30.44	1.08	993.27	26.17	0.82	1020.26	1020.9
	M_{45}	10.14	7.06	0.77	7.53	2.82	0.42	10.78	9.9

Table 4.2. This table reports the values of the coefficients for the expansion of the total energy as a function of the number of electrons, $E(N-q_i)$, when a charge q_i is removed from level i [137, 138]. The considered coefficients are both the atomic (A^a,B^a,C^a) and the bulk (A,B,C) ones for Cu (green values) and Zn (blue values). By $A_{M_{45}}$ we indicate the weighted average of the KS eigenvalue of the $3d$ band, with opposite sign; $B_{M_{45}}$ and $C_{M_{45}}$ are obtained according to Eqs.(4.19-4.20). All the values shown in the table are in eV.

as obtained by DFT calculations. The average DOS (shaded area in the figure), $\overline{d}(\omega) = \frac{1}{2(2l+1)} Tr[d(\omega)]$, is also shown. All the reported patterns have been shifted by $B_v + C_v$ to account for relaxation effects.

The $L_{23}M_{45}M_{45}$ Auger spectrum has been then calculated according to Eqs.(4.9-4.10). The result is shown in Fig.(4.7). To perform these calculations for both Zinc and Copper the Auger matrix elements have been taken from [133], while all the calculated patterns have been convoluted with a lorentzian curve having an FWHM (Full Width at Half Maximum) equal to the parent core-hole life time [146]. Each panel shows the superimposition between the $L_{23}VV$ Auger spectra evaluated both considering (curve with a grey filled area) and not (curve with a black filled area) spin orbit coupling effects. As it can be seen from the figure curves containing or not spin orbit coupling are quite undistinguishable for the considered case. Notwithstanding this finding, the general procedure we set up with this work will be a precious instrument for studying CVV Auger spectra from heavier materials at least. The position of peaks in the calculated spectra gives also important information about the reliability of the theory we formulated to evaluate ab initio Coulomb interactions. To analyze these results, let us focus on the principal peak (^1G) in each spectrum, which can be associated with the absolute position of the multiplet [6].

First we notice that the agreement with the experimental values [133] (see the vertical dashed line for the principal peak in both panels of Fig.(4.7)), as far as the position of this

[6]The internal structure of the multiplet in our description only depends on the values of F^2 and F^4 which, as previously specified, we took from the literature.

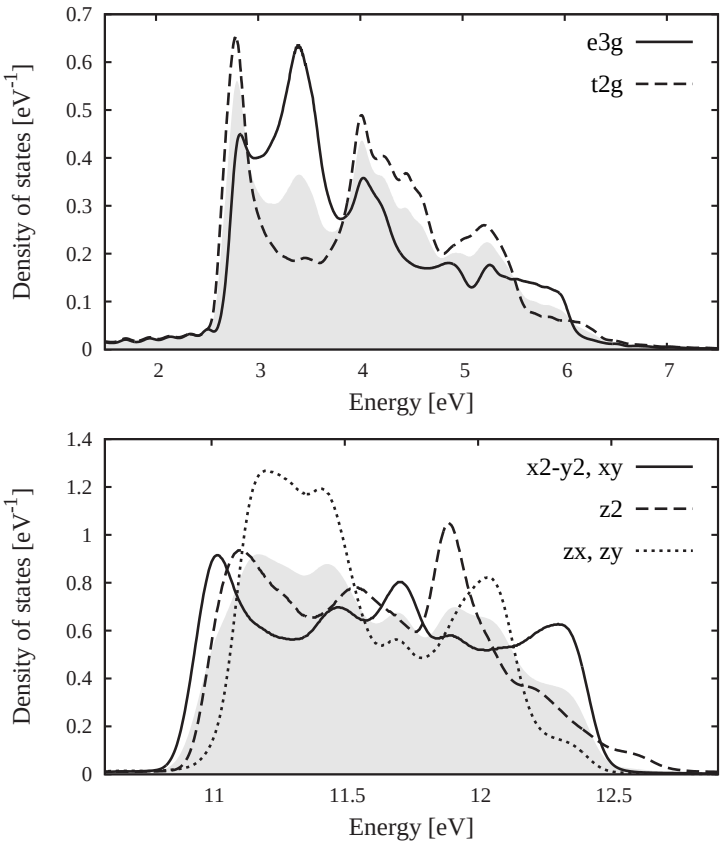

Figure 4.6. *Top and bottom panels show the $3d$ components of the 1hLDOS respectively for bulk Zinc and Copper [137, 138]. One-hole density area represents instead the average density of states, $\bar{d}(\omega) = \frac{1}{2(2l+1)} Tr[d(\omega)]$.*

		ε_c	$-2\varepsilon_v$	$-U^{^1G}$	$\omega^{^1G}$
Cu	Theory	931.31	-7.67	-3.34	920.29
	Exp.	932.2	-6.2	-8.0	918.0
	Diff.	-0.9	-1.5	4.7	2.3
Zn	Theory	1020.26	-21.55	-9.26	989.45
	Exp.	1020.9	-19.8	-9.5	991.5
	Diff	-0.6	-1.8	0.2	-2.1

Table 4.3. *Decomposition of the ^1G L_3VV Auger kinetic energy into its contributions, according to Eq.(4.22). Values corresponding to "Theory" have been obtained by using the present work [137, 138, 152], while the experimental ones ("Experiment") come from [133].*

peak is concerned, is rather good considering the absence of adjustable parameters in the theory. Our result for Cu overestimates the peak position by about 2 eV, while the one for Zn is underestimated by a slightly smaller amount. To have further insight into this comparison,

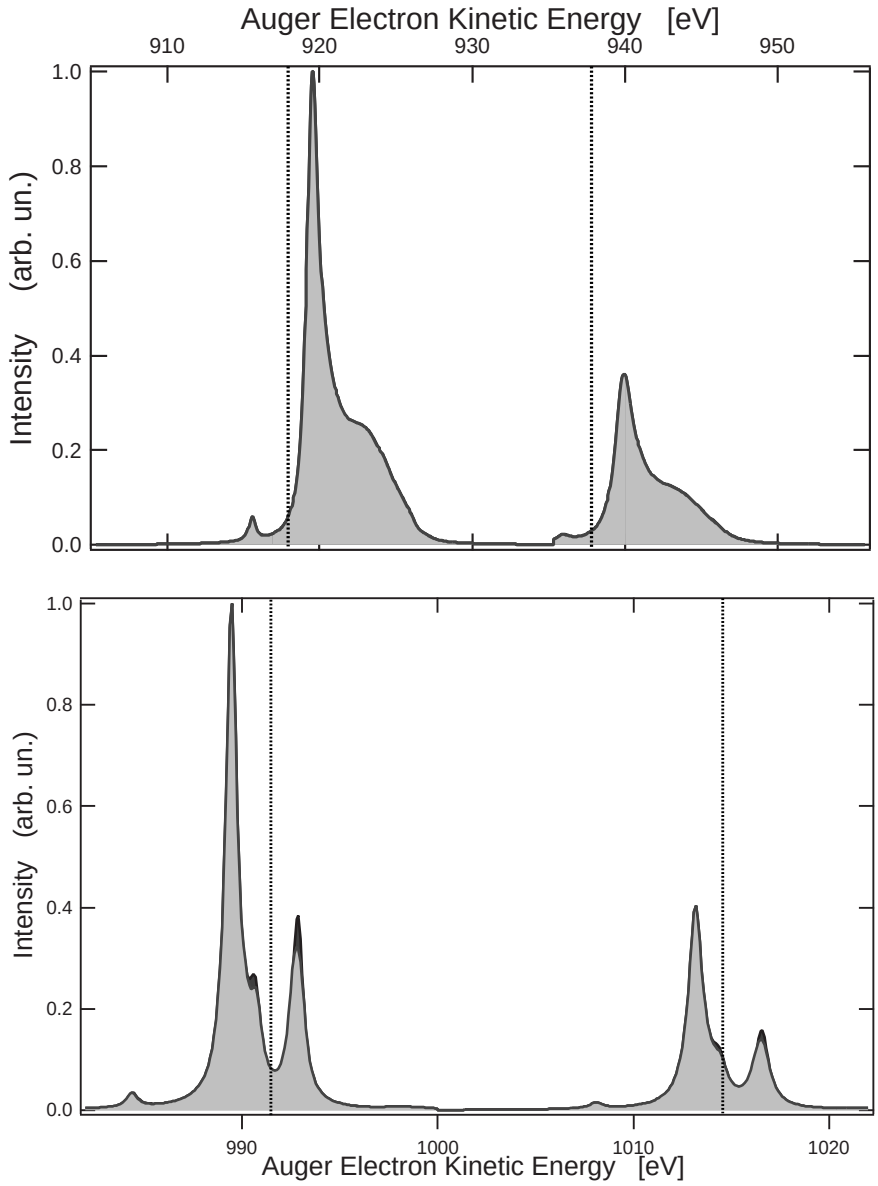

Figure 4.7. *Top and bottom panels display the comparison between the $L_{23}VV$ Auger spectra respectively for Copper and Zinc metals which have been calculated both considering (curve with a grey filled area) or not (curve with a black filled area) spin-orbit coupling effects. The dashed vertical lines represent the measured position of $^1G_4$ peak taken from [133]. As it can be seen from the figure the patterns with and without spin-orbit effects are superimposed for the case of copper (top panel), while for zinc (bottom panel) some little differences arise.*

we decomposed the Auger kinetic energy ω for the most most intense peak (the ^1G in the L_3VV part of the spectrum) into its contributions in Table 4.3 as:

$$\omega = \varepsilon_c - 2\varepsilon_v - U_{LS}. \tag{4.22}$$

We choose to perform this analysis on the most intense peak. Despite the fact that the overall agreement is similar in magnitude, it is important to realize that this finding has different origins. In both metals, we underestimate slightly the core photoemission energy and overestimate the valence ones.

As it can be seen from Fig.(4.7) and Table 4.3 our methodology provides an agreement with experimental photoemission energies of the order of 1 eV and of 2 eV for Auger energies. We consider this a rather good result, as a starting point, considering the absence of adjustable parameters in the model which is the novelty of our approach for CVV transitions in correlated systems. Of course, a much better agreement would be obtained by inserting phenomenological parameters, but at the cost of loosing predictive power. As for the internal structure of the line shape, i.e., the multiplet splitting, this is given very precisely. However, let us remember that a first-principles treatment of the latter is not a novelty of our approach, which is indeed based for this aspect on atomic results available in the literature since decades. Let us instead focus again on the estimated position of the multiplet, which crucially depend on the parameters evaluated by our ab initio method. Even if the magnitude of the agreement with the experiment is similar, the results for Zn are much better than those for Cu. In Zn, the $3d$ band is deep and narrow, and electronic states bear most of their atomic character. Their hybridization with the states closer to the Fermi level, which mostly contribute to the screening, is limited, similarly somehow to what happens for core states. Consequently, our approximations which transfer the values of ΔB and ΔC from the core states to the valence ones produces very good results. In Cu, instead, the $3d$ band is higher and broader, and hybridizes significantly with the s-like wavefunctions operating the screening. Our approximations turn out to be rather poor, since the resulting U is about half the one derived from experiments.

We have also shown that the inclusion of a cubic term in the expansion of the total energy with respect to a hole charge proves to be quite important. This term has a limited impact on photoemission energies, for which its factor C is counted only once, but it is summed six times to get U. Our very good agreement for the value of U in Zn crucially depend on C: neglecting such cubic term, our estimate of U would be 2.52 eV lower. We remind that this is

meant to adopt for our model the interaction parameter U as the curvature in the systems with $N-1$ electrons rather than in the neutral ground state. This seems naturally a better choice as we are interested in energy differences amongst the $N-2$ and the N electrons system. The purpose of this work has been to keep the treatment as simple as possible. We now briefly mention possible refinements and extensions, which could be the subject of future investigations. One possible improvement could be avoiding the assumptions behind Eqs. (4.19-4.20), which enter in two distinct aspects concerning the photoemission energies and the interaction between the two holes in the final state, respectively. Firstly DFT-GW [147] calculations of the 1hDOS could be used to compute the 1hDOSs accounting for relaxation energies. Results available in literature for Cu [148] are very promising in that sense. It is interesting to notice that the factor $B+C$ plays the role of a self-energy expectation value, and that the use of a single value of $B+C$ to shift rigidly the band is formally analogous to the scissor operator often adopted to avoid expensive self-energy calculations. The accuracy of such rigid shifts for valence-band photoemission in Cu is discussed in [148].

Besides this, it would be interesting to use methods which are capable to compute the total energy in presence of holes in the valence state. The methodology presented in [149], in which the valence occupation is changed by means of Lagrange multipliers associated with the KS eigenvalues, could be a possibility worth to investigate. One should pay some attention in that some arbitrariness is anyway introduced, i.e., the value of U does depend on the chosen form of the valence wavefunctions, an arbitrariness which is compensated in LDA+U calculations [149].

As far as the used CS model is concerned, the role of interatomic (off-site) correlation effects has been to be considered (see Sec.2.3.2). Recent studies [123] shows off-site interaction magnitude in copper is not negligible. This suggests a further improvement to the present theory which is represented by the development of an ab-initio method to evaluate this quantity. Till today in fact it has been gained only by fitting experimental spectra (see Sec.2.3.2).

In order to treat systems with larger band width or smaller hole-hole interaction, it would be desirable to extend the methodology to treat simultaneously the dependence of the matrix elements on energy, and the interaction in the final state. This would enable releasing either the assumption that matrix elements equal the atomic ones or that particles are non-interacting. Such possibility is currently under investigation. Finally, it would probably take a long effort to release the assumption that the valence shell is closed, which is crucial to the CS model in its original form, here adopted. Efforts have been spent in this direction,

resulting in a formulation through more complicated three-hole Green's functions [81]. No ab-initio treatment in this direction is present to our knowledge and this work is devoted to provide one.

4.3 The KVV Auger spectra from HOPG Graphite and Carbon Nanotubes

Carbon nanostructures continue to be an intense field of fundamental and applied research because of the recent discoveries of several of their unusual properties, such as the observation of the anomalous integer quantum Hall effect in planar graphene [155, 156] or the intrinsic superconductivity in multiwall [157] and ultrasmall [158] carbon nanotubes at temperatures of respectively 12 and 15 K. Within this framework, the understanding of electronic correlations is fundamental and we need to achieve their quantitative measurement in these carbon nanostructures.

In this work we measured the KVV[7] Auger spectra of HOPG (Highly Oriented Pyrolitic Graphite) Graphite and carbon nanotubes and gave a theoretical explanation of the measured data [150, 151, 152]. This allowed to extract a sensible estimate of the on-site screened Coulomb repulsion in these materials, which is a key quantity since it enters as a parameter in realistic LDA+U calculations. A comparison between the KVV spectra from HOPG and POCO Graphite[8] [154] is also presented, showing qualitative differences between the corresponding Auger line shapes which calls for further studies. As far as the SWCNT (Single-Wall Carbon NanoTubes) are concerned, this work is particularly useful in throwing light on the magnitude of hole-hole interaction in these compounds: only few experimental data on these materials are found in literature till today and no theoretical work introducing Coulomb repulsion is available.

4.3.1 The Experiment

Here we only sum up the fundamental steps needed to prepare and characterize the SWCNT samples which were adopted in the proposed experiment, while deferring a more detailed

[7]The transition of interest involves the creation of a $1s$ deep hole, which then decays through an Auger process leading to a final state with two holes in the sample valence band.

[8]The KVV Auger line shape of POCO Graphite has been measured several years ago [153]. Here we wish to improve over that theoretical analysis that was based on three fit parameters and neglected multiplet effects.

treatment to a dedicated issue [160].

As a starting point the SWCNT were synthesized by ablating a CoNi-doped Graphite target using a pulsed Nd:YAG laser in a superimposed pulse configuration [159]. Raman spectroscopy indicated that the tube is single-walled, characterized by a low degree of defects and with diameters of 1.2-1.3 nm [159]. This is consistent with Transmission Electron Microscopy (TEM) observations that, though showing tubes aggregated in bundles of various dimensions and twisting, allowed us to measure a tube diameter of (1.2±0.1) nm through a statistical analysis [160]. Moreover electron energy loss spectroscopy performed by means of the TEM apparatus directly on SWCNT bundles at the Co and Ni $L_{2,3}$ edges did not detect any traces of these catalysts [160]. The SWCNT samples were then obtained by diluting a droplet of the synthesis product in isopropyl alcohol and dispersing on a metallic surface.

As far as the HOPG Graphite is concerned, a freshly cleaved sample was used for measuring the KVV Auger features. The Auger spectra were acquired using a $K\alpha$ (1486.6 eV) X-ray source with a resolution of about 1 eV. Fig.(4.8) shows the comparison between the obtained experimental spectra from HOPG Graphite (red solid line) and SWCNTs (black line) after the subtraction of secondary electron background. These patterns display clear differences especially in the width and position of the main structure centered at approximately 260 and 264 eV, while instead both of them show a peak placed at 240 eV.

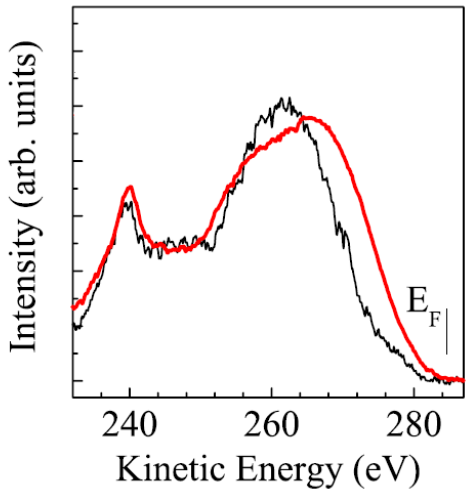

Figure 4.8. *Comparison between the experimental KVV Auger line shape from HOPG Graphite (bold red curve) and SWCNTs (black pattern) [150, 151, 152].*

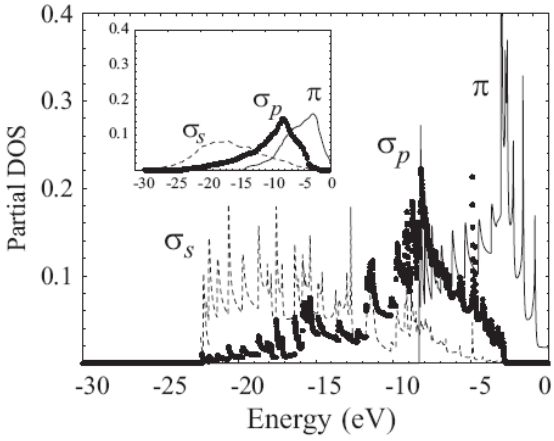

Figure 4.9. *One-particle partial DOS of (10,10) SWCNTs (diameter close to 1.3 nm) o[150, 151, 152] btained by the tight banding method of Ref.[161]. The inset shows the same quantity from Graphite as taken from [153]. The Fermi level corresponds to the x-axis origin and the antibonding part is not displayed.*

4.3.2 The Model

The experimental patterns have been modeled by using again the CS theory from closed bands materials we described previously (see Sec.2.3.1) but with some modifications so as to better adapt it to the considered materials [150, 151, 152]. The theoretical study of Auger spectra from HOPG and SWCNTs is indeed far from straightforward because the σ and π bands are half filled. However in these systems some special features allow the use of closed-band theory with slight but crucial modifications.

As it can be seen from Fig.(4.9), where the calculated single-particle density of states for Graphite and SWCNTs are displayed, the 1hLDOS is largely suppressed in proximity of the Fermi level, so that screening is not very efficient. This would imply only a static renormalization of the bare atomic Coulomb interaction term, which is used in the CS theory. Besides this it is worth noticing that the bonding portion of the $\sigma_{s,p}$ bands is separated by several eV from the corresponding antibonding part located above the Fermi level. As long as such a separation is larger than the effective interaction, one can treat the band as if it was closed, thus justifying the CS approach. The situation is different for the π band whose bonding and antibonding portions are separated by a very small energy region. Here the CS theory cannot be used without appropriate modifications: in this case in fact the contribution to the Auger spectrum originating from π and mixed $\pi - \sigma$ holes would be strongly influenced by open band effects. It is also expected that such a region should reveal the main differences between the HOPG and SWCNT spectra. This conjecture seems to be confirmed by the experimental data. The two measured patterns show in fact clear differences properly in the π and mixed $\pi - \sigma$ portions of the spectra (i.e. $\omega \geq 250$ eV), while in the σ_s region (i.e. $\omega \leq 250$ eV) the SWCNT and HOPG spectra are quite similar. In particular for $250 \leq \omega \leq 280$ eV the SWCNT line shape is narrower with vanishing and much weaker intensity near the Fermi energy as compared to the one for Graphite. This fits well with a scenario where the screening properties of π electrons are less efficient in SWCNTs.

The previous arguments authorize us to apply the CS theory for modeling the measured KVV Auger line shapes [150, 151, 152]. As it will be shown in the following some modifications to this approach have been used with the aim of better taking into account the described effects produced by the behavior of the π band. Within this model, which makes use of a two step approach to represent the photoemission and the following Auger decay, the Auger current can be written as Eq.(2.17):

$$S(\omega) \propto \sum_{\alpha_1,\alpha_2,\alpha_3,\alpha_4,\sigma} A^*_{\alpha_1,\alpha_2}(\overrightarrow{k}) D_{\alpha_1,\alpha_2,\alpha_3,\alpha_4,\sigma}(\omega) A_{\alpha_3,\alpha_4}(\overrightarrow{k}), \tag{4.23}$$

where α_i denote all the single particle valence orbitals available in the solid, while A_{α_i,α_j} and $A^*_{\alpha_i,\alpha_j}$ are the Auger matrix elements and their hermitian conjugates evaluated when the two final valence holes are produced in the α_i and α_j orbitals. $D_{\alpha_1,\alpha_2,\alpha_3,\alpha_4,\sigma}(\omega)$ is as usual the interacting two particles LDOS, which can be gained as the anti-hermitian part of the corresponding correlated Green's function $G_{\alpha_1,\alpha_2,\alpha_3,\alpha_4,\sigma}(\omega)$. This one can be evaluated by the matrix Dyson equation [163]:

$$\widehat{G}_\sigma(\omega) = \widehat{G}^{(0)}_\sigma(\omega)[1 + U_\sigma \widehat{G}^{(0)}_\sigma(\omega)]^{-1}, \tag{4.24}$$

in which U is the matrix of screened on-site repulsion for valence states, while $\widehat{G}^{(0)}_\sigma(\omega)$ represents the two holes non interacting Green's function matrix when one of the two final holes has spin σ [9]. $\widehat{G}^{(0)}_\sigma(\omega)$ can be collected building up firstly its anti-hermitian part by means of the simple convolutions of 1hLDOS, which were evaluated for each kind of valence states. In the case of HOPG we made use of the DOS coming from [162], which have been taken from experiments. The single particle LDOS for SWCNTs instead have been obtained by performing a tight binding calculation, where both $2s$ and $2p$ orbitals were included but neglecting overlap integrals for semplicity. The results of these calculations for the bonding part of the 1hLDOS of a typical (10,10) armchair nanotube with diameter close to 1.3 nm are plotted in Fig.(4.9) together with the LDOS of HOPG. The remaining part of $\widehat{G}^{(0)}_\sigma(\omega)$ can then be easily obtained by Hilbert transforming the corresponding non interacting two holes LDOS.

As far as the Auger matrix elements are concerned, we used both for HOPG and SWCNT the spin-independent values A_{ssss}=0.8, A_{sspp}=0.5 and A_{pppp}=1.0, which have been obtained from atomic calculations [162].

To gain the theoretical Auger line shape the last ingredient which is left to evaluate is the hole-hole Coulomb interaction. The evaluation of U starting from its atomic bare value U^b:

$$U^b_{\alpha_1,\alpha_2,\alpha_3,\alpha_4,\sigma} = \langle v | c_{\alpha_1,\uparrow} c_{\alpha_2,\sigma} | \frac{e^2}{r} | c^+_{\alpha_3,\uparrow} c^+_{\alpha_4,\sigma} | v \rangle \tag{4.25}$$

[9] The other hole is supposed to have spin $\uparrow$. This does not reduce the generality of the adopted treatment.

is generally a delicate task and in particular in this work we have to properly introduce the previously described effects on the π band of HOPG and SWCNT so as to make the CS theory still a good starting point for a description of the measured spectra, notwithstanding the fact we are no more in the closed band case.
Within the closed band theory, the Auger spectrum is obtained by taking the Auger matrix elements and the on-site interactions from atomic calculations which neglect solid state effects. On this basis one introduces the static screening operated by the closed-band system simply by shifting all the $F^0(i,j)$ Slater integrals [164] that contribute to U^b of the same amount representing the screening energy Δ[10]: $F^0(i,j) \rightarrow F^0(i,j) - \Delta$. Δ can be taken as the unique free fitting parameter of the theory or alternatively it can also be estimated within the Random Phase Approximation (RPA) or ab initio methods [149]. A further shift in the Coulomb interaction has to be added to take into account also the effect of the off-site interaction (see Sec.2.3.2).
To introduce the open band effects in this approach, we made use of orbital dependent *form factors* $f_{\alpha_1,\alpha_2,\alpha_3,\alpha_4}$ [150, 151, 152], which can be justified on the basis of the following phenomenological arguments. These quantities have to be used to correct all the ingredients appearing in the CS theory which measure local properties. Therefore both the effective on-site repulsions, $U_{\alpha_1,\alpha_2,\alpha_3,\alpha_4,\sigma}$ (where F^0 has been already rescaled by Δ), and the Auger matrix elements A_{α_i,α_j} will be corrected by a common multiplying factor $f_{\alpha_1,\alpha_2,\alpha_3,\alpha_4}$, where in our case the α_i states are the σ_s, σ_x, σ_y and π orbitals. The form factor f takes into account the fact that the $2s$ states of carbon behave as atomic orbitals, while the $2p$ ones are delocalized in the lattice and can use only a half of the total σ_p and π states to form occupied localized states because the p bands are half-filled. In this way three independent form factors appear which correspond to the cases where the quartet $\{\alpha_1,\alpha_2,\alpha_3,\alpha_4\}$ is made up of:

1. four σ_s orbitals;
2. two σ_s and two $\sigma_{x,y}$, π orbitals;
3. four $\sigma_{x,y}$, π orbitals.

According to the above discussion the three independent form factors were estimated to be $f_{ssss} \approx 1$, $f_{sspp} \approx 1/2$ and $f_{pppp} \approx 1/4$. In the following we will show that this

[10]This quantity has the same origin and meaning of the homonym screening energy described in Sec.4.1.3

choice works quite well in the case of HOPG, while we need $f_{pppp} \approx 1/2$ to reproduce the Auger spectrum of nanotubes, whose reason may be due to the nanotubes geometry which constraints the holes. It is worthwhile to note that the analysis performed in [165] does not apply to p holes and in fact no shift is seen in this case (presumably the pairs extend further than a nearest neighbor distance).

The bare (atomic) on-site Coulomb repulsions were obtained by appropriate combinations of the Slater integrals $F^{(0,2)}(i,j)$ and $G^{(1)}(i,j)$ found in literature [166]. In particular the used values for the independent bare interactions are reported in Table 4.4.

$U^b_{ssss\downarrow}$	$U^b_{sxsx\downarrow}$	$U^b_{sxxs\downarrow}$	$U^b_{\pi\pi\pi\pi\downarrow}$	$U^b_{xx\pi\pi\downarrow}$
15.5	15.0	1.5	14.6	-0.1
$U^b_{x\pi x\pi\downarrow}$	$U^b_{x\pi\pi x\downarrow}$	$U^b_{ssxx\downarrow}$	$U^b_{sxsx\uparrow}$	$U^b_{x\pi x\pi\uparrow}$
13.9	0.8	11.9	13.1	13.1

Table 4.4. *On-site hole-hole Coulomb bare interactions calculated by using the Slater integrals $F^{(0,2)}(i,j)$ and $G^{(1)}(i,j)$ found in literature [166].*

As discussed above, these values have to be shifted so as to include the screening effect through the constant Δ, which represents the only free fitting parameter of the theory and has to be subtracted to the $F^{(0)}(i,j)$ Slater integrals. Then to gain the Auger current, the resulting U and A matrix were multiplied by the f form factors.

The theoretical spectra of HOPG and SWCNTs were computed by solving a 16×16 matrix problem for $\sigma = \downarrow$ and a 6×6 one for the opposite spin, as it is shown in Eq.(4.24). The spectra shown in Fig.(4.10) have been obtained by applying the aforementioned theory and for a screening constant value equal to 6.0 and 5.5 eV respectively for HOPG and SWCNTs, which yielded the best fits. As it can be seen from the figure the agreement between theory and experiment is quite good and is particularly satisfactory for Graphite.

4.3.3 Discussion

The approach adopted to model the HOPG and SWCNTs Auger spectra allowed us to determine the most relevant parameter of the used model, that is the screened on site repulsion between $2p$ states. The values gained for Δ by a procedure of best fit yielded $U_{pppp} = 2.1$ eV for HOPG and $U_{pppp} = 4.6$ eV for SWCNTs, which allow to understand the lack of features near the Fermi level for SWCNTs, making their Auger spectrum more symmetric and narrower than that of HOPG. This is understood by looking at Fig.(4.9.b) , which shows

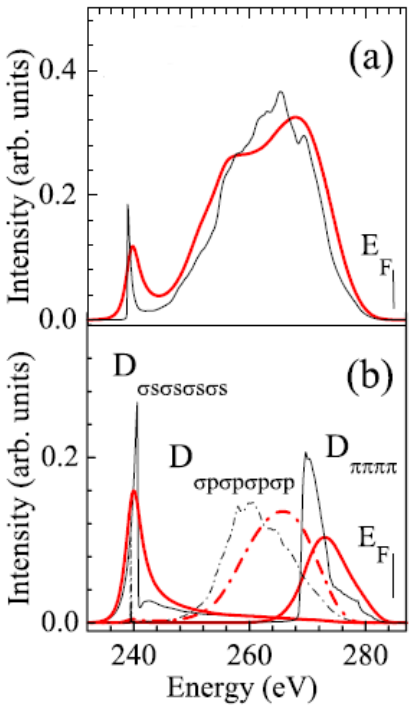

Figure 4.10. *[150, 151, 152]. Panel (a) shows the theoretical line shape (calculated by using Eq.(4.23)) from HOPG (bold red solid line) and SWCNTs (black curve) samples. Panel (b) displays instead the diagonal contributions to the interacting 2hLDOS for HOPG (bold red line) and SWCNTs (black pattern), where the two valence holes have the same simmetry. The $D_{\sigma_p,\sigma_p,\sigma_p,\sigma_p}$ contribution has to be understood as the sum of the $D_{\sigma_x,\sigma_x,\sigma_x,\sigma_x}$ and $D_{\sigma_y,\sigma_y,\sigma_y,\sigma_y}$ ones. In both panels the x-axis represents the Auger electron kinetic energy in eV, where the reported position of the Fermi level, E_F, has been obtained by shifting the position of the Fermi level of Fig.(4.9) by the binding energy of the $1s$ core hole, 284.6 eV.*

the diagonal contributions of the interacting DOS where the valence holes were taken in the same state. The off-diagonal contributions are not shown for the sake of clarity but are essential to reproduce the experimental spectra.

Concerning the line shape, the most striking feature is the narrow structure at 240 eV, which also appears as a shoulder in experimental spectra gained by Houston and coworkers [162]. In their work they assigned this structure to a plasmon replica of the main structure at 265 eV, attributing its origin to a plasmon of energy ω_p=27 eV. Instead, we interpreted the narrow structure as due to a quasi-two holes resonance produced by two σ_s Auger holes. This is consistent with the predicted values of screened on-site repulsion between σ_s holes which are $U_{ssss} = 9.5$ eV and 10.0 eV respectively for HOPG and SWCNTs. The non interacting $D^{(0)}_{ssss}(\omega)$ in fact has a maximum at ε_s=252 eV for Graphite and 251 eV for the nanotubes and therefore a narrow structure at about $\varepsilon_s - U_{ssss} \approx 241$ eV is correctly expected. The fact that a full split off resonance has not been observed in this case is due to σ_s bandwidth which is about 20 eV. This does not prevent the formation of a strongly distorted band-like behavior.

Another important finding of this work is the observation of a very small dependence of the observed correlation in SWCNTs on the nanotube diameter. The Auger spectrum

from a sample consisting of SWCNTs with average diameter of 2 nm in fact does not show significant changes with respect to that one reported in Fig.(4.8). Moreover by performing a similar theoretical analysis on a (20,20) SWCNT, no substantial changes were found for the values of correlation interaction.

In conclusion the line shape of the KVV Auger spectra for Graphite and SWCNTs has been interpreted in terms of a modified CS approach by using a single fitting parameter that is the screening on-site interaction Δ. The U_{pppp} Coulomb repulsion resulted to be doubled passing from HOPG to SWCNTs. This explains the sizeable shift of the SWCNT Auger main feature towards higher kinetic energies respect to the center of the HOPG one. This increase in the U_{pppp} is consistent with the theoretical prediction of the enhancement of the superconductive critical temperature recently observed [167] in carbon nanotubes.

4.4 The First Application of TDGA to High T_c Superconductors

The aim of this section is to throw some light on the problem of CVV Auger transition from open band materials through the application of a time dependent approach, the Gutzwiller Approximation (GA), and the comparison between its results and the BLA (Bare Ladder Approximation) ones [180].

The first step to fulfil this task consists in extending the Sawatzky approach [36] to a three band case, which was initially devised to explain the CVV Auger transitions from a single closed band (see Chapt.2). The need for this development comes from our choice of modeling CVV decays from CuO_2 planes as a first test-bed for the theory. These planes are characteristic of high T_c superconductors[11]. Since their first discovery in 1986 [168], these compounds have been the subject of intense research for their quite unusual features and behaviour [2] but no theory to date gained a general acceptance.

A major proposal, which is being investigated (see [2] for a review), relates their properties to electronic correlation. Since Auger spectroscopy is the optimal approach for this kind of interaction, the study of CVV Auger transition from these compounds appears to be promising to gain a deeper understanding.

[11] Indeed, a superconducting compound is said to belong to the family of high T_c superconductors only if it has CuO_2 planes [2]

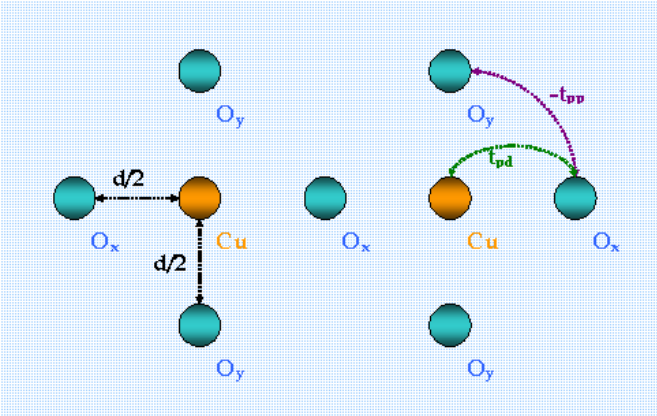

Figure 4.11. *Schematic representation of the atoms disposition in the considered cluster for CuO_2 planes. As it can be seen from the figure the nearest neighbours distance between Copper and Oxygen is always $d/2$ both in the x and in the y directions. In the text we refer to two types of oxygens, labeled as O_x and O_y, whose meaning is only to help the reader to keep in mind their position respect to the Cu site.*

4.4.1 The Model

This section contains a detailed description of the adopted model [180]. As previously stated the test-system to which this approach has been applied is a CuO_2 plane. To describe it, the plane has been subdivided in primitive cells. Each one of them is made up of a single Copper and two Oxygen atoms, which will be labeled as O_x and O_y to indicate their position respect to the Cu site, as it is shown in Fig.(4.11).

Taking this last one as the origin of our coordinate axis, O_x and O_y are placed in fact at a $d/2$ distance (where d is the lattice parameter) from the origin, respectively in the x and y directions. For each atom within each primitive cell we considered only one available orbital for the active holes involved in the Auger transition ($d_{x^2-y^2}$ for Copper and one p orbital per Oxygen): this gives rise to three energy bands. Two of them are fully occupied by electrons, while the remaining one is taken to be half filled. This corresponds to the antiferromagnetic phase, while superconducting phases are obtained by electron doping and by hole doping.

An Hubbard-like Hamiltonian has been adopted and splitted as:

$$\widehat{H} = \widehat{H}_0 + \widehat{H}_1 \tag{4.26}$$

where $\widehat{H}_0$ represents the kinetic term, that is the core hole and the ordinary hole band energies.

Correlation effects are included only through $\widehat{H}_1$, which is the Coulomb interaction between the two holes when both of them are localized on the copper atom or on one of the two “types” of oxygen:

$$\widehat{H}_1 = U_{dd} \sum_i n_{d_i\uparrow} n_{d_i\downarrow} + U_{pp} \sum_i (n_{p_{x_i}\uparrow} n_{p_{x_i}\downarrow} + n_{p_{y_i}\uparrow} n_{p_{y_i}\downarrow}). \tag{4.27}$$

Here summations run over each single atom but they can be understood also as summations on cells, properly because in each cell we have a single atom per chemical "species". The terms $n_{d_i\sigma}$, $n_{p_{x_i}\sigma}$ and $n_{p_{y_i}\sigma}$ represent the number operators for a hole created with spin σ respectively on the d shell of copper or on the p shell of one of the two types of oxygens, O_x and O_y, inside the same cell.

The interacting two holes Green's function matrix element between Cu sites can be labeled as:

$$G^{dd}_{mn}(\omega) = \langle dd,m| \frac{1}{\omega - \widehat{H} + i\delta} |dd,n\rangle. \tag{4.28}$$

The basis states represent hole pairs on the Copper d orbital in the nth and mth cell.

Starting from a Dyson-like equation:

$$\frac{1}{\omega - \widehat{H} + i\delta} = \frac{1}{\omega - \widehat{H}_0 + i\delta} + \frac{1}{\omega - \widehat{H}_0 + i\delta} \widehat{H}_1 \frac{1}{\omega - \widehat{H} + i\delta} \tag{4.29}$$

we can reach a system of coupled equations giving Eq.(4.28) in terms of all the other possible interacting and non interacting two holes Green's functions, which can be obtained projecting Eq.(4.29) on localized $|dd,i\rangle$ and $|pp,j\rangle$ states.

As an example we can build $G^{dd}_{mn}(\omega)$ closing Eq.(4.29) between $\langle dd,m|$ and $|dd,n\rangle$:

$$G^{dd}_{mn}(\omega) = g^{dd}_{mn}(\omega) + U_{dd} \sum_s g^{dd}_{ms}(\omega) G^{dd}_{sn}(\omega) + U_{pp} \sum_r g^{dp_x}_{mr}(\omega) G^{p_x d}_{rn}(\omega) + U_{pp} \sum_l g^{dp_y}_{ml}(\omega) G^{p_y d}_{ln}(\omega), \tag{4.30}$$

where:

$$\begin{aligned}
g^{dd}_{mn}(\omega) &= \langle dd,m| \frac{1}{\omega - H_0 + i\delta} |dd,n\rangle; \quad g^{dp_x}_{mn}(\omega) = \langle dd,m| \frac{1}{\omega - H_0 + i\delta} |p_x p_x,n\rangle; \\
g^{dp_y}_{mn}(\omega) &= \langle dd,m| \frac{1}{\omega - H_0 + i\delta} |p_y p_y,n\rangle; \quad G^{p_x d}_{rn}(\omega) = \langle p_x p_x,r| \frac{1}{\omega - H + i\delta} |dd,n\rangle; \\
G^{p_y d}_{ln}(\omega) &= \langle p_y p_y,l| \frac{1}{\omega - H + i\delta} |dd,n\rangle;
\end{aligned} \tag{4.31}$$

By using these projections, the total system can be represented in a compact matrix form as[12]:

$$\widehat{G}_{mn}(\omega) = \widehat{g}_{mn}(\omega) + \sum_s \widehat{g}_{ms}(\omega)\widehat{U}\widehat{G}_{sn}(\omega), \tag{4.32}$$

where:

$$\begin{aligned}
\widehat{G}_{mn}(\omega) &:= \begin{pmatrix} G^{dd}_{mn}(\omega) & G^{dp_x}_{mn}(\omega) & G^{dp_y}_{mn}(\omega) \\ G^{p_x d}_{mn}(\omega) & G^{p_x p_x}_{mn}(\omega) & G^{p_x p_y}_{mn}(\omega) \\ G^{p_y d}_{mn}(\omega) & G^{p_y p_x}_{mn}(\omega) & G^{p_y p_y}_{mn}(\omega) \end{pmatrix}, \\
\widehat{g}_{mn}(\omega) &:= \begin{pmatrix} g^{dd}_{mn}(\omega) & g^{dp_x}_{mn}(\omega) & g^{dp_y}_{mn}(\omega) \\ g^{p_x d}_{mn}(\omega) & g^{p_x p_x}_{mn}(\omega) & g^{p_x p_y}_{mn}(\omega) \\ g^{p_y d}_{mn}(\omega) & g^{p_y p_x}_{mn}(\omega) & g^{p_y p_y}_{mn}(\omega) \end{pmatrix}
\end{aligned} \tag{4.33}$$

and finally:

$$\widehat{U} := \begin{pmatrix} U_{dd} & 0 & 0 \\ 0 & U_{pp} & 0 \\ 0 & 0 & U_{pp} \end{pmatrix}. \tag{4.34}$$

We are interested in expressing the above equations in terms of delocalized Bloch states rather than localized single-particle atomic orbitals, to reconcile with the Sawatzky formalism [36] and to represent in a manifest way the lattice periodicity. In the present case the Bloch wave functions can be expressed as:

$$\psi_{k\nu}(\overrightarrow{r}) = e^{i\overrightarrow{k}\cdot\overrightarrow{r}} \begin{pmatrix} u^{Cu}_{k\nu}(\overrightarrow{r}) \\ u^{Ox}_{k\nu}(\overrightarrow{r}) \\ u^{Oy}_{k\nu}(\overrightarrow{r}) \end{pmatrix} \tag{4.35}$$

The index ν runs over the three bands, while k spans the Brillouin zone.

As previously stated we take one Copper atom as origin ($m = 0$), this way Eq.(4.28) can be written in the total momentum reference system $\overrightarrow{Q}$ as:

[12] Here and henceforth we adopt the convention to use $\widehat{\ }$ for representing a matrix operator.

$$G^{dd}_{0R}(\omega) = \langle dd,0|\frac{1}{\omega - \widehat{H} + i\delta}|dd,R\rangle = \frac{1}{N}\sum_{\overrightarrow{Q}} e^{i\overrightarrow{Q}\cdot\overrightarrow{R}} G^{dd}_{Q}, \tag{4.36}$$

where

$$G^{dd}_{Q} = \langle dd,Q|\frac{1}{\omega - \widehat{H}_Q + i\delta}|dd,Q\rangle, \tag{4.37}$$

and where the transformed Hamiltonian has been decomposed in:

$$\widehat{H}_Q = \widehat{H}_{0_Q} + \widehat{H}_{1_Q}. \tag{4.38}$$

Here $\widehat{H}_{0_Q}$ and $\widehat{H}_{1_Q}$ are simply the $\widehat{H}_0$ and $\widehat{H}_1$ terms appearing in Eq.(4.26) which have been transformed in the $\overrightarrow{Q}$-space. Actually Q is a good quantum number because of total momentum conservation and because we are interested in the propagation of the two interacting final holes as a pair. This is apparent from Eq.(4.27) where we included only Coulomb interactions between two holes, when they are both localized on a d or p orbital of the same atom.

By applying to Eq.(4.32) the transformation expressed in Eq.(4.36) we arrive to:

$$\frac{1}{N}\sum_{\overrightarrow{Q}} e^{i\overrightarrow{Q}\cdot\overrightarrow{R}}[\widehat{G}_Q(\omega) - \widehat{g}_Q(\omega)] = \frac{1}{N^2}\sum_{\overrightarrow{Q},\overrightarrow{Q'}} e^{i\overrightarrow{Q}\cdot\overrightarrow{R_s}}\widehat{g}_Q(\omega)\widehat{U}e^{i\overrightarrow{Q'}\cdot(\overrightarrow{R_n}-\overrightarrow{R_s})}\widehat{G}_{Q'}(\omega). \tag{4.39}$$

Here $\widehat{G}_Q(\omega)$ and $\widehat{g}_Q(\omega)$ are the whole square matrices representing the corresponding operators in the transformed Q-space (whose 11 elements are for example respectively $G^{dd}_Q(\omega)$ and $g^{dd}_Q(\omega)$). Summations over s and $\overrightarrow{Q'}$ can be immediately evaluated by considering that:

$$\sum_{s} e^{i(\overrightarrow{Q}-\overrightarrow{Q'})\overrightarrow{R_s}} = N\delta_{\overrightarrow{Q},\overrightarrow{Q'}}. \tag{4.40}$$

We are left with:

$$\frac{1}{N}\sum_{\overrightarrow{Q}} e^{i\overrightarrow{Q}\cdot\overrightarrow{R}}[\widehat{G}_Q(\omega) - \widehat{g}_Q(\omega)] = \frac{1}{N}\sum_{\overrightarrow{Q}} e^{i\overrightarrow{Q}\cdot\overrightarrow{R_n}}\widehat{g}_Q(\omega)\widehat{U}\widehat{G}_Q(\omega). \tag{4.41}$$

From this last expression we can obtain the wanted relation for our two holes Green's function in $\overrightarrow{Q}$ space:

$$\widehat{G}_Q(\omega) - \widehat{g}_Q(\omega) = \widehat{g}_Q(\omega)\widehat{U}\widehat{G}_Q(\omega) \Rightarrow \widehat{G}_Q(\omega) = [\widehat{I} - \widehat{g}_Q(\omega)\widehat{U}]^{-1}\widehat{g}_Q(\omega), \tag{4.42}$$

where $\widehat{I}$ is the identity matrix.

4.4.2 Calculation of the $\widehat{g}_Q$ Matrix Elements

In this section we report the description of the way we used to extend the explicit expression for the g_Q^{dd}, firstly written by G. Seibold [169], to a more convenient and general form which is suitable for our matricial approach.

We write the Schrödinger equation for the Bloch state of Eq.(4.35), eliminate the plane wave, rephrasing it as an equation for the local d, p_x and p_y amplitudes of periodic functions; then, the latter are rewritten as annihilation operators, in the hole picture, with a slight simplification of the notation, and the second-quantized Hamiltonian in the new representation is obtained. Thus, the tight binding Hamiltonian describing the system without any interaction can be written in the localized atomic orbitals representation, $\{d_{x^2-y^2},p,p\}$, as:

$$\widehat{H}_{tb} = \sum_{\overrightarrow{k},\sigma} \Lambda^{+}_{\overrightarrow{k},\sigma} \widehat{H}_{tb\overrightarrow{k},\overrightarrow{k}} \Lambda_{\overrightarrow{k},\sigma}, \tag{4.43}$$

where:

$$\overrightarrow{k} = (k_x,k_y);\ \ \Lambda_{\overrightarrow{k},\sigma} = \begin{pmatrix} d_{\overrightarrow{k},\sigma} \\ p^x_{\overrightarrow{k},\sigma} \\ p^y_{\overrightarrow{k},\sigma} \end{pmatrix} \text{ and} \tag{4.44}$$

$$\widehat{H}_{tb\overrightarrow{k},\overrightarrow{k}} = \begin{pmatrix} \varepsilon_d & 2\cdot t_{pd}Cos(\frac{k_x}{2}) & 2\cdot t_{pd}Cos(\frac{k_y}{2}) \\ 2\cdot t_{pd}Cos(\frac{k_x}{2}) & \varepsilon_p & -4\cdot t_{pp}Cos(\frac{k_x}{2})Cos(\frac{k_y}{2}) \\ 2\cdot t_{pd}Cos(\frac{k_y}{2}) & -4\cdot t_{pp}Cos(\frac{k_x}{2})Cos(\frac{k_y}{2}) & \varepsilon_p \end{pmatrix}.$$

The $d_{\overrightarrow{k},\sigma}$, $p^x_{\overrightarrow{k},\sigma}$ and $p^y_{\overrightarrow{k},\sigma}$ components[13] of $\Lambda_{\overrightarrow{k},\sigma}$ are the annihilation operators for a hole with momentum $\overrightarrow{k}$ and spin σ respectively in the d and p single-particle orbitals of energy

[13]The apices x and y refer to the fact that the corresponding p orbitals are localized respectively on the O_x and O_y types of oxygens in the given lattice cell.

ε_d and ε_p; t_{pd} and t_{pp} are related to the amplitude that a hole can hop respectively from a d to a p orbital (and viceversa) or between two p orbitals belonging to different types of oxygens.

To evaluate the uncorrelated two holes Green's function, it is useful to write $\widehat{H}_{tb}$ as:

$$\widehat{H}_{tb} = \sum_{\overrightarrow{k},\sigma} \Lambda^{+}_{\overrightarrow{k},\sigma} \widehat{A}^T \widehat{A} \widehat{H}_{tb_{\overrightarrow{k},\overrightarrow{k}}} \widehat{A}^T \widehat{A} \Lambda_{\overrightarrow{k},\sigma} = \sum_{\overrightarrow{k},\sigma} \Gamma^{+}_{\overrightarrow{k},\sigma} \widehat{D}_{tb_{\overrightarrow{k},\overrightarrow{k}}} \Gamma_{\overrightarrow{k},\sigma}, \tag{4.45}$$

where $\Gamma_{\overrightarrow{k},\sigma} = \widehat{A}\Lambda_{\overrightarrow{k},\sigma}$ and $\widehat{D}_{tb_{\overrightarrow{k},\overrightarrow{k}}} = \widehat{A}\widehat{H}_{tb_{\overrightarrow{k},\overrightarrow{k}}}\widehat{A}^T$ is the diagonal matrix representing the Hamiltonian written on the basis set of its eigenvectors. $\widehat{A}$ is the unitary matrix of the basis change, its rows are the components of the $\widehat{H}_{tb_{\overrightarrow{k},\overrightarrow{k}}}$ eigenvectors.

To keep notation in its most general form, we use $(\Lambda_{\overrightarrow{k},\sigma})_\alpha$ to indicate the αth component of $\Lambda_{\overrightarrow{k},\sigma}$ ($\alpha = 1,2,3$), i.e. $(\Lambda_{\overrightarrow{k},\sigma})_1 = d_{\overrightarrow{k},\sigma}$.

The $\alpha\beta$ matrix element of the noninteracting time-ordered two holes Green's function calculated on the ith and jth lattice cells can be written in the $\overrightarrow{R}$ and ω space as:

$$\widetilde{g}^{\alpha\beta}_{ij}(\omega) = \frac{1}{i}\int dt e^{i\omega t} \langle T\{[\Lambda_{i,\uparrow}(t)]_\alpha [\Lambda_{i,\downarrow}(t)]_\alpha [\Lambda^{+}_{j,\downarrow}(0)]_\beta [\Lambda^{+}_{j,\uparrow}(0)]_\beta\}\rangle \tag{4.46}$$

By using the fact that:

$$[\Lambda_{i,\sigma}(0)]_\alpha = \frac{1}{\sqrt{N}} \sum_{\overrightarrow{k}} e^{i\overrightarrow{k}\cdot\overrightarrow{R_i}} \sum_n [\widehat{A}^T(\overrightarrow{k})]_{\alpha n} \cdot [\Gamma_{\overrightarrow{k},\sigma}]_{n1} \tag{4.47}$$

$$[\Lambda_{i,\sigma}(t)]_\alpha = \frac{1}{\sqrt{N}} \sum_{\overrightarrow{k}} e^{i\overrightarrow{k}\cdot\overrightarrow{R_i}} \sum_n [\widehat{A}^T(\overrightarrow{k})]_{\alpha n} \cdot [\Gamma_{\overrightarrow{k},\sigma}]_{n1} e^{-iE^{(n)}_k t} \tag{4.48}$$

and transforming to the system of the total ($\overrightarrow{Q}$) and the relative ($\overrightarrow{q}$) momenta, we arrive to the following expression for Eq.(4.46):

$$\begin{aligned}\widetilde{g}^{\alpha\beta}_{ij}(\omega) \;=\; & \frac{1}{i}\int dt e^{i\omega t} \frac{1}{N^2} \sum_{n,m} \sum_{\overrightarrow{Q},\overrightarrow{k}} e^{i\overrightarrow{Q}\cdot(\overrightarrow{R}_i - \overrightarrow{R}_j)} e^{-i(E^{(n)}_{k+Q} - E^{(m)}_{-k})t} [\widehat{A}^T(\overrightarrow{k} + \overrightarrow{Q})]_{\alpha n} [\widehat{A}^T(\overrightarrow{-k})]_{\alpha m} \\ & \cdot [\widehat{A}(\overrightarrow{-k})]_{m\beta} [\widehat{A}(\overrightarrow{k} + \overrightarrow{Q})]_{n\beta} \langle T\{[\Gamma_{k+Q,\uparrow}]_{n1} [\Gamma_{-k,\downarrow}]_{m1} [\Gamma^{+}_{-k,\downarrow}]_{1m} [\Gamma^{+}_{k+Q,\uparrow}]_{1n}\}\rangle, \end{aligned} \tag{4.49}$$

which gives:

$$\begin{aligned}\widetilde{g}_{ij}^{\alpha\beta}(\omega) &= \frac{1}{i}\int dt e^{i\omega t}\frac{1}{N^2}\sum_{n,m}\sum_{\overrightarrow{Q},\overrightarrow{k}} e^{i\overrightarrow{Q}\cdot(\overrightarrow{R}_i-\overrightarrow{R}_j)}e^{-i(E^{(n)}_{k+Q}-E^{(m)}_{-k})t}[\widehat{A}^T(\overrightarrow{k}+\overrightarrow{Q})]_{\alpha n}[\widehat{A}^T(\overrightarrow{-k})]_{\alpha m}\\ &\cdot[\widehat{A}(\overrightarrow{-k})]_{m\beta}[\widehat{A}(\overrightarrow{k}+\overrightarrow{Q})]_{n\beta}\{\theta(t)[1-\langle(\Gamma^+_{k+Q,\uparrow})_{1n}(\Gamma_{k+Q,\uparrow})_{n1}\rangle]\\ &\cdot[1-\langle(\Gamma^+_{-k,\downarrow})_{1m}(\Gamma_{-k,\downarrow})_{m1}\rangle]+\theta(-t)\cdot\langle(\Gamma^+_{k+Q,\uparrow})_{1n}(\Gamma_{k+Q,\uparrow})_{n1}\rangle\\ &\cdot\langle(\Gamma^+_{-k,\downarrow})_{1m}(\Gamma_{-k,\downarrow})_{m1}\rangle\}. \qquad (4.50)\end{aligned}$$

Terms, such as for example $(\Gamma^+_{-k,\downarrow})_{1m}(\Gamma_{-k,\downarrow})_{m1}$ appearing in the previous equation, are number operators counting the holes present in the mth band with momentum $-k$ and spin down.

Making use of the integral representation of the θ function, the integral in dt can be easily evaluated and after some other algebra we finally obtain:

$$\begin{aligned}\widetilde{g}_{ij}^{\alpha\beta}(\omega) &= \frac{1}{N^2}\sum_{\overrightarrow{Q},\overrightarrow{k}} e^{i\overrightarrow{Q}\cdot(\overrightarrow{R}_i-\overrightarrow{R}_j)}\sum_{n,m}[\widehat{A}^T(\overrightarrow{k}+\overrightarrow{Q})]_{\alpha n}[\widehat{A}^T(\overrightarrow{-k})]_{\alpha m}[\widehat{A}(\overrightarrow{-k})]_{m\beta}[\widehat{A}(\overrightarrow{k}+\overrightarrow{Q})]_{n\beta}\\ &\cdot\left\{\frac{1-\theta(E_F-E^{(n)}_{k+Q})-\theta(E_F-E^{(m)}_{-k})}{\omega-(E^{(n)}_{k+Q}+E^{(m)}_{-k}-2E_F)+i\eta Sign(E^{(n)}_{k+Q}+E^{(m)}_{-k}-2E_F)}\right\}. \qquad (4.51)\end{aligned}$$

Comparing this expression with Eq.(4.36), it clearly appears what have to be $\widehat{g}_Q$, which is the only other ingredient we need, besides $\widehat{U}$, to build $\widehat{G}_Q$. Its $\alpha\beta$ matrix element in fact is:

$$\begin{aligned}g_Q^{\alpha\beta}(\omega) &= \frac{1}{N}\sum_{\overrightarrow{k}}\sum_{n,m}[\widehat{A}^T(\overrightarrow{k}+\overrightarrow{Q})]_{\alpha n}[\widehat{A}^T(\overrightarrow{-k})]_{\alpha m}[\widehat{A}(\overrightarrow{-k})]_{m\beta}[\widehat{A}(\overrightarrow{k}+\overrightarrow{Q})]_{n\beta}\\ &\left\{\frac{1-\theta(E_F-E^{(n)}_{k+Q})-\theta(E_F-E^{(m)}_{-k})}{\omega-(E^{(n)}_{k+Q}+E^{(m)}_{-k}-2E_F)+i\eta Sign(E^{(n)}_{k+Q}+E^{(m)}_{-k}-2E_F)}\right\}. \qquad (4.52)\end{aligned}$$

Here $[\widehat{A}(\overrightarrow{-k})]_{m\beta}$ represents the βth component of the $\widehat{H}_{tb_{\overrightarrow{-k},\overrightarrow{-k}}}$ eigenvector in the mth band evaluated with momentum $-\overrightarrow{k}$.

It is worth noticing that to gain the correlated two holes Green's function in $\overrightarrow{Q}$-space, $\widehat{G}_Q$, by using Eq.(4.42), we have to use the whole time ordered uncorrelated two holes Green's function $\widehat{g}_Q$. Only at the end of our calculation the retarded part has to be selected from $\widehat{G}_Q$ to make possible a comparison with the experiment.

Summing up, these are the main steps to get the correlated two holes Green's function that we are interested in:

1. Calculation of the uncorrelated two holes Green's function matrix, $\widehat{g}_Q$, using Eq.(4.52).

2. Application of Eq.(4.42) to evaluate the $\widehat{G}_Q$ matrix.

3. The CVV Auger spectra of copper and oxygen will be proportional to the retarded part of $-\frac{1}{\pi}Im[G(\omega)]_{\alpha\alpha}$, where α is respectively d or p^x (p^y) and $\widehat{G}(\omega) = \left[\frac{1}{N}\sum_{\overrightarrow{Q}}\widehat{G}_Q(\omega)\right]$. N is the total number of k-points we took to build the Brillouin zone.

4.4.3 From Theory to Practice

To obtain the CVV Auger spectra of Copper and Oxygen which will be shown in the following two subsections, the procedure described a few lines ago has been adopted both for BLA and GA. The results given by these two methods differ one from the other only because of the different way BLA and GA treat and introduce electronic correlations.

The Bare Ladder Approximation in fact introduces correlation effects only through the Coulomb Hamiltonian $\widehat{U}$ (see Sec.2.3.3), so $\widehat{g}_Q$ in this case represents a completely uncorrelated two particles Green's function where interactions enter only by means of an Hartree-Fock renormalization of the input ε_d and ε_p values, qualifying the approach we adopted as a sort of HFBLA (Hartree Fock - BLA). In the spectra calculated within the BLA in fact we take into account the effect of a mean Coulomb interaction treated in the Hartree-Fock approximation (see Sec.2.3.3). Its effect is to produce a renormalization of the ε_d and ε_p parameters, which have been used as input for the model, by $(U_{dd}/2)\cdot n_{Cu}$ and $(U_{pp}/2)\cdot n_O$ respectively. This renormalization was not present in the original BLA.
In the Gutzwiller approach instead electronic correlations are present not only in $\widehat{U}$, but also in $\widehat{g}_Q$ by means of the hopping parameters and the energies ε_d and ε_p, which result to be renormalized by Coulomb interactions. In the Gutzwiller approximation all the parameters we need are calculated by using a self-consistent procedure (see Chapter 3).

Another fundamental difference between these two theories is in the way they evaluate the Coulomb Hamiltonian $\widehat{U}$. In the Gutzwiller approach the Hubbard repulsion U is replaced by $V^{\sigma\sigma}_{\alpha\alpha}$, which is the extension of the effective interaction of Ref [119] for a multiband case:

$$V^{\sigma\sigma}_{\alpha\alpha} = \frac{U - 2\Sigma^{\sigma\sigma}_{G_{\alpha\alpha}}}{1 - n^{\sigma}_{h}}. \tag{4.53}$$

Here n^{σ}_{h} denotes the concentration of holes having spin σ, while α may represent in our case

a d or a p single-particle orbital; $\Sigma^{\sigma\sigma}_{G_{\alpha\alpha}}$ is a self-energy term. For paramagnetic materials one has: $V^{\sigma\sigma}_{\alpha\alpha} = V^{-\sigma-\sigma}_{\alpha\alpha}$, that is $\Sigma^{\sigma\sigma}_{G_{\alpha\alpha}} = \Sigma^{-\sigma-\sigma}_{G_{\alpha\alpha}}$ and $n^{\sigma}_{h} = n^{-\sigma}_{h}$.

It is interesting to notice that Eq.(4.53) is a general expression returning, for whatever approximation is used, the effective interaction which is consistent with that approximation. As an example by replacing $\Sigma^{\sigma\sigma}_{G_{\alpha\alpha}}$ with the Hartree-Fock self-energy, $\Sigma^{\sigma\sigma,(HF)}_{G_{\alpha\alpha}}$, we get the BLA. Appendix A reports in a very schematic way the procedure which has to be followed to evaluate the several $\Sigma_{G_{\alpha\alpha}}$ values for the case of interest.

The GA ε_d and ε_p input parameters have been renormalized by the effect of interaction too. In accordance with the Gutzwiller's theory [119] they have been respectively shifted of $\Sigma_{G_{dd}}$ and $\Sigma_{G_{pp}}$.

One last observation before showing the calculated patterns: the Fermi energies, ε_{Fermi}, have been obtained by evaluating firstly the lowest band[14] of the tight binding Hamiltonian of Eq.(4.44), which has been built up for the considered parameter set. Then the Fermi energy has been determined by taking that value which yields the correct filling for the lowest band, that is by using a simple *aufbau* principle. Fig.(4.12) displays, as an example, two different views of the lowest band (in the hole picture), which have been obtained using the parameters shown in the first row of Table 4.6.

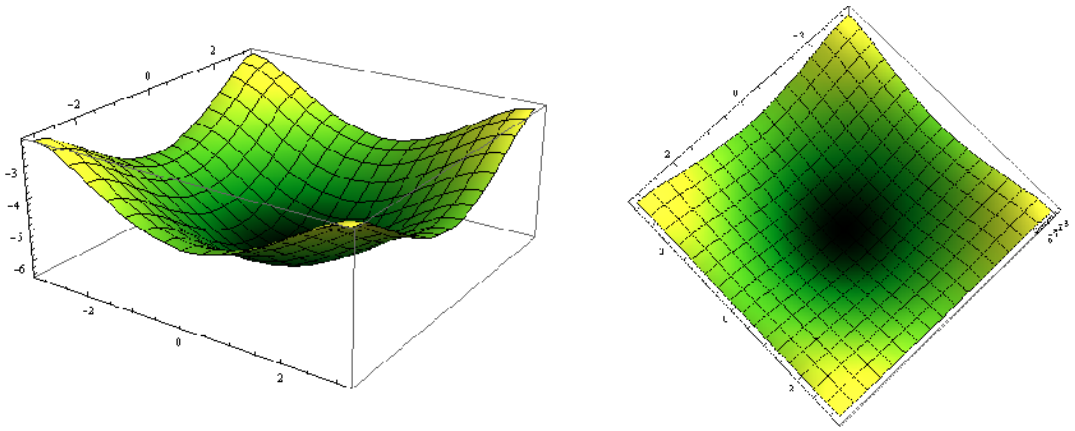

Figure 4.12. *These figures show two different views of the lowest band (in the hole picture) of the system made up of a CuO_2 plane. This band has been calculated using the tight binding Hamiltonian reported in Eq.(4.44). In particular to get the band here presented, this Hamiltonian has been evaluated using the parameters shown in the first row of Table 4.6 corresponding to the case of the Bare Ladder Approximation for a 12×12 system (that is a system which is characterized by 144 k-vectors) with hole filling $n_h = 0.514$.*

In the next two sections some results we gained both applying BLA and GA to the Auger

[14] which is the only one (half) filled by holes in the hole picture.

spectra from CuO_2 planes will be presented. In particular in the next section these two approaches will be compared with the results given by the exact solution of the Eq.(4.42) for a finite cluster for many U values, while the following one contains comparisons between BLA and GA for a more extended system and for different possible choices of the parameter sets.

BLA and GA against the exact results of a finite cluster

Despite the abundance of experimental data reporting CVV Auger spectra from high T_c superconductors (i.e. [170, 171, 172]), we decided to probe the goodness of GA as applied to CVV decay by comparing its results to the ones of an exactly solvable cluster of finite size. One reason for this choice is that a two holes density of states is not enough to understand the line shape; besides this, all the spectra which can be found in literature display broad Auger line shapes, so there are no sharp two holes features to look for.

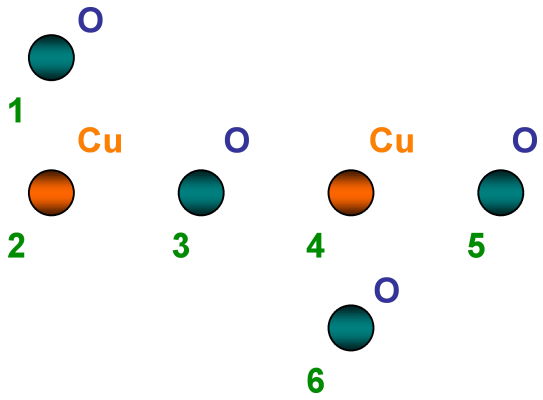

Figure 4.13. *Schematic representation of the finite cluster for a CuO_2 plane adopted to gain the exact solution of Eqs.(4.42). As it can be seen, the considered system is made up of six atoms. Two k-vectors, $(k_x,k_y) = \{(0,0),(\pi,0)\}$, have been used to perform calculations. Periodic boundary conditions have been applied.*

Fig.(4.13) shows the geometry of the cluster used to gain the exact solution of Eqs.(4.42). This 6-sites cluster allows two k_x components and one k_y value, thus $(k_x,k_y) = \{(0,0),(\pi,0)\}$. The reason for the reduced size of the cluster is the feasibility of calculation by using a "Mathematica" program [173] without recurring to other programming languages. Simply increasing only by one the number of considered atoms in fact requires the use of a more complex code. This has been done to compare the BLA and GA results in more extended (and so more realistic) systems. To this purpose a program in the Python language [174]

has been written and used to simulate CVV Auger spectra for systems with 144 k-vectors[15]. The results of these calculations are described in the following section, while Appendix B is devoted to a brief description of the Python program which has been written to this purpose.

The calculations for the exact solution have been performed by evaluating the correlated two holes Green's function of the system for the chosen atom:

$$-G^j(t) = \langle \Phi | T\{c_{j\uparrow}(t) c_{j\downarrow}(t) c^+_{j\downarrow} c^+_{j\uparrow}\} | \Phi \rangle, \tag{4.54}$$

where j (with j = 1,2,..,6) accounts for the number labeling each atom in the system and $|\Phi\rangle$ is the system ground state where no holes are present; T represents the time-ordered product, while $c_{j\uparrow}(t)$ ($c_{j\downarrow}(t)$) and $c^+_{j\uparrow}$ ($c^+_{j\downarrow}$) are the hole operators which respectively destroy and create a hole on the atom i with spin up (down) at times t and zero. In the ω space this Green's function can be re-written using the Lehmann representation as (see e.g. Refs. [83, 175]):

$$G^j(\omega) = |A|^2 \frac{(-i)}{\omega - E^{(2)}_{0j} - i\delta} + i \sum_\nu \frac{|B_\nu|^2}{\omega + (E^{(2)}_{0j} - E^{(4)}_{\nu j}) + i\delta}, \tag{4.55}$$

with

$$A = \langle \Phi | c^+_{j\downarrow} c^+_{j\uparrow} | 0 \rangle; \quad B_\nu = \langle \nu | c^+_{j\downarrow} c^+_{j\uparrow} | \Phi \rangle. \tag{4.56}$$

In Eq.(4.55) $E^{(2)}_{0j}$ is the eigenvalue of the two particles Hamiltonian corresponding to a state where two holes are created on the atom j starting from a two bodies vacuum state, $|0\rangle$; $E^{(4)}_{\nu j}$ represents instead the eigenvalue of the four bodies Hamiltonian corresponding to one of the ν possible ways to create two holes on states yet characterized by two vacancies, $|\nu\rangle$.

The Auger current from the atom j can be obtained as usual as the imaginary part of the corresponding correlated two holes Green's function, $G^j(\omega)$. This way the only things we

[15] A program written for "Mathematica" and evaluating the correlated two holes Green's function given by Eq.(4.42) takes about 445 seconds to evaluate a single point per frequency for a 10×10 system (that is a system made up of 100 k-vectors), while only 17 seconds are needed by the Python program we wrote to perform the same calculation. "Mathematica" is not able to evaluate patterns for systems which are larger than a 10×10 one because its kernel crashes down. The only limit of the Python program instead is time: this means that in principle it can calculate the wanted Green's function for a system of whatever dimension, but the larger will be the considered system, the longer will be the time the program takes. The user has to find a compromise between the timing of calculations and the system extension which is needed to gain reliable results.

need to gain the calculated spectra are the eigenvalues of the two and four bodies Hamiltonian matrix and the corresponding eigenvectors. In particular the spectra that will be shown in the following lines have been obtained considering the Copper and Oxygen atoms labeled respectively with 2 and 3 in Fig.(4.13). Periodic boundary conditions have been applied to atoms 1, 2, 5 and 6 to simulate as most as possible an infinite lattice.

Each one of the following figures displays the comparison between the spectra calculated in the HFBLA (blue dashed line), GA (purple solid line) and by exactly solving the finite cluster previously described (red solid line), for CVV Auger transitions from both Copper and Oxygen. All these patterns have been calculated for $n_h = n_{Cu} + 2n_O = 1$, that is for the case of an half filled valence band per unit cell, where n_h represents the total hole number of the system. Different values of the Coulomb interactions for two holes both localized in the d or p orbitals respectively of Copper and Oxygen have been considered, U_{dd} and U_{pp}. No interaction between the p and d orbitals, U_{pd}, has been taken into account.

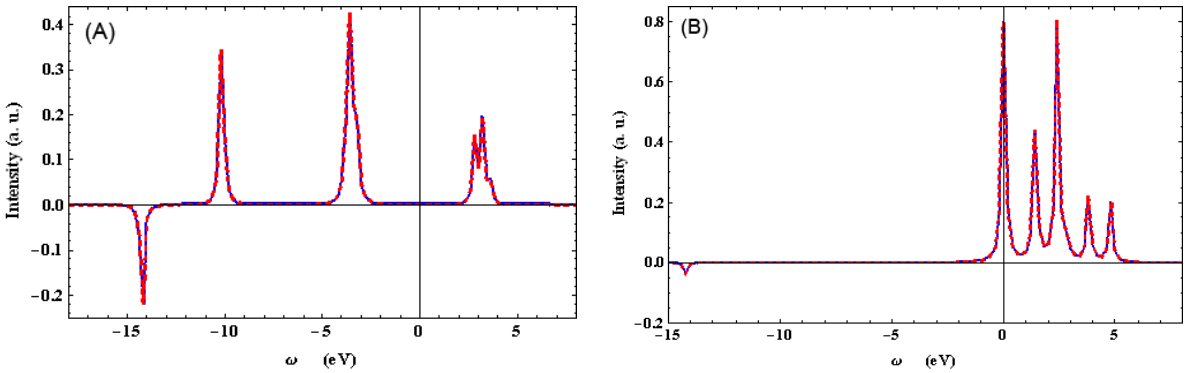

Figure 4.14. *Comparison between the exact (red dashed line) and the HFBLA/GA (blue solid line) correlated two particles Green's function for the case of Copper (panel A) and Oxygen (panel B) and for $U_{dd} = U_{pp} = 0$. In both panels the exact and the approximated patterns are equal as expected.*

Fig.(4.14) can be used as a check for the validity of the several codes that have been used. From this figure in fact one can notice that HFBLA and GA results coincide in absence of Coulomb interactions as expected. Furthermore these patterns results to be perfectly superimposed to the exact one as expected too, because BLA (and HFBLA) becomes exact in the limit of zero Coulomb interactions.

By observing the series of panels (A), going from Fig.(4.15) to Fig.(4.17), one can see that the U_{dd} magnitude results to be too small, even at $U_{dd}/3$ (and $U_{pp}/3$), to produce sensitive changes between the HFBLA, GA and exact time-ordered Green's function of the Copper atom. From the patterns calculated for $U/5$ and $U/3$ a characteristic of the GA curve comes

out which is confirmed and stressed in panel (A) of Fig.(4.18): the peaks evaluated by means of GA result to be centered on higher energies than the HFBLA ones. This is due to the effective interaction V adopted by the former method, which is always greater than the bare one, U. The overall effect is the production of spectra which are more atomic-like than the corresponding ones evaluated within the HFBLA, as it is shown in Fig.(4.18). This feature obviously needs high magnitudes for the Coulomb interaction (respect to the band width) to be evident, as it is shown by Figs.(4.15÷4.18).

The series of panels (B) of Figs.(4.15÷4.18) shows instead that the magnitude of Coulomb interaction U_{pp} on Oxygen is too small, for all the considered values, to observe any kind of sensitive difference among the reported patterns.

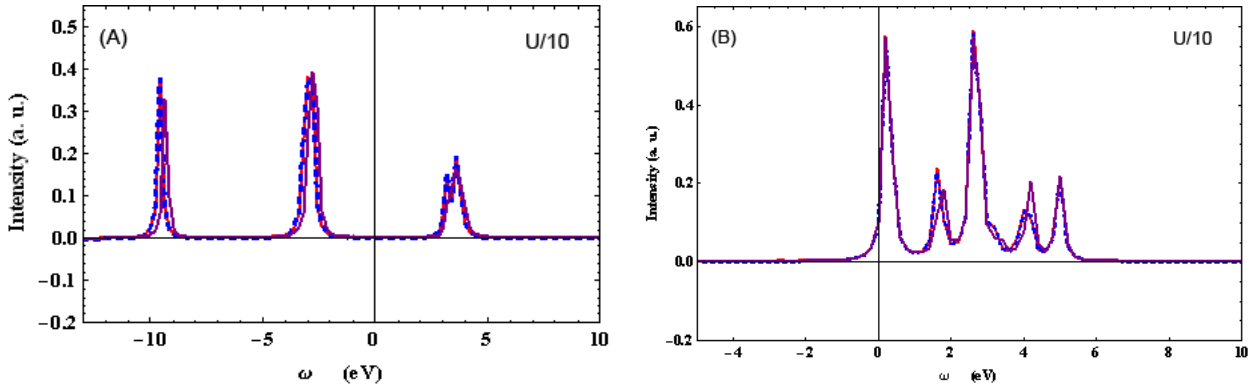

Figure 4.15. *Comparison between the exact (red solid line), the HFBLA (blue dashed line) and the GA (purple solid line) correlated two particles Green's function for the case of Copper (panel A) and Oxygen (panel B). All the reported patterns have been obtained by using as input the Coulomb interactions values present in literature [178] as divided by a factor 10.*

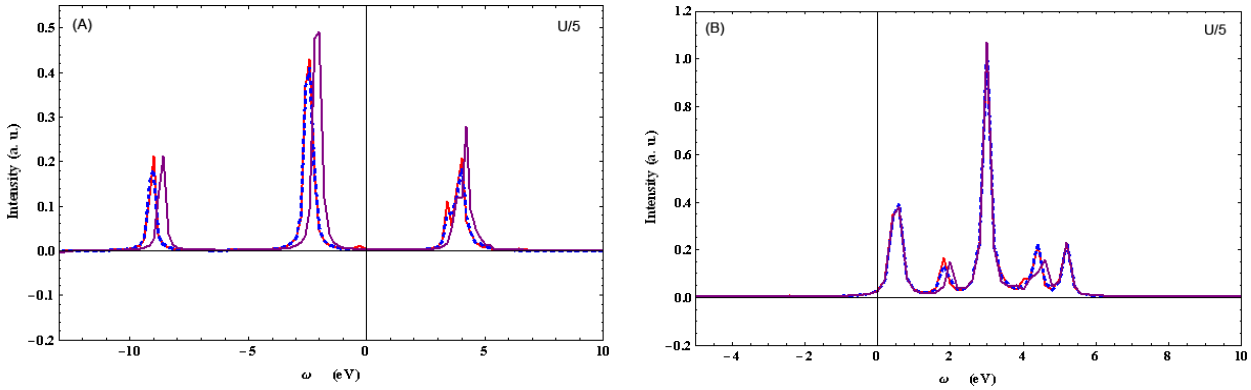

Figure 4.16. *Comparison between the exact (red solid line), the HFBLA (blue dashed line) and the GA (purple solid line) correlated two particles Green's function for the case of Copper (panel A) and Oxygen (panel B). All the reported patterns have been obtained by using as input the Coulomb interactions values present in literature [178] as divided by a factor 5.*

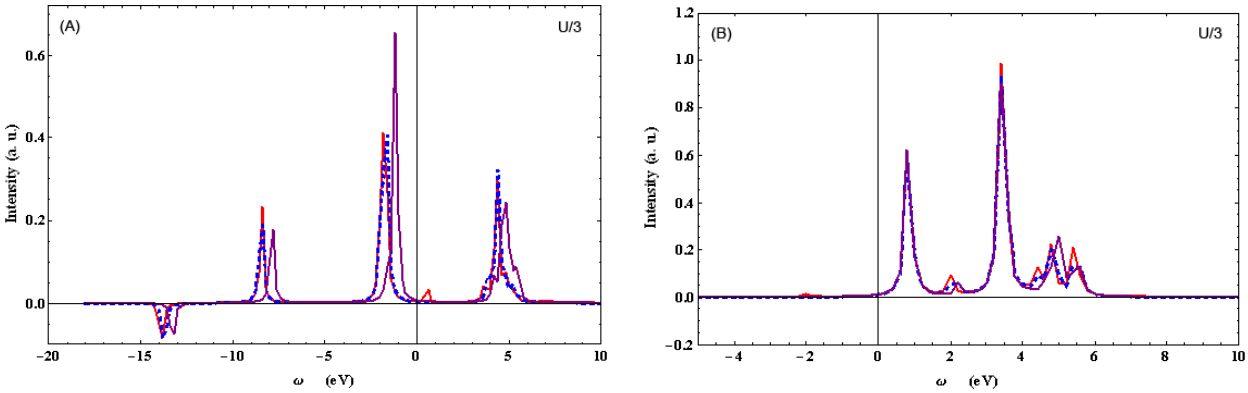

Figure 4.17. *Comparison between the exact (red solid line), the HFBLA (blue dashed line) and the GA (purple solid line) correlated two particles Green's function for the case of Copper (panel A) and Oxygen (panel B). All the reported patterns have been obtained by using as input the Coulomb interactions values present in literature [178] as divided by a factor 3.*

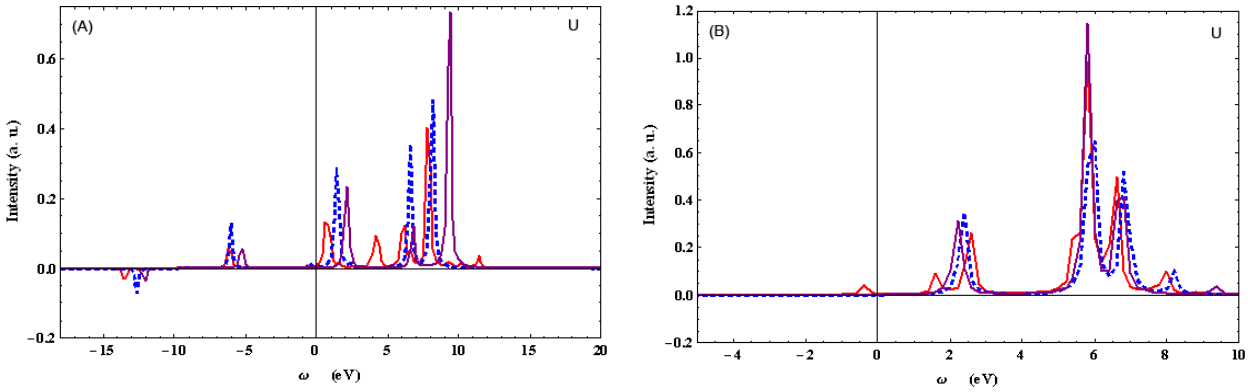

Figure 4.18. *Comparison between the exact (red solid line), the HFBLA (blue dashed line) and the GA (purple solid line) correlated two particles Green's function for the case of Copper (panel A) and Oxygen (panel B). All the reported patterns have been obtained by using as input the Coulomb interactions values present in literature [178].*

The good accuracy provided by HFBLA in describing both the number and the energy position of the structures which are present in the evaluated spectra (for all the considered U values) is the real surprising finding gained by these calculations. Despite the one band case [119], it seems that in a three band case the HFBLA still gives quite reliable results as compared to the exact pattern despite we are dealing with an open band material. However it is worth to note that properly because we are facing with a three band problem, the hole band filling n_h on each atom of a primitive cell is far from being 1. This means that we are not really dealing with an half-filling case, because the hole concentration on each Copper and Oxygen atom per primitive cell is lesser than one and only the total number of holes per primitive cell is equal to 1.

GA results for wider systems

In this subsection the results of CVV spectra from CuO_2 planes evaluated in the HFBLA and GA are shown. The considered system this time is a more extended one, characterized by 144 k-vectors[16]. As previously stated these calculations have been performed by using a Python program which is described in details, together with the other used procedures, in Appendix B. The mathematical steps followed to calculate the Auger current for both the considered approximations are the ones described in Secs.4.4.1 and 4.4.3.

Table 4.5 shows the results of $\Sigma_{G_{\alpha\alpha}}$ calculations gained, for the case of a 12×12 system and for several values of filling n_h, starting from the parameter set given by McMahan and coworkers [178]. This table gives evidence to the dependence of $\Sigma_{G_{\alpha\alpha}}$ from both the Coulomb interaction magnitude (as it can be seen by comparing $\Sigma_{G_{dd}}$ and $\Sigma_{G_{pp}}$ at fixed n_h) and the hole filling n_h (increasing n_h at fixed $U_{\alpha\alpha}$ increases the corresponding $\Sigma_{G_{\alpha\alpha}}$ value).

n_h	$n_{h_{Cu}}$	n_{h_O}	$\Sigma^{\sigma\sigma}_{G_{dd}}$ [eV]	V_{dd} [eV]	$\Sigma^{\sigma\sigma}_{G_{pp}}$ [eV]	V_{pp} [eV]
0.514	0.291	0.111	0.528	9.650	0.148	3.718
0.847	0.477	0.185	1.053	11.080	0.249	3.805
1.125	0.619	0.253	1.635	12.169	0.346	3.891
2.0	0.952	0.524	3.636	13.094	0.775	4.304

Table 4.5. *This table reports the values obtained for $\Sigma^{\sigma\sigma}_{G_{dd}}$ and $\Sigma^{\sigma\sigma}_{G_{pp}}$ starting from the McMahan parameter set [178], which gives for U_{dd} and U_{pp} respectively the values 7.9 eV and 3.6 eV. All the reported values have been gained for a 12×12 system characterized by an hole number $n_h = n_{h_{Cu}} + 2 \cdot n_{h_O}$, which is specified in the first column of the table. The case of an half-filled lowest band (in the hole picture) corresponds to $n_h = 1$, while $n_h = 2$ represents a completely filled case. The expressions used to evaluate $\Sigma^{\sigma\sigma}_{G_{dd}}$ and $\Sigma^{\sigma\sigma}_{G_{pp}}$ are explained in details in A, while the corresponding V_{ii} values (with $i = d$,p) have been calculated making use of Eq.(4.53).*

In the following pages some preliminary results will be shown. Before presenting them, we report in the table below all the values used to calculate the predicted Auger profiles by adopting the two mentioned approaches. In particular the rows in Table 4.6 contain all the parameters used for doing calculations for a 12×12 system in the BLA (black values) and in the GA (green values). All the reported ε_d and ε_p values have to be further shifted to take into account the effect of the interaction as explained in Sec.4.4.3, that is to apply HFBLA.

[16]These 144 k-vectors are nothing else than all the possible combinations of 12 k_x-vectors and 12 k_y-vectors, this is the reason why we will refer to this kind of system also as a 12×12 one.

In particular the parameters used for the calculations performed within the HFBLA corresponds - obviously except the Fermi energies - to the same values of the starting parameter set [178] as it is expected.

n_h	ε_d [eV]	ε_p [eV]	t_{pd} [eV]	t_{pp} [eV]	U_{dd} [eV]	U_{pp} [eV]	ε_{Fermi} [eV]
0.514	-3.3	0.0	1.5	0.6	7.9	3.6	-5.249
0.514	-2.920	0.0	1.464	0.599	9.650	3.718	-5.294
0.847	-3.3	0.0	1.5	0.6	7.9	3.6	-4.188
0.847	-2.493	0.0	1.436	0.597	11.080	3.805	-4.040
1.125	-3.3	0.0	1.5	0.6	7.9	3.6	-3.425
1.125	-2.006	0.0	1.416	0.595	12.169	3.892	-2.967
2.0	-3.3	0.0	1.5	0.6	7.9	3.6	0.484
2.0	-0.429	0.0	1.400	0.587	13.094	4.304	0.775

Table 4.6. *Here the several sets of parameters used to evaluate the theoretical CVV Auger profiles for CuO_2 are shown. The reported values have been obtained for a 12×12 system starting from the McMahan parameter set [178] and performing calculations in the Bare Ladder (black) and in the Gutzwiller (green) approximations. The reported BLA ε_d and ε_p have to be further shifted to take into account the effect of the interaction as explained in Sec.4.4.3, that is to apply HFBLA.*

The GA values instead result to be all different from the ones of the McMahan parameter set, because they all feel the effects of interaction by means of a self-consistent procedure as the GA prescribes.

It is worth to note that the results presented in Tabs. 4.5 and 4.6 shows very little differences between HFBLA and GA values for low-filling cases, while increasing n_h produces increasing differences between the values obtained by using the two different approaches, as expected.

Figs.(4.19 ÷ 4.22) report the results we gained by applying HFBLA and GA to a 12×12 system, going from $n_h = 0.514$ to $n_h = 2$, that is at increasing the hole filling per primitive cell. All the calculated spectra have been obtained making use of the values reported in Tabs.4.5 and 4.6. Physical values of the Coulomb interactions [178] have been used as starting point for calculations. The graphs shown for the case of a 2×1 system have been obtained by varying the interaction magnitude at fixed n_h ($n_h = 1$).

In my opinion it is worth to note that the information given by the two sets of spectra, which have been shown in this subsection and the previous one, can not be considered as complementary as far as GA is concerned. This means that the GA results gained for a 2×1 and a 12×12 system do not allow to isolate the effects on each spectrum which are due to only the Coulomb interaction magnitude and to only the hole filling n_h. Varying in fact

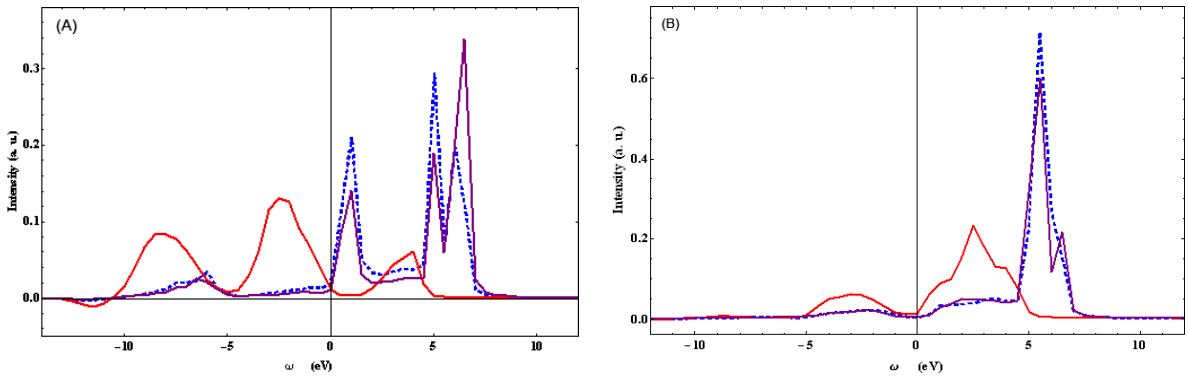

Figure 4.19. *Comparison between the non interacting (red solid line) and the interacting HFBLA (blue dashed line) and GA (purple solid line) two particles Green's function for the case of Copper (panel A) and Oxygen (panel B). In this case the hole-filling per primitive cell has been fixed to* $n_h = 0.514$.

the Coulomb interaction magnitudes (U_{dd} and U_{pp}) at fixed hole filling per primitive cell $n_h = n_{h_{Cu}} + 2 \cdot n_{h_O}$ induces variations on the hole filling per atom, $n_{h_{Cu}}$ and n_{h_O} (but not on n_h), which will influence the renormalized U values used for the spectra. The same happens if we vary the n_h values keeping fixed the starting Coulomb interactions. This is the reason why the discussion of the results here presented should be considered in the light of the results of the previous subsection.

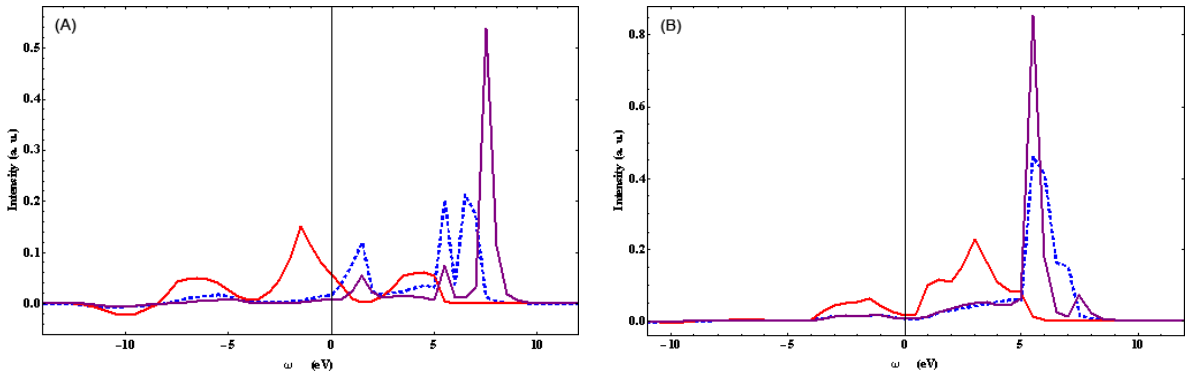

Figure 4.20. *Comparison between the non interacting (red solid line) and the interacting HFBLA (blue dashed line) and GA (purple solid line) two particles Green's function for the case of Copper (panel A) and Oxygen (panel B). In this case the hole-filling per primitive cell has been fixed to* $n_h = 0.847$.

As previous stated, Figs.(4.19 ÷ 4.22) display a comparison between the non interacting (red solid line) and the interacting HFBLA (blue dashed line) and GA (purple solid line) two particles Green's function for the case of Copper (panels A) and Oxygen (panels B) and for several values of hole filling n_h.

The reported spectra seem not only to confirm all the findings which have been discussed

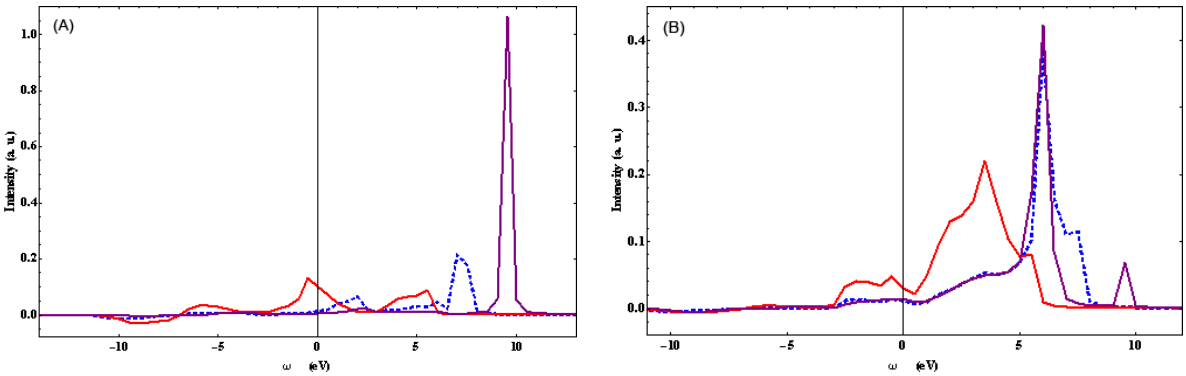

Figure 4.21. *Comparison between the non interacting (red solid line) and the interacting HFBLA (blue dashed line) and GA (purple solid line) two particles Green's function for the case of Copper (panel A) and Oxygen (panel B). In this case the hole-filling per primitive cell has been fixed to* $n_h = 1.125$.

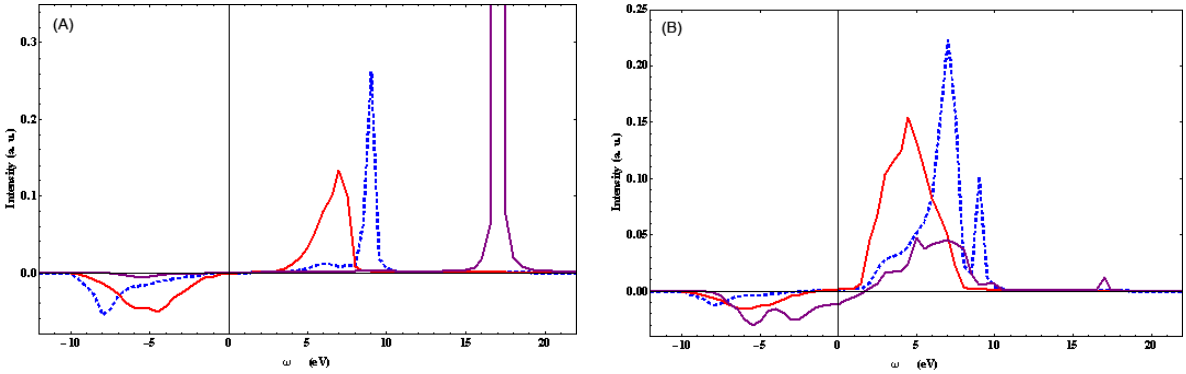

Figure 4.22. *Comparison between the non interacting (red solid line) and the interacting HFBLA (blue dashed line) and GA (purple solid line) two particles Green's function for the case of Copper (panel A) and Oxygen (panel B). In this case the hole-filling per primitive cell has been fixed to* $n_h = 2$.

for the case of a 2×1 system, but show some new features too.

The series of spectra from Copper (Figs.(4.19.A $\div$ 4.22.A)) shows that for small hole filling HFBLA and GA results are very similar as expected, while at increasing n_h (and so also n_{hCu}) GA patterns are more atomic-like than the HFBLA ones.

The series of spectra from Oxygen (Figs.(4.19.B $\div$ 4.22.B)) instead shows that for all the considered n_h values (except for the case of $n_h = 2$) GA and HFBLA spectra are very similar as expected. This happens because of the lower value of U_{pp} than U_{dd}. For the case of Oxygen, GA patterns display also a little peak on the high energy side of the main structure, which recalls to the mind the partner resonances of Ref. [179]. We attribute in fact this structure to the effect of U_{dd} on the Oxygen atom. By setting U_{dd} to zero in fact this structure disappears as it is shown in Fig.(4.23) for the cases of $n_h = 1.125$ and $n_h = 0.872$,

which have been chosen as an example. The same phenomenon happens also for $n_h = 0.514$ as expected.

A comparison with the exact results of a finite cluster for $n_h = 2$

To better understand the case for $n_h = 2$, we performed the same calculation as the one described in the previous subsection. In this case again the same 6-atoms cluster of Fig(4.13), with periodical boundary conditions, has been considered. Two k-vectors, $(k_x,k_y) = \{(0,0),(\pi,0)\}$, have been used. The starting input values for the Coulomb interaction magnitudes are the ones taken from literature [178]. Figs.(4.24.A) and (4.24.B) report the gained results, which have been obtained by comparing the exact (red solid line) and the interacting HFBLA (blue dashed line) and GA (purple solid line) two particles Green's function for the case of Copper (panel A) and Oxygen (panel B). As it can be seen from the figure, the patterns gained for the case of Copper seem to confirm the findings obtained for a 12×12 system, that is a more atomic like character of GA respect to HFBLA. In this case however HFBLA seems to underestimate the energy position of the main structure respect to the exact solution. For the case of Oxygen instead we found again a result which is similar to what we obtained for a 12×12 system, but only as far as the main structure energy position is concerned. The line shapes we found in fact seem to be quite different from the ones of a 12×12 system, especially for the GA patterns.

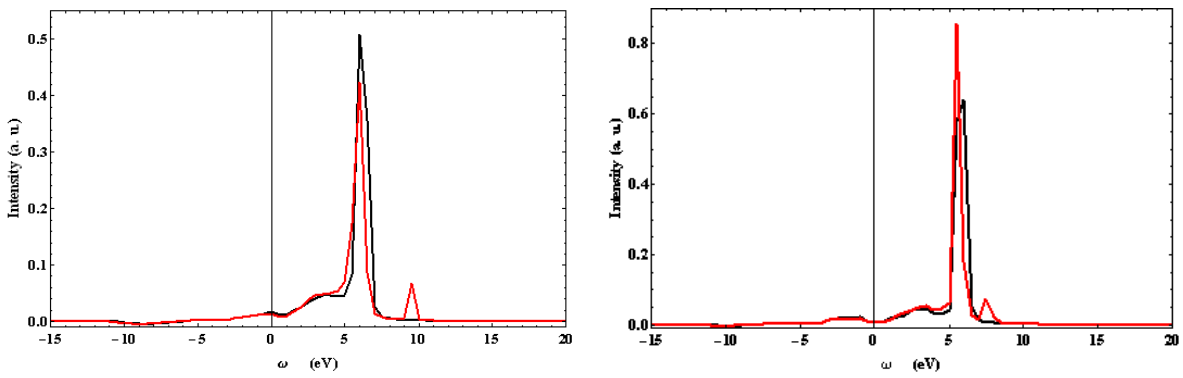

Figure 4.23. *Comparison between the correlated GA two holes Green's functions from an Oxygen atom of a CuO_2 plane. The two patterns reported in each panel have been obtained by using Eq.(4.42) and the same set of parameters except for the U_{dd} magnitude. The black solid curve in fact has been calculated for $U_{dd} = 0$, while the red one corresponds to the GA U_{dd} value reported in Table 4.6 for the corresponding hole filling n_h. The two panels differ for the used n_h value, which has been set to 1.125 for the right one and to 0.872 for the left panel.*

In Fig.(4.24) one can notice that the integrated intensities of the two approximations

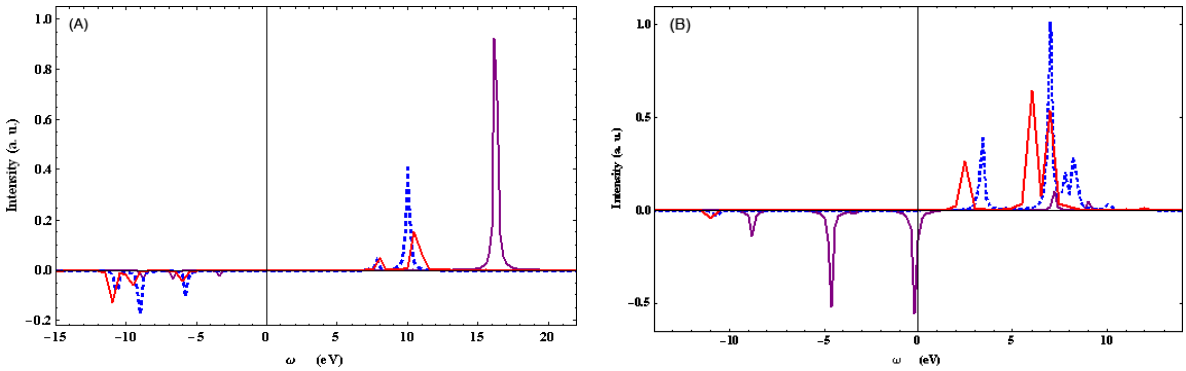

Figure 4.24. *Comparison between the exact (red solid line) and the interacting HFBLA (blue dashed line) and GA (purple solid line) two particles Green's function for the case of Copper (panel A) and Oxygen (panel B). In this case the hole-filling per primitive cell has been kept fixed to $n_h = 2$. In both panels calculations have been performed on a six atoms cluster with periodical boundary conditions and only two k vectors ($(k_x,k_y) = \{(0,0),(\pi,0)\}$), which is completely identical to the one described in the previous subsection. The used Coulomb interaction magnitudes are the ones reported in literature [178]. For Copper and Oxygen were considered respectively the atoms labeled with 2 and 3 in Fig.(4.13).*

differ remarkably in both Cu and O cases. The GA predicts too much intensity at positive ω and too little intensity at negative ω for Cu; for O, quite the other way, too little intensity is seen at positive ω and too large intensity at negative ω. The HFBLA, on the other hand, yields intensities that are about right in all cases.

All the found discrepancies deserve a deeper analysis and more other calculations in order to be completely understood. However we expect they are due to the considered very small number of k-vectors which introduces a little indetermination in the values used for the input parameters. For example the GA $\Sigma_{G_{ii}}$ (with $i = d,p$), and so also the effective Coulomb interactions, are very sensitive to the values of the parameters which are used to evaluate them. For timing reasons it has not been possible to deepen our inquiry about this argument within this thesis work, but it will be performed for the completeness of the forthcoming paper we are preparing on this subject [180].

Summing up the very surprising finding of this work is represented by the quite reliable results given by the HFBLA even if we are dealing with an open band material, in particular with a system with an half filled valence band. This one has always been thought as the case where surely the HFBLA has to break down. Besides being unexpectedly good an approximation for the line shape, the HFBLA is also remarkably reliable for the overall intensity both in the hole and in the electron sides for both Cu and O. In my opinion this result deserves however more studies because:

1. the three band case is obviously different from a single band one. This means that the hole-filling per atom within each primitive cell is far from being one ($n_{Cu} \ll 1$ and $n_O \ll 1$), so we are not properly considering the case of an half-filled band per atom. Besides this, the presence of three bands can produce some peculiar effects which are different from the ones appearing in a single band material. We should not argue on the basis of only the behavior which is expected for the single band case;

2. we compared the several results gained by using the HFBLA and GA only with the exact patterns for the case of a 2×1 system, because of the lack in literature of Auger spectra from CuO_2 planes which have been measured with enough resolution. The few considered k-vectors allows to determine the needed GA parameters with insufficient accuracy and this reflects mostly to the used Σ values (and so also on the renormalized Coulomb interactions) which are very sensitive.

To a decisive confirmation of the HFBLA reliability we need firstly to embed the theory we developed here in the approach proposed by Cini and Drchal [79, 80] (see Sec.2.3.3). A comparison with an enough resolved experiment or the exact solution of a more extended cluster are then necessary and we hope to go along one of these two ways as soon as we complete the writing of the forthcoming paper [180] where we describe the results here presented.

4.5 Coster-Kronig Preceded Auger Line Shapes in Solids

Looking for a theory for modeling three holes satellites has been part of the strategy to face the problem of Auger spectra from open band materials; another part of the same strategy also involved the application of the TDGA to the unrelaxed features. The case of study was provided in 1977 by E. Antonides and coworkers [133], who measured the $L_{23}M_{4,5}M_{4,5}$ Auger spectra from transition metals.

The experimental patterns displayed their overall similarity, except for the presence of some intensity in the low kinetic energy side of the Auger spectra from Copper and Zinc, which instead resulted to be absent in the Germanium and Gallium cases. They attributed these features to Coster-Kronig (CK) $L_2 - L_2L_3M_{4,5} - M_{4,5}M_{4,5}(M_{4,5})$ satellites[17] that are

[17]The bracketed hole is a spectator one, according to a notation proposed by Lund et al.[184]. These transitions involve the creation of the first core hole in the $2p_{1/2}$ shell, which decays by a Coster-Kronig transition

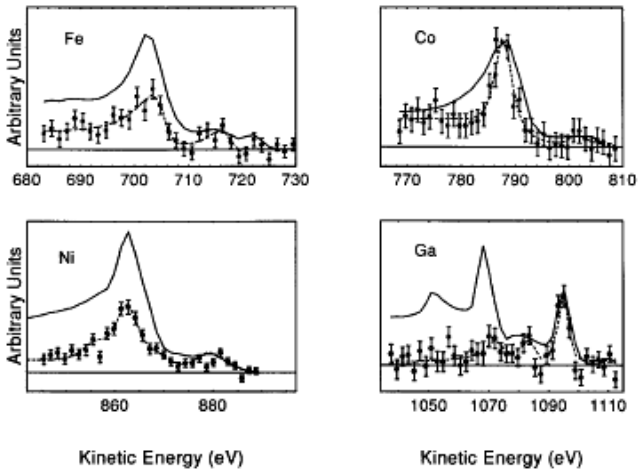

Figure 4.25. *Comparison between the $L_{23}VV$ Auger spectra measured by using (points and dashed line) or not (solid line) a coincidence spectroscopic technique for Fe, Co, Ni and Ga samples [187]. The APECS spectra were acquired by measuring only the Auger electrons emitted in coincidence with the $2p_{1/2}$ photoelectron. The presence of some intensity under the region of the L_3VV line shape in all cases except Ga represents a proof of the existence of the $L_2 - L_2L_3M_{4,5} - M_{4,5}M_{4,5}(M_{4,5})$ CK satellites.*

forbidden in Ga and Ge for energy conservation reasons, as it can be seen for the cases of Fe, Co, Ni and Ga from the collection of free atom binding energies shown in Table 4.7. It is worth noticing that the values displayed in the table cannot be applied literally to solids and that in Ga the $3d$ binding energy is lesser than the $L_2 - L_3$ energy difference, but nevertheless the CK transition is forbidden because of the $L_3M_{4,5}$ repulsion. It is forbidden in atomic Zn as well, but becomes allowed in the metal because the $L_3M_{4,5}$ repulsion is reduced by screening.

The real demonstration of the existence of structures attributed to CK $L_2 - L_2L_3M_{4,5} - M_{4,5}M_{4,5}(M_{4,5})$ satellites came a few decades later with the coincidence experiments performed by Thurgate's group [184, 187] on open band transition metals such as Ni, Fe, Co and Ga. The data measured in these cases allowed the authors to decouple these satellites from their parent diagrammatic lines and to attribute their origin to the L_2 core-hole decay.

Furthermore the measured spectra showed that, contrary to a naive intuition and despite the core lifetime broadening, the processes involving more than one Auger electron and more than two holes in the final state may yield sharper features than the parent diagrammatic lines. This remarkable fact implies that the corresponding satellites may be expected to be atomic-like for high hole-hole Coulomb interaction, that is when the final state level is outside the three holes continuum in analogy with the two holes resonances of the CS model.

towards a final state characterized by two final holes in the $2p_{3/2}$ shell and in the $3d$ valence band. The $2p_{3/2}$ then decays by a normal CVV Auger transition in presence of a localized $3d$ spectator hole.

Element	$2p_{1/2}$ [eV]	$2p_{3/2}$ [eV]	$2p_{1/2} - 2p_{3/2}$ [eV]	$3d$ [eV]
Fe	719.9	706.3	13.6	9.34
Co	793.2	778.1	15.1	8.99
Ni	870	852.7	17.3	10.21
Ga	1143.2	1116.4	26.8	18.7

Table 4.7. *Free atom binding energies [185, 186] for holes created in the $2p_{1/2}$, $2p_{3/2}$ and $3d$ shells of transition metals.*

With this work [181, 182, 183] we set up a model aimed for the calculation of such line shapes, allowing to identify the sharpest structures in the Auger spectra from open band materials and to arrive to a general recipe for evaluating correlated three holes Green's functions.

4.5.1 The Model

As we anticipated a few lines ago we address to the L-LLM-MM(M) processes although our considerations are completely general and apply to M-MMN-NN(N) and many other kinds of CK preceded processes. The total Hamiltonian of the system can be decomposed as:

$$\widehat{H}_{tot} = \widehat{H} + \widehat{H}_A + \widehat{T}_A + \widehat{T}_p, \tag{4.57}$$

where $\widehat{T}_A$ and $\widehat{T}_p$ account for the kinetic energy respectively of the Auger electron and the photoelectron in the hole picture:

$$\widehat{T}_A = \sum_k \xi_k c_k c_k^+, \quad \widehat{T}_p = \sum_p \xi_p c_p c_p^+. \tag{4.58}$$

$\widehat{H}_A$ of Eq.(4.57) represents instead that part of the Coulomb interaction operator which is responsible for the Auger transitions and which can be further split in the sum of two operators accounting for the CK and the CVV processes:

$$\widehat{H}_A = \widehat{H}_A^{(CK)} + \widehat{H}_A^{(CVV)}, \tag{4.59}$$

thereby disregarding the possible contributions of other decay channels. The corresponding explicit expressions for these two operators in the hole picture are:

$$\begin{aligned}\widehat{H}_A^{(CK)} &= \sum_k \sum_{dd'} \sum_{\alpha} (W_{\alpha d' dk} c_{d'}^+ c_\alpha^+ c_d c_k + h.c.), \\ \widehat{H}_A^{(CVV)} &= \sum_k \sum_{d} \sum_{\alpha\alpha'} (W_{\alpha\alpha' dk} c_{\alpha'}^+ c_\alpha^+ c_d c_k + h.c.).\end{aligned} \tag{4.60}$$

Here $\widehat{H}_A^{(CK)}$ produces the precursor CK decay and the sums, which are present in its expression in Eq.(4.60), run over k and α, that is respectively over all CK electron states and over valence M states. Summations over d and d' run instead over all deep electron states. In a similar way $\widehat{H}_A^{(CVV)}$ describes the CVV Auger transition following the precursor CK decay and the sum over α and α', appearing in the explicit formulation of this operator, runs over all final hole states in the M shell. All the remaining terms are included in $\widehat{H}$, which hence describes the dynamic of the systems with no Auger transitions.

The expression we used to evaluate the Auger current is deeply rooted in the one step theory for Auger transitions made by Gunarsson and Schönhammer [13], whose main principle have been described in Chapter 2. The formula they give to describe the Auger current can be easily extended to the case with two emitted Auger electrons (when the first Auger electron is not detected). Neglecting contributions which are off-diagonal in the deep hole states, the Auger current can be written as:

$$\begin{aligned}J_k(\omega) &= 2\pi f^2 \sum_{p,d} |\tau_{pd}|^2 \langle \phi_g | c_d \frac{1}{z^* - \widehat{H} - \widehat{H}_A - \widehat{T}_A - \xi_p} \widehat{H}_A n_k \delta(E + \omega - \widehat{H} - \widehat{T}_A - \xi_p) \cdot \\ &\quad \cdot n_k \widehat{H}_A \frac{1}{z - \widehat{H} - \widehat{H}_A - \widehat{T}_A - \xi_p} c_d^+ |\phi_g\rangle.\end{aligned} \tag{4.61}$$

The several terms appearing in this equation are:

- $|\phi_g\rangle$ = the ground state of the system Hamiltonian $\widehat{H}$, with energy E;
- ω = the energy of the impinging photon (we set here and henceforth $\hbar = 1$);
- $z = E + \omega + i\delta$ with $\delta = 0^+$;
- τ_{pd} = the radiation-matter interaction connecting the photoelectron to the deep electron state;
- f = the amplitude of the external electromagnetic field;

- n_k = the Auger electron number operator.

The H_A operators in the denominators of Eq.(4.61) produce any number of virtual Auger transitions after the deep hole creation and before the real transition take place: this can mix different decay channels giving interference effects. Treating H_A as a perturbation, virtual transitions and the mixing with other channels can be neglected and Eq.(4.61) reads as:

$$\begin{aligned} J_k(\omega) \simeq\ & 2\pi f^2 \sum_{p,d} |\tau_{pd}|^2 \langle\phi_g| c_d \frac{1}{z^* - \widehat{H} - \xi_p} \widehat{H}_A^{(CK)} \frac{1}{z - \widehat{H} - \widehat{T}_A - \xi_p} \widehat{H}_A^{(CVV)} n_k \cdot \\ & \cdot\delta(E + \omega - \widehat{H} - \widehat{T}_A - \xi_p) n_k \widehat{H}_A^{(CVV)} \frac{1}{z - \widehat{H} - \widehat{T}_A - \xi_p} \widehat{H}_A^{(CK)} \frac{1}{z - \widehat{H} - \xi_p} \cdot \\ & \cdot c_d^+ |\phi_g\rangle, \end{aligned} \tag{4.62}$$

where we made use of:

$$\widehat{H}_A \frac{1}{z - \widehat{H} - \widehat{H}_A - \widehat{T}_A - \xi_p} c_d^+ |\phi_g\rangle \simeq \widehat{H}_A^{(CVV)} \frac{1}{z - \widehat{H} - \widehat{T}_A - \xi_p} \widehat{H}_A^{(CK)} \frac{1}{z - \widehat{H} - \xi_p} \cdot c_d^+ |\phi_g\rangle \tag{4.63}$$

and of its hermitian conjugate expression. Reading Eq.(4.63) from the right it describes the evolution of the deep hole which is followed by the Auger decay and the creation of the first Auger electron. The latter evolves with the systems while the second Auger electron is finally created by $\widehat{H}_A^{(CVV)}$.

Eq.(4.62) is still too involved and, for a first orientation in this complex problem, we searched for some other simplification which lead us to what we called the "*three step approximation*", in analogy with the two step model described in Chapt.2. To understand the physics underlying this approximation some considerations about the main mechanisms suspected to be the responsible of the observed spectra have a fundamental importance. First we remark that correlation effects must play a dominant role in these transitions and the observed structures are strictly connected with the breaking of the independent particle picture for the description of the valence holes. In the independent particle picture there would be ample time for the M spectator hole to delocalize before the L_3 hole decays, since the valence band width is expected to be much larger than the L_3 core-level width. In this case the influence of a far away spectator hole should be negligible and one should observe a normal L_3VV decay initiated by the L_2 hole. There should be no reason to expect any narrowing of the satellite

line shape, but on the contrary, one would predict a broadening due to a convolution with the L_2 core line. Any deviation from this result as the ones observed in Co and Ni [184, 187] must come from processes starting with a local $M_{4,5}$ spectator hole during the Auger decay of the L_3 hole, before the $M_{4,5}$ hole escapes and/or bound to a resonance. For the reasons above we expect that the two holes resonances of the CS theory must be involved in keeping the spectator hole on site. The intensity of the three holes satellite should be computed in terms of the probability of decay in presence of a localized spectator hole in the sample valence band, ($M_{4,5}$), and the probability that this spectator sticks on the same site where it was created may be estimated as the intensity of the split-off peak of the $L_3M_{4,5}$ resonance. Since this intensity vanishes or is small unless the hole-hole interaction U is comparable with the band width, one should see no change at all compared to the $L_3M_{4,5}M_{4,5}$ line shape unless we are rather close to the atomic-like limit. In the light of the above discussion, we argue that the ($M_{4,5}$) hole is localized with high probability in a two holes resonance, a property which requires strong correlation. The same spectral region should also contain intensity arising from the band-like part of the $L_3M_{4,5}$ resonance contributing with a normal L_3VV feature that will show no narrowing and will tend to broaden the sharp features and hence complicate the diagnosis. It is worth to note that the narrow CK line shapes observed from transition metals entail strong contributions coming from the $L_2M_{4,5}$ two holes resonance, $|i\rangle = c^+_{L_2}c^+_M|\phi_g\rangle$, when $\widehat{H}^{(CVV)}_A$ acts on the wave packet representing the state of the system. The spectral features must be then referred to an initial state energy $E = \langle i|\widehat{H}|i\rangle$.

Returning to the three step approximation, we can say that it consists in treating the initial photoionization, the CK transition and the following Auger decay as three independent processes not interfering one with the other, that is we are assuming that the system undergoes photoionization and CK transition getting ionized but not excited. This brings to a further simplification of Eq.(4.63), which now reads as:

$$\widehat{H}^{(CVV)}_A \frac{1}{z-\widehat{H}-\widehat{T}_A-\xi_p}\widehat{H}^{(CK)}_A \frac{1}{z-\widehat{H}-\xi_p}\cdot c^+_d|\phi_g\rangle \simeq c^+_{\alpha_1}c^+_{\alpha_2}c^+_{\alpha_3}|\phi_g\rangle. \tag{4.64}$$

Within the three step model one can compute the multiplet of final ionic states arising from the CK decay and their probabilities providing the initial states for the final CVV Auger decay. Each of the initial LM states gives access to a MMM multiplet final state. Once again the Auger spectrum is calculated, up to a constant, by means of the expression:

$$S(\omega) = -Im\{Tr[A^+(\omega)\Phi(\omega)A(\omega)]\}, \tag{4.65}$$

where A is the Auger matrix and Φ is the three holes Green's function matrix. The density of states for the MMM satellite can be obtained within the three step model from a three holes Green's function:

$$\Phi_{\alpha_1,\alpha_2,\alpha_3;\beta_1,\beta_2,\beta_3}(z) = \langle 0|c_{\alpha_3}c_{\alpha_2}c_{\alpha_1}\frac{1}{z-H}c^+_{\beta_1}c^+_{\beta_2}c^+_{\beta_3}|0\rangle. \tag{4.66}$$

Here the α's and the β's represent spin-orbital states on the valence shell of the Auger site, while the average is over the vacuum, $|0\rangle$, since we are specializing to the closed band case.

4.5.2 Modeling the Three Particle Green's Function

To gain the three particles Green's function expressed by Eq.(4.66) an Anderson-like model has been used:

$$\widehat{H} = \widehat{H}_{at} + \widehat{H}_S + \widehat{V}, \tag{4.67}$$

where $\widehat{H}_S$ and $\widehat{H}_{at}$ describe respectively the solid and the atom where the considered Auger decay is taking place, while $\widehat{V}$ accounts for one-body hopping terms between the two:

$$\begin{aligned} \widehat{H}_S &= \sum_\alpha \sum_k \varepsilon_{k\alpha} c^+_{k\alpha} c_{k\alpha}, \\ \widehat{V} &= \sum_\alpha \sum_k V_{k\alpha}(c^+_{k\alpha} c_\alpha + c^+_\alpha c_{k\alpha}). \end{aligned} \tag{4.68}$$

The $\widehat{V}$ expression is based on the assumption that a hole in the atomic state α can only hop into the corresponding continuum of states $\{k\alpha\}$. By labeling with α the k-states we are assuming that the solid does not significantly perturb the spherical symmetry of each atom. This hypothesis is reasonable for metals, whose local fields are very weak. As far as the atomic Hamiltonian is concerned, it is given instead by the sum:

$$\widehat{H}_{at} = \widehat{H}^{(0)}_{at} + \widehat{H}_C, \tag{4.69}$$

where $\widehat{H}^{(0)}_{at} = \sum_\alpha \varepsilon_\alpha c^+_\alpha c_\alpha$ is the one-body term and $\widehat{H}_C$ the Coulomb interaction one:

$$H_C = \sum_{\alpha_1,\alpha_2,\alpha_3,\alpha_4} U_{\alpha_1,\alpha_2,\alpha_3,\alpha_4} c^+_{\alpha_1} c^+_{\alpha_2} c_{\alpha_4} c^+_{\alpha_3}. \tag{4.70}$$

This model tacitly assumes that the screening modes are fast compared to hole hopping times (essentially $\omega_p \gg V_{k\alpha}$, with ω_p the plasma frequency), otherwise the dynamics of polarization should be included explicitly.

The procedure we adopted to obtain the interacting three particles Green's function consists in projecting a Dyson-like equation on all the states making up the Hilbert space of the treated problem. This yields to a system of coupled equations which are closed thanks to the initial assumption of closed valence band and so we were able to solve the problem. The equations are not easy but can be handled by the cunning to be discussed below.
Starting from the final three holes state, $|A\rangle = c^+_{\alpha_1} c^+_{\alpha_2} c^+_{\alpha_3}|0\rangle$, we can generate all the other states making up the Hilbert space of the system by simply allowing the delocalization in the solid firstly of one hole, then of two and finally of three ones, leading respectively to states characterized by two, one and no holes on the Auger atom. Introducing a short hand notation these states can be indicated as for example $|A^1_k\rangle = c^+_{k\alpha_1} c^+_{\alpha_2} c^+_{\alpha_3}|0\rangle$ for a three particle states with two holes localized on the Auger site and one hole delocalized in the solid, or as $|A^2_k\rangle = c^+_{k\alpha_1} c^+_{k\alpha_2} c^+_{\alpha_3}|0\rangle$ for states with only one localized hole and so on. The dynamics mixes determinants with different labels. In this way as a starting point of our procedure we would not have to consider only the state $|A\rangle$ to generate the Hilbert space of the system, but also $|B\rangle = c^+_{\beta_1} c^+_{\beta_2} c^+_{\beta_3}|0\rangle$, $|C\rangle = c^+_{\gamma_1} c^+_{\gamma_2} c^+_{\gamma_3}|0\rangle$,...
Once the Hilbert space of the system has been built, the non interacting three holes Green's function is defined according to:

$$\Phi^{(0)}_{A,B}(z) = \langle A|\frac{1}{z-\widehat{H}_0}|B\rangle, \tag{4.71}$$

where $\widehat{H}_0 = \widehat{H} - \widehat{H}_C$ is the non interacting part of the system Hamiltonian. $\Phi^{(0)}_{A,B}$ is used then to generate the following Dyson equation for the interacting three particles Green's function:

$$\Phi_{A,B}(z) = \Phi^{(0)}_{A,B} + \sum_{\gamma_1,\gamma_2,\gamma_3,\gamma_4} U_{\gamma_1,\gamma_2,\gamma_3,\gamma_4} \langle A|\frac{1}{z-\widehat{H}_0} c^+_{\gamma_1} c^+_{\gamma_2} c_{\gamma_4} c_{\gamma_3} \frac{1}{z-\widehat{H}}|B\rangle. \tag{4.72}$$

As we anticipated we can take advantage of the initial assumption of a fully occupied valence band allowing these equations to be closed and so exactly solved. Thanks to this

assumption in fact the insertion of the operator $\widehat{I} = \sum_\beta (c^+_\beta c_\beta + \sum_k c^+_{k,\beta} c_{k,\beta})$ between $c^+_{\gamma_2}$ and $c^+_{\gamma_3}$ in Eq.(4.72) is equivalent to the insertion of a complete set of states. Due to particle conservation, the insertion of $\widehat{I}$ allows to recast Eq.(4.72) as [181, 182, 183]:

$$\underline{\Phi} = \underline{\Phi}^{(0)} + \underline{\Phi}^{(0)} \cdot \underline{U} \cdot \underline{\Phi} + \sum_k \underline{\Phi}^{(0)}_k \cdot \underline{U} \cdot \underline{\Phi}_k. \tag{4.73}$$

In the above expression each amplitude is a matrix in the three particles Hilbert space of the atom, i. e. $(\underline{\Phi})_{A,B} = \Phi_{A,B}$, $(\underline{\Phi}_k)_{A,B} = \Phi_{A^1_k,B}$, $(\underline{\Phi}^{(0)}_k)_{A,B} = \Phi^{(0)}_{A^1_k,B} = \Phi^{(0)}_{B,A^1_k}$, $(\underline{\Phi}^{(0)}_k p)_{A,B} = \Phi^{(0)}_{A^1_k,B^1_k}$, etc., while the matrix $\underline{U}$ has matrix elements $U_{C,D} = U_{\gamma_1,\gamma_2,\gamma_3;\delta_1,\delta_2,\delta_3} = \delta_{\gamma_3\delta_3} U_{\gamma_1,\gamma_2;\delta_1,\delta_2}$. Proceeding along similar lines, one finds the second system of coupled equations which have to be solved together with Eq.(4.73) [181, 182, 183]:

$$\underline{\Phi}_k = \underline{\Phi}^{(0)}_k + \underline{\Phi}^{(0)}_k \cdot \underline{U} \cdot \underline{\Phi} + \sum_p \underline{\Phi}^{(0)}_{kp} \cdot \underline{U} \cdot \underline{\Phi}_p. \tag{4.74}$$

4.5.3 The Rectangular Band Case and the ^4F State

As a first simple application of this model we restrict our analysis to consider the case of a single monodeterminantal three holes final state, the ^4F, which can be written in the three step approach as $c^+_{m_l=0\uparrow} c^+_{m_l=1\uparrow} c^+_{m_l=2,\uparrow} |0\rangle$. The atomic Hamiltonian is the sum of:

$$\widehat{H}^{(0)}_{at} = \sum_{m_{l_i}=-2}^{2} \varepsilon_{m_{l_i}} c^\dagger_{m_{l_i}} c_{m_{l_i}}; \qquad \widehat{H}_C = \sum_{m_{l_1}+m_{l_2}=m_{l_3}+m_{l_4}} U_{m_{l_1} m_{l_2} m_{l_3} m_{l_4}} c^\dagger_{m_{l_1}} c^\dagger_{m_{l_2}} c_{m_{l_4}} c_{m_{l_3}} \tag{4.75}$$

To further simplify our analysis we restrict to degenerate atomic levels, $\varepsilon_{m_{l_i}} = \varepsilon_0$ for all i, and to hopping integrals independent of the magnetic quantum number m_{l_i}, $V_{k m_{l_i}} = V_k$. In this case the two holes states of the Hilbert space of the system, geometrically represented in Fig.(4.26), are given not only by the four states obtained setting free one electron from the $|^4F\rangle$, $\{|i,k\rangle\} = \{|m_{l_p} \uparrow, m_{l_q} \uparrow, m_{l_r} k \uparrow\rangle\}$[18] ($m_{l_{p,q,r}} = 0,1,2$), that is all those states which can be reached by diagonal scattering $(i,j) \leftrightarrow (j,i)$. We must take into account in

[18]Here and henceforth we will drop the spin index for each hole quantum numbers set, being implied it is always $\uparrow$.

fact also another state, $c^{+}_{m_l=2,k}c^{+}_{m_l=-1}c^{+}_{m_l=2}|0\rangle$, which can be reached only by the Coulomb interaction $\widetilde{U}$ with the $c^{+}_{m_l=0\uparrow}c^{+}_{m_l=1\uparrow}c^{+}_{m_l=2k,\uparrow}|0\rangle$ and not by hopping[19] from $|^4F\rangle$. In this way $\widehat{H}_C$ in (4.75) can be re-written as:

$$\begin{aligned}\widehat{H}_C &= U_0 c_1^\dagger c_2^\dagger c_2 c_1 + U_1 c_0^\dagger c_2^\dagger c_2 c_1 + U_2 c_0^\dagger c_1^\dagger c_1 c_0 \\ &+ \tilde{U}(c_0^\dagger c_1^\dagger c_2 c_{-1} + c_{-1}^\dagger c_2^\dagger c_1 c_0) + \dots \end{aligned} \tag{4.76}$$

where the remaining terms can be neglected as they do not contribute.

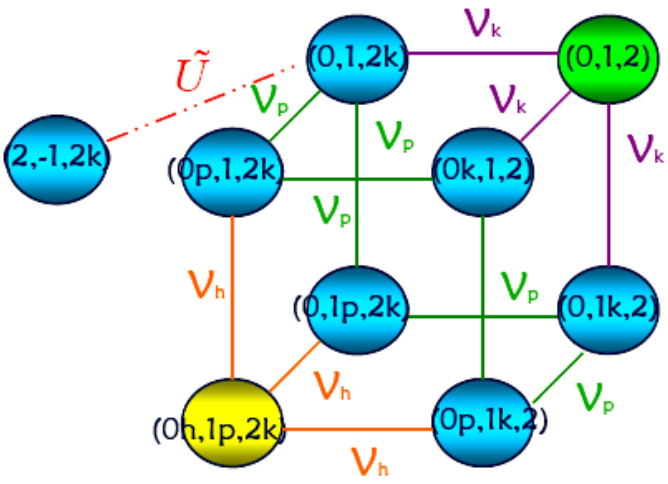

Figure 4.26. Schematic representation of the Hilbert space of the system for the case of a final ^4F state. The green vertex of the cube represents the ^4F generating all the other states making up the Hilbert space of the system. All the blue vertices, connected to ^4F by the hopping term V_k, are the states characterized by two holes localized on the Auger atom and another one which is delocalized in the solid. From these states we can jump by V_p on all the remaining states represented as blue vertices of the cube, which are the states characterized by only one localized hole and two delocalized ones. The state where all the three holes are delocalized in the solid is represented instead by the yellow vertex. This geometric representation of the Hilbert space of the system gives evidence to the fact that all the vertices of the cube represent states which are reachable by hopping from each "vertex state" that is connected to them by "hopping edges" V_i ($i = k,p,h$). There exists also another state (outside of the cube), the off-diagonal scattering one (see text), which can be get only by Coulomb interaction, $\widetilde{U}$, from the $c^{+}_{m_l=0\uparrow}c^{+}_{m_l=1\uparrow}c^{+}_{m_l=2k,\uparrow}|0\rangle$ state.

As anticipated, to gain a prediction for the CK three holes line shape the quantity we are interested in is the interacting three holes Green's function which is in this case:

[19] For this reason we refer to this state as *off-diagonal scattering state*.

$$\Phi(z) = \langle {}^4F | \frac{1}{z - \widehat{H}} | {}^4F \rangle, \tag{4.77}$$

where:

$$\widehat{H}_C | {}^4F \rangle = \Omega | {}^4F \rangle; \quad \Omega = U_0 + U_1 + U_2. \tag{4.78}$$

Solution for $\widetilde{U} = 0$

This special case is useful as the simplest possible three holes model which shows the mixing of local and band features and is a counterpart of Ref.[35].

For this case in fact we found an approximate solution of the system given by Eqs.(4.73) and (4.74), which is valid for all cases where the final three holes state is a monodeterminantal one. To make easier the understanding of the formula we found, we illustrate the problem for the narrow band limit, involving a single k state, with the Hamiltonian:

$$\widehat{H} = \begin{pmatrix} \varepsilon_0 + \Omega & \sqrt{3}V_k & 0 & 0 \\ \sqrt{3}V_k & 2\varepsilon_0 + \varepsilon_k + U & 2V_k & 0 \\ 0 & 2V_k & \varepsilon_0 + 2\varepsilon_k & \sqrt{3}V_k \\ 0 & 0 & \sqrt{3}V_k & 3\varepsilon_k \end{pmatrix}. \tag{4.79}$$

Here we take $U_i \equiv U$. The three holes Green's function $\Phi(z)$ is given by the $(1,1)$ element of the inverse of the $(z - \widehat{H})$ operator, which can be written as:

$$\Phi(z) = \cfrac{1}{z - 3\varepsilon_0 - \Omega - \cfrac{V_k^2}{z - 2\varepsilon_0 - \varepsilon_k - U_i - 4\cfrac{V_p^2}{z - \varepsilon_0 - \varepsilon_k - \varepsilon_p - 3\cfrac{V_p^2}{z - 3\varepsilon_k}}}}. \tag{4.80}$$

We seek an extension of this formula to three different U_i and a finite bandwidth centered at ε_0 knowing that the result must be symmetric on U_i. Thus we write [181, 182, 183]:

$$\Phi(z) = \cfrac{1}{z - 3\varepsilon_0 - \Omega - \sum_{i,k} \cfrac{V_k^2}{z - 2\varepsilon_0 - \varepsilon_k - U_i - 4\sum_p \cfrac{V_p^2}{z - \varepsilon_0 - \varepsilon_k - \varepsilon_p - 3\Sigma(z - \varepsilon_k - \varepsilon_p)}}},$$

(4.81)

where $\Sigma(z) = \sum_k V_k^2/(z - \varepsilon_k)$ is the self-energy. This is a strikingly good formula having the correct normalization and the Herglotz property (see Chapter 2).

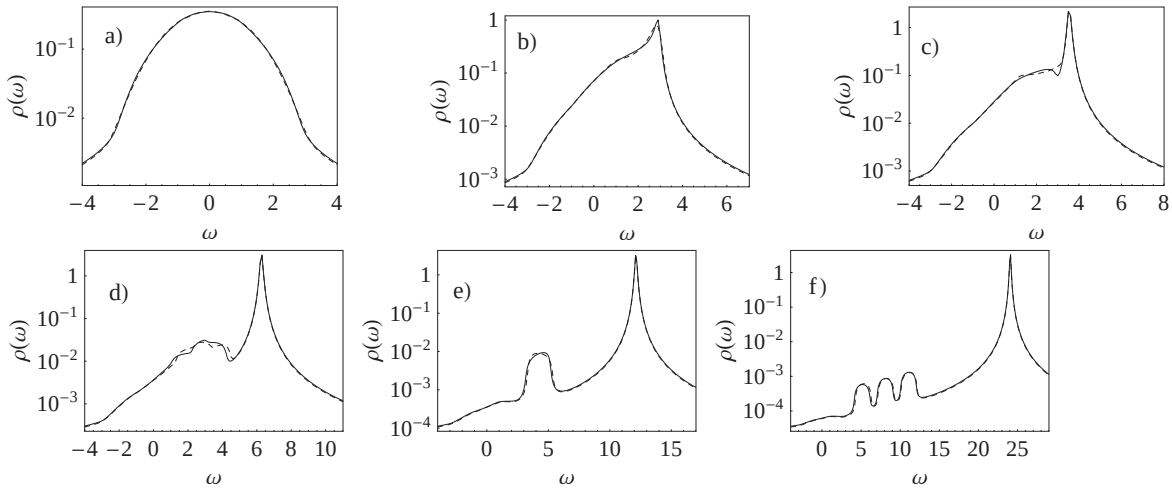

Figure 4.27. [181, 182, 183]. Plot of $\rho(\omega) = -(1/\pi)\mathrm{Im}[\Phi(\omega + i0^+)]$ for the exact numerical solution (solid line) and for the approximate solution of Eqs.(4.73-4.74) (dashed line) in the case of a rectangular band for different values of the Coulomb parameters U_i: a) $U_0 = U_1 = U_2 = 0$; b) $U_0 = 0.4$, $U_1 = U_2 = 0.8$; c) $U_0 = U_1 = U_2 = 1$; d) $U_0 = U_1 = 1.5$, $U_2 = 3$; e) $U_0 = U_1 = U_2 = 4$; f) $U_0 = 5$, $U_1 = 8$, $U_2 = 11$. The values of U and ω are in units of a. The exact solution has been obtained with $N_k = 24$ states.

To illustrate the physical meaning of the result provided by the powerful Eq.(4.81), this formula has been applied as a test-bed to the case of a rectangular valence band. To this end the Anderson model parameters ε_0 and V_k have been chosen in such a way that the corresponding expression for the 1hLDOS is:

$$\rho(z) = -\frac{1}{\pi} Im[g(z)] = \frac{\theta(\frac{W}{2} - |z|)}{W}, \tag{4.82}$$

where W is the bandwidth and $g(z)$ is the single particle Green's function. Fig.(4.27) displays the comparison between the interacting three particles Green's function, $\rho(\omega) = -\frac{1}{\pi} Im[\Phi(\omega + i\delta)]$, gained by Eq.(4.81) (dashed line) and the exact numerical solution (solid line) of the system of coupled equations (Eqs.(4.73) and (4.74)) obtained by taking a finite number of k-states[20], $N = 24$. The several panels of Fig.(4.27) refer to similar calculations which have been performed starting from different sets of U_i values.

[20]The numerical results have been proved to converge rather quickly with increasing the number of k-states, N_k. The way the exact numerical solution has been gained is described in Appendix C.

As one can see the approximate solution cannot be distinguished from the exact one. As expected, by analogy with the two holes resonances, the spectra remain band-like when $\gamma \equiv U/W \ll 1$ but the line shape is progressively distorted with increasing γ, see panel b). Intermediate cases [panels c) to d)] show new features, and besides the distorted continuum one can observe a non-split-off two holes resonances around $\omega \sim U$ and three holes resonances at energies of about Ω. For $\gamma \gg 1$ [panel e) and f)] split-off two holes resonances and a quasi-atomic three holes resonance develop. The two holes resonances are not sharp but rather smeared out and their width is of the order of W. This is due to the bound hole that virtually explores the valence band. We observe that the two holes resonances have rather small and unequal intensity as compared to the pronounced three holes peak and that the residual spectral weight of the original band is quite small. APECS however would allow to observe these structures because the background measured by this technique is usually so small that weak continua can be detected as in the case of the Cu band residuum [14].
The approximation given by Eq.(4.81) is remarkably good: the only ones that show some differences are the patterns displayed in panel c), which have been obtained for all U_i equal to half of the bandwidth ($\gamma = 1$). Despite this modest discrepancy occuring in special cases, the approximation is about as reliable as the model itself can be.

Solution for $\widetilde{U} \neq 0$

In the more general case of a nonvanishing off-diagonal scattering, $\widetilde{U} \neq 0$, $\Phi(z)$ is obtained as $[g \otimes P](z)$ where $\otimes$ stands for a convolution product, g is the single particle Green's function and P is the interacting two holes Green's function [181, 182, 183]:

$$P(z) = \frac{1}{P_0^{-1}(z) - \tilde{U}^2 P_0(z)}, \tag{4.83}$$

while $P_0(z) = [g \otimes g](z)$ is the non-interacting one. The effects produced by having $\widetilde{U} \neq 0$, can be understood from Fig.(4.28), where the underlying mechanism of off-diagonal scattering is represented. In this figure the hole with $m_l = 2$ propagates freely, while holes with $m_l = 0$ and $m_l = 1$ undergo multiple scattering processes due to the $\widetilde{U}$ coupling with holes characterized by $m_l = 2$ and $m_l = -1$.

In Fig.(4.29) the interacting three holes Green's function calculated for different values of U_i is compared with the exact results obtained again for a finite k-number, $N_k = 24$.

Also this time we observed in the calculated spectra the same analogies with the two holes phenomenology of the CS theory as we found for the $\tilde{U} = 0$ case, but for $\tilde{U} \neq 0$ new

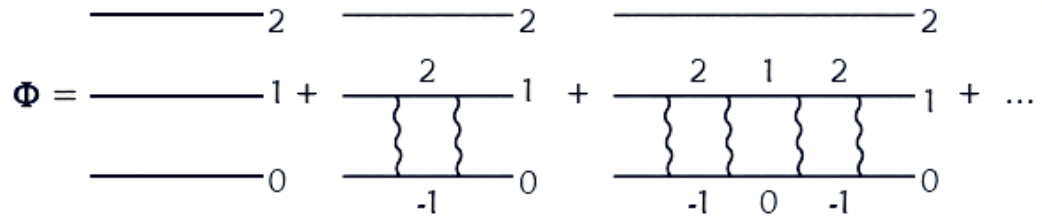

Figure 4.28. Diagrammatic representation of the three hole Green's function $\Phi(z) = [G \otimes P](z)$ [181, 182, 183]. The label on each propagator specifies the magnetic quantum number m_l of the hole, while wiggly lines represent the interaction $\widetilde{U}$.

interesting features arise. It is found in fact that the presence of a non vanishing $\tilde{U}$ acts only on one of the three U_i, namely U_2, which undergoes a sort of "dynamical renormalization" of U_2. Physically this is due to the possibility of multiple scattering of the two holes with $m_l = 0{,}1$ between the states $c^+_{m_l=2,k}c^+_{m_l=-1}c^+_{m_l=2}|0\rangle$ and $c^+_{m_l=2,k}c^+_{m_l=0}c^+_{m_l=1}|0\rangle$, making U_2 behave as $\widetilde{U}^2/z$ for large z. This explains the splitting of the resonance at about U_2 in two ones at energies $\sim U_2 \pm |\tilde{U}|$.

The results for the exactly solvable model for $U_0 = U_1 = U_2 = 0$ and $\tilde{U} \neq 0$ are shown in panel (a) of Fig.(4.29). Panel (b.1) ($\tilde{U} = 0$) exhibits instead a spectrum with a split-off three holes peak at energy $\sim W$ and a distorted continuum but, increasing $\tilde{U}$, well defined two holes structures start to develop. They eventually split off from the top and the bottom of the continuum as in panels (b.2) and (b.3). The same behavior is observed for $U_0 = U_1 = U_2 = 4$ (panel (c)), where the only difference is the fact that the continuum is completely dominated by the degenerate two holes resonance. The strong coupling limit is considered in panel (d). The effect of the dynamical renormalization of U_2 is evident in the strong coupling limit, which is shown in panel (d). Indeed in fact the two holes resonances at U_0 and U_1 are not affected by $\tilde{U}$, while the one at U_2 splits into a double resonance at energies $\sim U_2 \pm |\tilde{U}|$ (see panels (d.2) and (d.3)).

A direct consequence of the Pauli Exclusion Principle is the complete lack of sensitiveness of the three holes resonance to the strength of $\tilde{U}$, which is evident from all panels of Fig.(4.29). This is due to the fact that the scattering $(m_{l_i},m_{l_j}) = (0{,}1) \leftrightarrow (2,-1)$ is forbidden in presence of a hole with $m_l = 2$ on the local site.

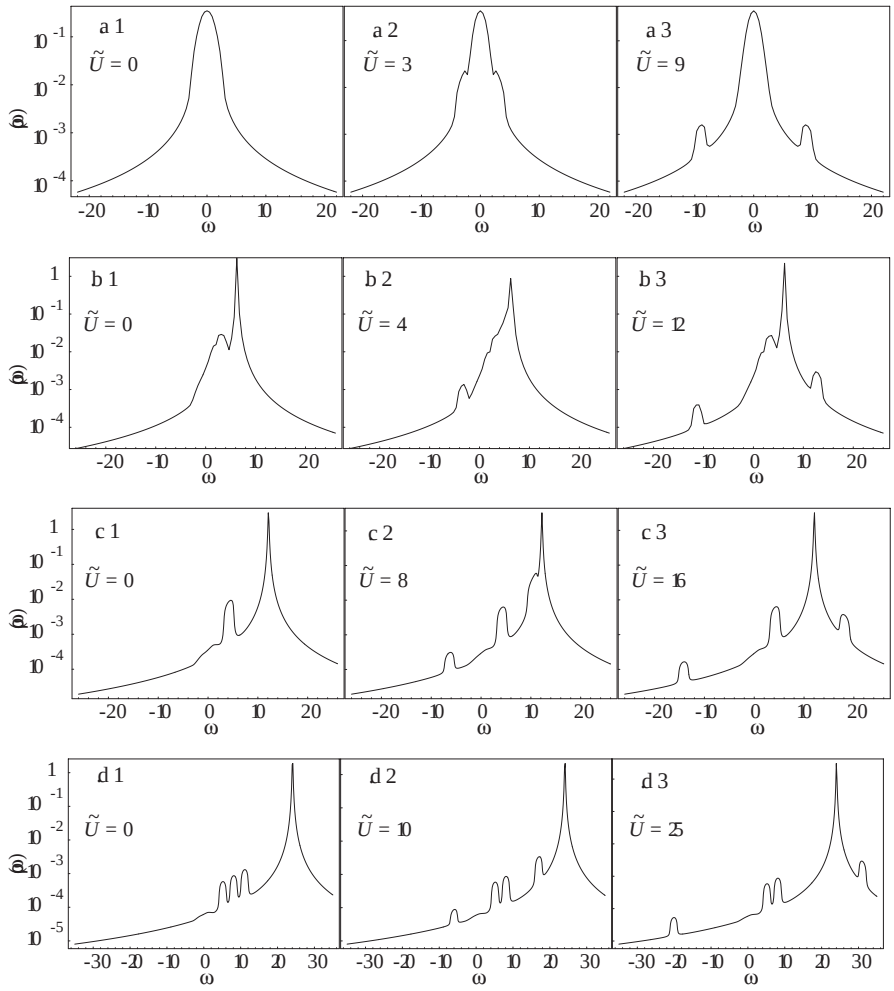

Figure 4.29. Each panel displays the plot of $\rho(\omega) = -(1/\pi)\mathrm{Im}[\Phi(\omega + i0^+)]$ as obtained from the numerical solution of the Eqs.(4.73-4.74) in the case of a rectangular band [181, 182, 183]. All the showed pattern are calculated for different values of the Coulomb parameters U_i and increasing $\tilde{U}$. a) $U_0 = U_1 = U_2 = 0$; b) $U_0 = U_1 = 1.5$, $U_2 = 3$; c) $U_0 = U_1 = U_2 = 4$; d) $U_0 = 5$, $U_1 = 8$, $U_2 = 11$. The values of the U's and ω are in units of a.

4.5.4 Discussion

Till today the field of CK preceded Auger satellites was theoretically quite undiscovered and experimentally neglected because of the reputation of this kind of transitions as a mere background. This work clearly shows that CK preceded Auger satellites are instead a real mine of information about strongly correlated materials because they give us the opportunity to characterize the system by measuring what happens when a strongly correlated system responds to a strong local perturbation. The line shapes of these processes in fact contain information on three holes multiplet states of the atom and on the two holes multiplets that result when

one of the holes explores the surroundings. The two holes multiplet structures differ widely in shape and intensities from those of the Auger transitions leading to two valence holes. For instance peaks corresponding to forbidden Auger transitions can be prominent in CK satellites. Moreover, the two holes states displayed in Figs.(4.27) and (4.29) have a broadening of the order of the band width.

Also the position where the two holes structures are expected to be observed are quite different from the ones foreseen by the CS theory, that is by the corresponding parent diagrammatic transitions as we discuss in the following. A first attempt of peak position forecast may be done starting from values and coincidence spectra presented in Ref.[14] for the case of Copper. In this work in fact the $L_2M_{4,5}M_{4,5}$ and $L_3M_{4,5}M_{4,5}$ coincidence spectra of Cu were measured and the most prominent structures analyzed using the Cini [35] and Sawatzky [36] theories for the two-hole features and atomic multiplet calculations of the CK transitions. For both these features the atomic Slater integrals were employed. By using free-atom data [188], they were corrected for an extra-atomic relaxation, R_{ea}, which was evaluated as $\sim 13{,}5$ eV. Further semiempirical estimates were $U = 7$ eV for the $d_8\ ^1G$ configuration and $Q = 9$ eV for the average $2p$ hole-$3d$ hole interaction. Assuming that a representative value for the [184] Coulomb interaction in the three holes $M_{4,5}M_{4,5}(M_{4,5})$ multiplet is $3U$, and taking into account the interaction Q in the initial LM state, the three holes feature should be at $3U - Q$ lower kinetic energy than the M band residuum. Its kinetic energy was estimated to be lower than the ^1G peak of the $L_2M_{4,5}M_{4,5}$ by an energy:

$$\Delta E = E(CVV) - E(d^7) = 2U - Q. \tag{4.84}$$

In the case of Cu it turned out that $\Delta E \sim 5$ eV. This estimate was in good agreement with experiment, allowing for a clear-cut assignment of the spectral features. Therefore, in the interesting case [14] of the Cu $L_3M_{4,5}M_{4,5}$ spectrum, the ~ 2 eV wide two holes satellites described in the previous subsections should be sought at about $\sim 2U \sim 14$ eV on the high kinetic energy side of the three holes structure, or else at ~ 930 eV. The weak three holes continuum should be centered around 937 eV, where the $L_2M_{4,5}M_{4,5}$ transitions are much stronger. Unfortunately the spectra shown in Ref.[14] do not display any two holes feature coming from the three particles Green's function, but we expect they should be found by increasing the APECS signal to noise ratio.

In conclusion, more modeling and computational work is needed in order to compare the above results with experiment and such work is currently under way. Here we have tried

to address some simpler aspects of the theoretical problems that CK transitions pose, in order to prepare the ground to a future extended theory. Finally, we observe that the present formalism is expected to have a wider scope, since in most of the periodic Table one observes satellite lines like those seen in Mg [189] which are due to shake-off during the primary photoionization [190]. If the shake-off produces a hole in the valence band, the Auger line shape mirrors a three holes valence density of states modulated by the matrix elements. The method described here for computing the local three holes spectrum should apply to those satellites as well.

5 Conclusions

By recollecting together all the results we gained and which have been presented in Chapter 4, we can say that this thesis fulfilled all the aims we set at its very beginning. Even if they can be improved, the several models we developed give interesting and encouraging results, qualifying them as first steps in several still unexplored directions towards a complete understanding of Auger transitions from strongly correlated materials. Definitely, in this work we did progress in the field of Auger transitions from condensed matter, in particular as far as incompletely filled valence bands materials are concerned.

For solids with a quite completely filled valence band, our models show that the changes we proposed (see Secs.4.1 and 4.3 and Refs. [123]) to adapt the Cini-Sawatzky (CS) model [34, 35, 36] so as to include solid state and spin-orbit effects to describe the corresponding Auger spectra give reliable results by means again of closed formulas. This paves the way to important future perspectives about a more extensive use of Auger spectroscopy as a tool to investigate the role of correlations in complex materials, which are not so different from the closed band ones. As an example this approach as applied to an AR-APECS experiment on a Copper sample allowed to study the spin-selection ability of such a kind of technique [123]. It has been shown that the proposed approach is able in fact to reproduce some important features of the measured spectra, even if the used model is based on a two step approach (see Chapter 2). The fundamental differences between the spectra revealed in the two adopted geometrical configurations are in fact well reproduced by this theory, which is not able however to account for all the intensity difference between the two main peaks of each spectra. To attribute this effect to an effective spin-selective ability of the AR-APECS technique, further calculations are needed but framed this time in a one-step formulation within a multiple

scattering formalism.

By slightly increasing the band hole filling, the CS approach is expected to give no more reliable results. This is the reason why we adopted the Bare Ladder Approximation (BLA) [62, 63, 64] to describe the Auger spectra from Graphite and Single Walled Carbon Nanotubes (SWCN) [150, 151, 152]. In this case we introduce within the theory a novelty: the use of form factors (see Sec.4.3) to properly take into account the different electron population of the bands which are involved in the Auger transition, that is to adapt the model to the case of a quite open band, where more than one valence band take part to the transition. This new approach reproduced quite well the measured spectra. Only one fitting parameter has been used, that is the screening on-site interaction. The adopted model allowed not only to determine the magnitude of Coulomb interactions in SWCN and Graphite, but also to attribute the narrow structure at about 240 eV in the Auger spectra of Graphite to a quasi two holes resonance produced by two σ_s holes.

To set free the model from experimentally determined parameters we developed also a complete ab-initio approach which is based on the use of the Janak's theorem [142] and the Density Functional Theory (DFT) (see Sec.4.2 and Ref.[137, 138]). The position of the multiplet in each spectrum, which crucially depends on the parameters evaluated by our ab initio method, agrees quite well with the experimental one for the case of Zinc, while for Copper our approximations turn out to be rather poor. We attribute this effect mostly to the width and hybridization of the Copper $3d$ band. Other factors contributing to worsen the agreement between theoretical and experimental findings are the off-site interaction[1] (see Sec.2.3.2) and the possibility to compute the total energy in presence of holes in the valence state. The model we developed surely can be improved by taking into account at least these factors, but its current form gives reliable results for at least closed band materials and represents a first effort towards a fully ab-initio approach to set free the modeling of Auger spectra from the experimental brand.

For materials which are characterized by completely open valence bands (i.e. bands populated by an hole-filling $n_h \geq 1$), the spectrum is a combination of relaxed and unrelaxed features [79, 80] and only the latter are contained in a two holes Green's function. Moreover, the BLA breaks down for reasons discussed in Ref. [82] and summarized above. To face the problem of modeling at least the unrelaxed features, we extended the Time Dependent Gutzwiller Approximation (TDGA) [84, 114, 119], a time dependent variational theory, to a

[1] An estimate of the off-site interaction magnitude for Copper can be found in Ref.[123].

three band case so as to apply it to CuO_2 planes [180]. To our complete surprise, the comparison between HFBLA[2] and GA in the three-band model did not go in analogy with the one-band case. The HFBLA, which was expected to be poor, was seen to be rather good, instead, and even preferable in several cases to the GA. The calculated spectra showed also the more atomic-like character of GA patterns and their resemblance with the HFBLA ones for small hole-fillings as expected. A comparison with an experiment or with the exact solution of a cluster which is bigger than a 2×1 one is needed to fully understand which one of the two approximations, HFBLA and GA, is the best to describe this kind of spectra. This work however represents a valid grip for starting to climb the problem of modeling the Auger spectra from strongly correlated open bands materials.

Another instrument for modeling Auger spectra is represented by the theory we built up (see Sec.4.5 and Refs. [181, 182, 183]) to study three holes satellites which are due to Coster-Kronig preceded Auger transitions. This approach in fact can be used, together with the former one, to model Auger spectra from solids which are characterized by incompletely filled valence bands. It makes the user able to disentangle the structures produced by Coster-Kronig transitions from the corresponding parent diagrammatic lines. The model we developed shows that the production of this kind of three holes satellites reproduce a phenomenology which is very similar (even if with some slight modifications) to the one of the CS theory. Increasing in fact the ratio between the Coulomb interaction magnitude and the band width, two holes structures appear besides the sharp three holes one and display a progressively atomic-like appearance. We tested our theory only for the case of a rectangular valence band and assuming that the final three holes state was a monodeterminantal one. More modeling is in order to be performed but to arrive to a direct comparison with the experiment it will be enough to extend our theory at least to a three holes final state which is characterized by a combination of two or three Slater determinants. The formula we found however is of value also outside the particular problem for which it has been reached. It represents one of the few successful attempts that can be found in literature to evaluate a correlated three bodies Green's function.

As it has been said, much more work, both for modeling and computing, has to be done to gain a complete and full understanding of Auger spectra from open bands materials. Thanks

[2]The Hartree Fock BLA (HFBLA) is a BLA where we introduced an HF renormalization of the orbital energies, ε_p and ε_d, that we used as input parameters for the model. This allowed us to take into account the effects of of a mean Coulomb interaction as treated in the Hartree-Fock approximation. For more details see Sec.4.4.3.

also to the little bricks which have been built up by this thesis, it appears however no more a too far target to be fulfilled. The explanation of the Auger spectra from CoO or other strongly correlated and complex materials will be reached soon, enabling us to have access to the mine of information about electronic correlations they promise.

Publications

The following lines report a list of the publications describing in full details the results which have been gained by this thesis:

- E. Perfetto, M. Cini, S. Ugenti, P. Castrucci, M. Scarselli, M. De Crescenzi, F. Rosei e M. A. El Khakani, *Phys. Rev. B* **76**, 233408 (2007);
- E. Perfetto, M. Cini, S. Ugenti, P. Castrucci, M. Scarselli, M. De Crescenzi, F. Rosei e M. A. El Khakani, *arXiv:0710.3721v1 [cond-mat.str-el]* (2007);
- M. Cini, E. Perfetto, G. Stefanucci and S. Ugenti, *Phys. Rev. B* **76**, 205412 (2007);
- E. Perfetto, M. Cini, S. Ugenti, P. Castrucci, M. Scarselli and M. De Crescenzi, *J. Phys.: Conf. Ser.* **100**, 052082 (2008);
- S. Ugenti, M. Cini, E. Perfetto, F. Da Pieve, C. Natoli, R. Gotter, F. Offi, A. Ruocco, G. Stefani, F. Tommasini, G. Fratesi, M. I. Trioni and G. P. Brivio, *J. Phys.: Conf. Ser.* **100**, 072020 (2008);
- M. Cini, E. Perfetto, G. Stefanucci and S. Ugenti, *J. Phys.: Conf. Ser.* **100**, 0720198 (2008);
- M. Cini, E. Perfetto, G. Stefanucci and S. Ugenti, *J. Phys.: Cond. Matt.* **20**, 474209 (2008);
- G. Fratesi, M. I. Trioni, G. P. Brivio, S. Ugenti, E. Perfetto and M. Cini, *Phys. Rev. B* **78**, 205111 (2008);
- G. Fratesi, M. I. Trioni, G. P. Brivio, S. Ugenti, E. Perfetto and M. Cini, *arXiv:0811.3872v1 [cond-mat.str-el]* (2008);

- S. Ugenti, M. Cini, J. Lorenzana, G. Seibold, E. Perfetto and G. Stefanucci, *"The First Application of TDGA to High T_c Superconductors"*, in preparation;

A

How to evaluate Σ_G

As it is shown in [176, 177], the several values of $\Sigma^{\sigma\sigma}_{G_{\alpha\alpha}}$ in Eq.(4.53)[1] can be obtained by using:

$$\Sigma^{\sigma\sigma}_{G_{\alpha\alpha}} = \frac{\partial(T^{\sigma\sigma}_{GA} + T^{-\sigma-\sigma}_{GA})}{\partial\rho_{\alpha_\sigma\alpha_\sigma}}; \tag{A.1}$$

here T_{GA} and $\rho_{\alpha_\sigma\alpha_\sigma}$ are respectively the kinetic term in the Gutzwiller's (GA) Hamiltonian and the operator describing the hole density in the single particle orbital α with spin σ, where in this case α represents the p or d single particle orbital.
The explicit expression for the GA kinetic operator is[2]:

$$T_{GA} = \sum_{ij\sigma'} z_{i_{\sigma'}} z_{j_{\sigma'}} t_{i_{\sigma'}j_{\sigma'}} \rho_{i_{\sigma'}j_{\sigma'}}, \tag{A.2}$$

where the summation is restricted to orbitals belonging to atoms which are the nearest neighbors of the considered one, while $t_{i_{\sigma'}j_{\sigma'}}$ denotes the transfer parameter between the sites i and j (characterized by spin σ'); $\rho_{i_{\sigma'}j_{\sigma'}}$ is the integral corresponding to the overlap between the charge densities of $i_{\sigma'}$ and $j_{\sigma'}$ spin-orbitals. Finally $z_{i_{\sigma'}}$ is given by [176]:

---

[1] In Eq.(4.53) Σ_G correspond to $\Sigma^{\sigma\sigma}_{G_{\alpha\alpha}}$ or to $\Sigma^{-\sigma-\sigma}_{G_{\alpha\alpha}}$, but in this case $\Sigma^{\sigma\sigma}_{G_{\alpha\alpha}} = \Sigma^{-\sigma-\sigma}_{G_{\alpha\alpha}}$ because we are interested in the paramagnetic case. For this reason we directly skipped the σ apices in Eq.(4.53).

[2] In Eq.(A.2) the term $-\Delta\rho_{dd}$ does not appear because to evaluate $\Sigma^{\sigma\sigma}_{G_{\alpha\alpha}}$ only the hopping terms in the GA kinetic operator are important.

$$z_{i_{\sigma'}} = \frac{\sqrt{(1-\rho_{i_{\sigma'}i_{\sigma'}}-\rho_{i_{-\sigma'}i_{-\sigma'}}+d_i)(\rho_{i_{\sigma'}i_{\sigma'}}-d_i)}+\sqrt{d_i(\rho_{i_{-\sigma'}i_{-\sigma'}}-d_i)}}{\sqrt{\rho_{i_{\sigma'}i_{\sigma'}}(1-\rho_{i_{\sigma'}i_{\sigma'}})}}. \tag{A.3}$$

In the previous equation d_i represents the doubly occupancy on the i ($i = d$,p) orbital, while $\rho_{i_{\sigma'}i_{\sigma'}}$ is the charge density localized on the $i_{\sigma'}$ spin-orbital of the same lattice site.
By applying Eq.(A.1) to Eq.(A.2) we gain:

$$\Sigma^{\sigma\sigma}_{G_{\alpha\alpha}} = \left[\sum_{j\sigma'} \frac{\partial z_{\alpha_{\sigma'}}}{\partial \rho_{\alpha_\sigma\alpha_\sigma}} z_{j_{\sigma'}} t_{\alpha_{\sigma'}j_{\sigma'}} \rho_{\alpha_{\sigma'}j_{\sigma'}} + \sum_{i\sigma'} z_{i_{\sigma'}} \frac{\partial z_{\alpha_{\sigma'}}}{\partial \rho_{\alpha_\sigma\alpha_\sigma}} t_{i_{\sigma'}\alpha_{\sigma'}} \rho_{i_{\sigma'}\alpha_{\sigma'}}\right]\Bigg|_{min}, \tag{A.4}$$

where the right hand side of Eq.(A.4) has to be evaluated taking as values for the several used parameters the ones coming from the minimization procedure as applied to the GA Hamiltonian.
Eq.(A.4) can be further simplified because in our case $t_{\alpha_{\sigma'}j_{\sigma'}} = t_{j_{\sigma'}\alpha_{\sigma'}}$ and $\rho_{\alpha_{\sigma'}j_{\sigma'}} = \rho_{j_{\sigma'}\alpha_{\sigma'}}$, i and j behaves as mute indices:

$$\Sigma^{\sigma\sigma}_{G_{\alpha\alpha}} = \left[\sum_{j} t_{\alpha_\sigma j_\sigma} \rho_{\alpha j} \left(\frac{\partial z_{\alpha_\sigma}}{\partial \rho_{\alpha_\sigma\alpha_\sigma}} z_{j_\sigma} + \frac{\partial z_{\alpha_{-\sigma}}}{\partial \rho_{\alpha_\sigma\alpha_\sigma}} z_{j_{-\sigma}}\right)\right]\Bigg|_{min} \tag{A.5}$$

where $\rho_{\alpha j} = \rho_{i_\sigma\alpha_\sigma} + \rho_{i_{-\sigma'}\alpha_{-\sigma'}}$, which is equal to $2\rho_{i_{\sigma'}\alpha_{\sigma'}}$ in the paramagnetic case. This expression gives for $\alpha = d$:

$$\Sigma^{\sigma\sigma}_{G_{dd}} = \left[4 \cdot t_{d_\sigma p_\sigma} \rho_{dp} \left(\frac{\partial z_{d_\sigma}}{\partial \rho_{d_\sigma d_\sigma}} z_{p_\sigma} + \frac{\partial z_{d_{-\sigma}}}{\partial \rho_{d_\sigma d_\sigma}} z_{p_{-\sigma}}\right)\right]\Bigg|_{min} \tag{A.6}$$

and for $\alpha = p$:

$$\Sigma^{\sigma\sigma}_{G_{pp}} = \left[2{\cdot}t_{d_\sigma p_\sigma}\rho_{dp}\left(\frac{\partial z_{p_\sigma}}{\partial \rho_{p_\sigma p_\sigma}} z_{d_\sigma} + \frac{\partial z_{p_{-\sigma}}}{\partial \rho_{p_\sigma p_\sigma}} z_{d_{-\sigma}}\right) + 4{\cdot}t_{p_\sigma p_\sigma}\rho_{pp}\left(\frac{\partial z_{p_\sigma}}{\partial \rho_{p_\sigma p_\sigma}} z_{p_\sigma} + \frac{\partial z_{p_{-\sigma}}}{\partial \rho_{p_\sigma p_\sigma}} z_{p_{-\sigma}}\right)\right]\Bigg|_{min} \tag{A.7}$$

These are the two expressions we have to evaluate to build the effective Coulomb interaction shown in Eq.(4.53) for the case of paramagnetic CuO_2 planes. The values gained this way for $\Sigma^{\sigma\sigma}_{G_{dd}}$ and $\Sigma^{\sigma\sigma}_{G_{pp}}$ for a 12×12 system and for different hole filling values (starting from the McMahan parameter set [178]) are reported in Tab.4.5 of Sec.4.4.3.

B

The Python Program and Other Codes

This appendix is devoted to the description of the procedure adopted to calculate the CVV Auger spectra from CuO_2 planes, which have been shown in Chapter 4.

The procedure is completely general and applies to both HFBLA (Hartree Fock - Bare Ladder Approximation) and GA , because the different ways these two approaches consider interactions enters in this calculation only through the used parameters, leaving unaltered the equations.

These are the fundamental steps of the adopted procedure:

1. **Calculation of the renormalized parameters**: To obtain the Auger spectra the first thing to do consists in evaluating the new values of the parameters adopted to calculate the Green's function as renormalized by interaction. For HFBLA this is accomplished by simply evaluating the shift which has to be applied to ε_d and ε_p, so as to take into account the effects of a mean Coulomb interaction treated in the Hartree-Fock approximation (see Sec.4.4.3). In the case of GA instead a self consistent procedure renormalizes all the needed parameters: ε_d, t_{pd}, t_{pp} and the hole numbers per site within each primitive cell, $n_{h_{Cu}}$ and n_{h_O}. These two tasks have been carried out by writing two simple "Mathematica" [173] programs.

2. **The Fermi energy**: Fermi energy is computed via a "Mathematica" program which takes as input parameters the renormalized quantities evaluated in the previous step. This is done by using a tight binding Hamiltonian and filling the lowest band (we are in the hole picture) until the wanted hole filling number is gained in accordance with a sort of aufbau principle (see Sec.4.4.3).

3. $\Sigma_{G_{\alpha\alpha}}$ **evaluation**: This step is needed to evaluate the effective Coulomb interaction $V_{\alpha\alpha}$ (see Sec.4.4.3) within the GA. $\Sigma_{G_{\alpha\alpha}}$ values are computed, following the equations of Appendix A, with a "Mathematica" code.

4. **The interacting two holes Green's function**: The following lines report the program written to calculate the CVV Auger spectra from Copper and Oxygen atoms embedded in a CuO_2 plane. The code is written in the Python [174] programming language, which has been chosen for the great flexibility it allows in testing and developing modeling ideas, together with an excellent mathematical support, allowing to obtain the performances which were required for the completion of the computations. From the user point of view the structure of the program is the following:

   (a) the user defines the general parameters of the computations, i.e. the number of k vectors in the cell, the number of digits to be kept in the computations, the width of the line shape δ, the energy range;

   (b) the user defines a set of configurations that she intends to compute (this amount to specifying the atomic species, the hopping parameters t_{pp},t_{pd}, the energies e_d,e_p, the Coulomb interactions u_{dd},u_{pp}, the Fermi energy, a description and the name of the output file for further processing);

   (c) for each configuration a computation is carried with the parameters required, and the results are saved on the requested files for being consulted afterwards. The program is object oriented, in the sense that it defines a GreenFunction class which is instanced according to the user input: in particular the compute method of the GreenFunction class takes a function as parameter: this function returns the required element of the interacting two holes Green's function matrix. This allows for good flexibility and code reuse. The program is fully commented (comments start from the "♯" symbol until the end of the line). The theory which lies at the root of the code is detailed in Chapt.3 and in Sects.4.4.1-4.4.3. Among the features of the program, it has to be noted that the upper bounds for the parameters are rather high, and mainly correspond to the amount of time that the user is willing to wait to gain a single spectrum. For instance up to 900 k-vectors on a typical desktop the program takes reasonable ranges of time to calculate a single pattern[1]. Great care has been devoted to profiling and timing the code to

[1]To quantify the timing performance of our Python code see the footnote on page 104.

reduce as much as possible the bottlenecks and to provide reliable results, which have been double checked with "Mathematica" code where possible. To this end, the program can provide timing information (argument timeit of the compute method) and uses the **psyco** module for *Just in Time* compilation and the **numpy** and **scipy** for optimal mathematical performance. In more detail the algorithm is the following:

- initialize the GreenFunction class, like in *my_greenfunction = GreenFunction(precision, parameter.energies, parameter.hopping, parameter.coulomb, parameter.fermi, parameter.label)*. This also computes the first Brillouin zone (self.brillouin);
- then call the compute method, which begins by building the tight binding Hamiltonian of Eq.(4.44) and compute its eigenvalues and eigenvectors as a function of the input parameters (ε_d, ε_p, t_{pp},t_{pd}, k_x, k_y, U_{dd} and U_{pp}) (this is stored in the kdata attribute of class GreenFunction);
- then compute the non interacting two particles Green's function matrix, $\hat{g}_Q(\omega)$ (see Eq.(4.52)), which is referred to as $g_0(\omega)$ in the code (method compute_g0);
- the interacting two particles Green's function matrix is computed following Eq.(4.42). It then takes its diagonal matrix element corresponding to the atom of the primitive cell which has been assumed to be the source for the signal. This means that element 11 is taken for the Auger spectrum from Copper while the 22 or 33 matrix would be taken for the two one other atoms, the Oxygen Ox and Oy (see Sec.4.4.1) (method compute_my_interacting);
- finally the spectrum is computed as the imaginary part of the chosen matrix element of the interacting two particles Green's function, multiplied by $-\frac{1}{\pi}$.

This is stored in:

```
######################################################################
######################################################################
##                                                                  ##
##  Program for the calculation of the correlated two holes         ##
##  Green's function for a CVV Auger transition from a CuO_2        ##
##  plane                                                           ##
##                                                                  ##
##  Authors: Dr. Simona Ugenti and Dr. Francesco Guerrieri          ##
##                                                                  ##
######################################################################
######################################################################

# Latest Revision on 26 June 2008
# Refactoring on october, 12 2008.

# Everything is packed in classes to achieve better usability and
# performances.

# Import of the modules needed for the computations
# and the GUI

from __future__ import division
from numpy import matrix
from math import cos
import scipy
import numpy

try:
    from pylab import axis, eig, plot, show, xlabel, ylabel, title
except:
    print 'Couldn\'t find pylab, do something about that.'
    from scipy.linalg import eig
import math
import time
```

```
import datetime
from pprint import pprint

# return_pairs() creates all the possible combinations of the k_x
# and k_y values calcuted on the First Brillouin zone of the
# considered system or else of the CuO_2 planes.

def return_pairs(seq):
    """
    return_pairs(seq) -> Given a sequence return a generator which
    yields all the possible pairs, with repetitions.
    Example:
    >>> for item in return_pairs(xrange(2)):    print item
    (0, 0)
    (0, 1)
    (1, 0)
    (1, 1)

    """
    copy_of_seq = seq[:]
    for i in seq:
        for j in copy_of_seq:
            yield i, j


# theta() is simply the definition by means of logic operators of
# the Heavyside function.

def theta(x):
    """ theta (x) -> 1 if x < 0, 0 if x >= 0.
    It is -1 times the Heavyside function.
    """
    return x < 0
```

```
def my_module(x):
    """
    my_modules (x) takes a value in R and brings it back into the
    first Brillouin zone, -infinity < x < infinity -> - pi <= x < pi
    """
    if scipy.sign(x) == 1:
        while x > scipy.pi:
            x = x-2*scipy.pi
    else:
        while x <= -1*scipy.pi:
            x = x + 2*scipy.pi
    return x

def my_range(start, stop, step):
    """
    my_range(start, stop, step) yields values from start (included)
    to stop incrementing by step. It is used for the omega vector:
    that is, the energies where the Green's function will be evaluated.
    It accepts any numeric values and not only integers like range and
    xrange.
    """
    value = start
    if step <= 0:
        print "Can only iterate forward! Step must be positive."
        raise StopIteration

    while value < stop:
        yield value
        value = value + step

# Main
class GreenFunction(object):
    """
        __init__(precision, energies, hopping, coulomb_interactions,
```

```
        fermi, label)

        where precision is the number of digits requested,
        energies is a dict with 'ed' and 'ep' keys,
        hopping is a dict with 'tpd' and 'tpp' keys,
        coulomb_interactions is a dict with 'udd' and 'upp' keys,
        fermi is the fermi energy of the system.
        tpd is the Cu-O hopping term;
        tpp is the O-O hopping term;
        ed is the 3d orbital binding energy
        Since the oxygen 2p binding energy, ep, has been
        set to zero,  ed corresponds to the energy difference ed-ep
        (we are in the hole picture);
        label is a description of the system.

    """
    def __init__(self, precision, energies, hopping,
                 coulomb_interactions, fermi, label):

        self.precision = precision
        # Parameter initialization

        self.ed = energies['ed'] # d orbital
        self.ep = energies['ep'] # p orbital
        self.udd = coulomb_interactions['udd']
        self.upp = coulomb_interactions['upp']
        self.tpd = hopping['tpd']
        self.tpp = hopping['tpp']
        self.fermi = fermi
        self.label = label
        self.brillouin = [scipy.pi*(-1+2*n/L) for n in range(1,L+1)]

    def hh(self, kx,ky):
        # Definition of the system Hamiltonian, which has as variables
```

```
        # the components of the wave vector k in the xOy plane and
        # as parameters tpd, tpp and ed. Here:



        ed = self.ed
        ep = self.ep
        tpd = self.tpd
        tpp = self.tpp
        return matrix([[ed,2*tpd*cos(kx/2),2*tpd*cos(ky/2)],
                   [2*tpd*cos(kx/2),ep,  -4*tpp*cos(kx/2)*cos(ky/2)],
                   [2*tpd*cos(ky/2),-4*tpp*cos(kx/2)*cos(ky/2),ep]])

    def compute(self, energy_range, interacting_green_function,
        timeit,output=None):
        """
        compute (energy_range, interacting_green_function, timeit,
        output) -> It computes the correlated time ordered two
        particles Green function, passed via interacting_green_function.
        If timeit is True, it computes the time.
        If output is an open file, it writes the results on it.
        """
        self.kdata = self.eigensystem() # eigensystem for all the
                                        # k vectors
        final_data = []
        print self.label
        print "Job starting."
        if timeit:
            start = time.time() # Time counter
        self.my_interacting = interacting_green_function
        for omega in energy_range:
            print '.',
            qresult = self.compute_g0(omega)
            final_data.append(self.compute_my_interacting(qresult))
```

```
        if timeit:
            end = time.time()
            print "\nJob done in ", end - start, "seconds\n"

        datapoints = [val.imag/(-1*math.pi*L**2) for val in final_data]

        if output is None:
            print datapoints
        else:
            output.write(self.label + '\n')
            datapoints = ", ".join(str(value) for value in datapoints)
            output.write(datapoints)
            output.close()

    def eigensystem(self):
        """
        For each k vector in the brillouin zone, compute eigenvalues
        and eigenvectors of the Hamiltonian.
        Returns a dictionary.
        """
        kdata={}
        for index, kvector in enumerate(return_pairs(self.brillouin)):
            kdata[index]=self.my_eig(*kvector)
        return kdata


    def my_eig(self, kx, ky):
        """
        my_eig computes the eigenvalues and eigenvectors of the given
        Hamiltonian and returns a Python dictionary:
        kx, ky -> {0:{'eigval':value of the 1st eigenvalue,
        'eigvec':1st eigenvector}, 1:{'eigval':value of the 2nd
        eigenvalue, 'eigvec':2nd eigenvector}, 2:{'eigval':value of
        the 3rd eigenvalue, 'eigvec':3rd eigenvector}} corresponding
```

```
        to hh(kx, ky).
        """
        precision = self.precision
        res =eig(self.hh(kx,ky))
        diz={}
        for index in range(3):
            diz[index]={'eigval':res[0][index],
            'eigvec':scipy.around(scipy.asarray(res[1][:,index]),
            decimals=precision)}
        return diz

    # compute_g0(omega) evaluates a 3*3 matrix for each considered
    # (qx,qy) vector which represents the not correlated two holes
    # Green's function of the system as a function of the hole
    # binding energies omega.

    def compute_g0(self, omega):
        """ compute_g0(omega) evaluates a 3*3 matrix for each
        (qx,qy) vector which represents the not correlated two
        holes Green's function of the system as a function of the
        hole binding energies omega.
        """
        # To speed up lookup, bind to local names E_Fermi and scipy.outer
        E_Fermi = self.fermi
        out = scipy.outer

        qsum = {}
        for index, qvector in enumerate(return_pairs(self.brillouin)):
            qx,qy = qvector
            qsum[index]=0
            for k_index, k_point in
                enumerate(return_pairs(self.brillouin)):
                kx, ky = k_point
                qeig = self.my_eig(my_module(qx+kx),my_module(qy+ky))
```

```
                for n in range(3):
                    for m in range(3):
                        v1=qeig[n]["eigvec"]*
                           self.kdata[k_index][m]["eigvec"]
                        num=out(v1,v1)*(1-theta(qeig[n]["eigval"]
                            -E_Fermi)-
                            theta(self.kdata[k_index][m]["eigval"]
                            -E_Fermi))
                        den=(omega - (qeig[n]["eigval"]
                             +self.kdata[k_index][m]["eigval"])
                             +1j*delta)*L**2
                        qsum[index] += num/den
        return qsum

    def compute_my_interacting(self, qresult):
        """
        compute_GintCu() -> Calculates GintCu(a,b,c,d,m,f) for every
        (qx,qy) in the first Brillouin zone and then sums all
        these values
        """
        Gnosum = 0
        for qres in qresult.values():
            Gnosum += self.my_interacting(qres[0,0],qres[0,1],
            qres[0,2],qres[1,1],qres[1,2],qres[2,2], self.upp, self.udd)
        return Gnosum


class ParameterSet(object):
    pass

def cu_GreenInteracting(a,b,c,d,m,f, upp, udd):
    """
    cu_GreenInteracting(a,b,c,d,m,f, upp, udd) ->
    Returns the element [0,0] of the interacting
```

```
    two holes Green's function matrix.
    Its arguments are respectively:
    a = g0[0,0], b = g0[0,1],c = g0[0,2],d = g0[1,1],m = g0[1,2],
    f = g0[2,2]
    """
    return (c*(c*upp - c*d*upp**2 + b*m*upp**2))/(1 - a*udd - d*upp
           - f*upp - (b**2)*udd*upp - (c**2)*udd*upp + a*d*udd*upp
           + a*f*udd*upp + d*f*upp**2 - (m**2)*(upp**2)
           + (c**2)*d*udd*upp**2 + (b**2)*f*udd*upp**2
           - a*d*f*udd*upp**2 - 2*b*c*m*udd*upp**2 + a*(m**2)*udd*upp**2)
           + (b*(b*upp - b*f*upp**2 + c*m*upp**2))/(1 -
           a*udd - d*upp - f*upp - (b**2)*udd*upp - (c**2)*udd*upp
           + a*d*udd*upp + a*f*udd*upp + d*f*upp**2 - (m**2)*(upp**2)
           + (c**2)*d*udd*upp**2 + (b**2)*f*udd*(upp**2)
           - a*d*f*udd*upp**2 - 2*b*c*m*udd*upp**2 +a*(m**2)*udd*upp**2)
           + (a*(1 - d*upp - f*upp + d*f*upp**2 - (m**2)*(upp**2)))
           /(1 - a*udd - d*upp - f*upp - (b**2)*udd*upp -
           (c**2)*udd*upp + a*d*udd*upp + a*f*udd*upp + d*f*upp**2
           - (m**2)*(upp**2) + (c**2)*d*udd*upp**2 +(b**2)*f*udd*upp**2
           - a*d*f*udd*upp**2 - 2*b*c*m*udd*upp**2 + a*(m**2)*udd*upp**2)

def o_GreenInteracting(a,b,c,d,m,f, upp, udd):
    """
    o_GreenInteracting(a,b,c,d,m,f, upp, udd) ->
    Returns the element [1,1] of the interacting
    two holes Green's function matrix.
    Its arguments are respectively:
    a = g0[0,0], b = g0[0,1],c = g0[0,2],d = g0[1,1],m = g0[1,2],
    f = g0[2,2]
    """
    return (d*(1-a*udd-f*upp-(c**2)*udd*upp+a*f*udd*upp))/(1-a*udd-
    d*upp-f*upp-(b**2)*udd*upp-(c**2)*udd*upp+a*d*udd*upp+
    a*f*udd*upp+d*f*(upp**2)-(m**2)*(upp**2)+(c**2)*d*udd*(upp**2)+
    (b**2)*f*udd*(upp**2)-a*d*f*udd*(upp**2)-2*b*c*m*udd*(upp**2)+
```

```
    a*(m**2)*udd*(upp**2))+(m*(m*upp+b*c*udd*upp-a*m*udd*upp))/(1-
    a*udd-d*upp-f*upp-(b**2)*udd*upp-(c**2)*udd*upp+a*d*udd*upp+
    a*f*udd*upp+d*f*(upp**2)-(m**2)*(upp**2)+(c**2)*d*udd*(upp**2)+
    (b**2)*f*udd*(upp**2)-a*d*f*udd*(upp**2)-2*b*c*m*udd*(upp**2)+
    a*(m**2)*udd*(upp**2))+(b*(b*udd-b*f*udd*upp+c*m*udd*upp))/(1-
    a*udd-d*upp-f*upp-(b**2)*udd*upp-(c**2)*udd*upp+a*d*udd*upp+
    a*f*udd*upp+d*f*(upp**2)-(m**2)*(upp**2)+(c**2)*d*udd*(upp**2)+
    (b**2)*f*udd*(upp**2)-a*d*f*udd*(upp**2)-2*b*c*m*udd*(upp**2)+
    a*(m**2)*udd*(upp**2))


if __name__ == '__main__':
    import psyco
    psyco.full()

    precision=5 # number of digits
    L = 12       # L*L is the total number of k-vectors
    delta = 0.1 # broadening of the calculated lineshape. It is
                # equivalent to convolve the computed line shape
                # with a Lorentzian curve having an HWHM of delta

    green = {"Copper":cu_GreenInteracting, "Oxygen":o_GreenInteracting}

    parameters = []

    first_set = ParameterSet()
    first_set.interacting = green["Copper"]
    first_set.hopping = {'tpd':1.5, 'tpp': 0.6}
    first_set.energies = {'ed': -3.3+(7.9/2)*0.273922,'ep':(3.6/2)*0.119984
    first_set.coulomb = {'udd':7.9,'upp': 3.6}
    first_set.fermi = -5.2489
    first_set.label = """
    Description of the first parameter set.
    """
```

```
first_set.outputname = "today_Copper_HFBLA_L12_nh08472.dat"

second_set = ParameterSet()
second_set.interacting = green["Oxygen"]
second_set.hopping = {'tpd':1.5, 'tpp': 0.6}
second_set.energies = {'ed': -3.3+(7.9/2)*0.273922,'ep':(3.6/2)*0.119984}
second_set.coulomb = {'udd':7.9,'upp': 3.6}
second_set.fermi = -5.2489
second_set.label = """
Description of the second parameter set.
"""
second_set.outputname = "today_Oxygen_HFBLA_L12_nh08472.dat"

parameters.append(first_set)
parameters.append(second_set)



for parameter in parameters:
    nrg=my_range(-20.0,-10.0,0.5) # omega vector
    my_greenfunction = GreenFunction(precision, parameter.energies,
    parameter.hopping, parameter.coulomb, parameter.fermi,
    parameter.label)

    try:
        today = str(datetime.datetime.today()).split()[0]
        filename = today + '_' + parameter.outputname
        my_file = open(filename, 'wb')
    except AttributeError:
        my_file = None
    my_greenfunction.compute(nrg, parameter.interacting,
    timeit=True, output=my_file)
```

C

Numerical Procedure for the Exact Three Particles Green's Function

The interacting three-particles Green's function, which has been used to test Eq.(4.81) and to observe what happens for $\widetilde{U} \neq 0$, can be computed by solving Eqs.(4.73-4.74) with an adequate number N_k of continuum states. It is a matter of algebra to show that Eqs.(4.73-4.74) require to compute the following non-interacting three-holes correlators, written in terms of the single particle Green's function $g(z)$:

$$\Phi^{(0)}_{A,A}(z) = [g \otimes g \otimes g](z); \tag{C.1}$$

$$\Phi^{(0)}_{A^i_k,A}(z) = [g \otimes g \otimes g_k](z); \tag{C.2}$$

$$\Phi^{(0)}_{A^i_k,A^j_p}(z) = [g \otimes g \otimes g_{k,p}\delta_{i,j} + g \otimes g_k \otimes g_p(1-\delta_{i,j})](z); \tag{C.3}$$

$$\begin{aligned} \Psi^{(0)}_{p,q}(z) &= \langle 0|c_{p2}c_2c_{-1}\frac{1}{z-H_0}c^+_{-1}c^+_2c^+_{q2}|0\rangle \\ &= [g \otimes g \otimes g_{q,p}](z) - [g \otimes g_q \otimes g_q](z). \end{aligned} \tag{C.4}$$

The need to calculate these quantities simply arises from projecting a Dyson-like equation on all the states making up the Hilbert space of the system (see Sec.4.5.2).

In the above expressions $|A\rangle$ is $|c^+_0c^+_1c^+_2|0\rangle$ and, besides the already defined three-particles states $|A^1_k\rangle$, we have introduced also the states $|A^2_k\rangle = |c^+_0c^+_{k1}c^+_2|0\rangle$ and $|A^3_k\rangle = |c^+_0c^+_1c^+_{k2}|0\rangle$. The symbol "$\otimes$" denotes a single convolution product, i.e. $[f \otimes p](z) = -\frac{1}{2\pi\imath}\int dz' f(z')p(z-z')$.

Eqs.(C.1-C.4) shift the problem of obtaining a numerical solution of Eqs.(4.73-4.74) to the calculation of the matrix elements of the one-hole Green's function, which can be obtained by:

$$\begin{aligned} g(z) &= \frac{1}{z-\varepsilon_0-\Sigma(z)}, \\ g_k(z) &= \frac{V_k}{z-\varepsilon_k} g(z), \\ g_{k,p}(z) &= \frac{\delta_{k,p}}{z-\varepsilon_k} + \frac{V_k}{z-\varepsilon_k} g(z) \frac{V_p}{z-\varepsilon_p}, \end{aligned} \tag{C.5}$$

where $\Sigma(z)$ is the embedding self-energy and V_i (with $i = k,p$) are the hopping integrals; ε_0 and ε_i ($i = k,p$) represent instead the energy of respectively a localized and a delocalized hole with momentum i.

To gain the above quantities, the only input parameters are the single particle density of states, $D(\omega)$, which are assumed to be zero for ω values outside the range $(-\frac{W}{2},\frac{W}{2})$ (where W is the band width), and the Coulomb repulsions U's. As a first step we Hilbert transform $D(\omega)$ to obtain the single-hole Green's function on the Auger site $g(z) = 1/[z-\varepsilon_0-\Sigma(z)]$, where ε_0 is given by $\int d\omega \cdot \omega D(\omega)$ (center of mass of the density of states). Assuming a linear dispersion for the continuum states of the solid, $\varepsilon_k = -\frac{W}{2} + (W/N)k$, $k = 1,...,N$, the hopping integrals V_k of the model can be evaluated from $V_k = \sqrt{|Im[\Sigma(\varepsilon_k)]|/\pi}$.
Once we gained all the needed parameters of the model, we compute the triple convolutions of Eqs.(C.1-C.4). This is done by expressing the single-hole Green's function in the Lehmann representation, which requires the solution of the (N_k + 1)-dimensional one-body problem.

D

Acronyms

- **1hLDOS** = One hole Local Density of States.
- **2hLDOS** = Two holes Local Density of States.
- **AED** = Auger Electron Diffraction.
- **AES** = Auger Electron Spectroscopy.
- **AF** = Anti-Ferromagnetic.
- **ALOISA** = Advanced Line for Overlayer, Interface and Surface Analysis.
- **APECS** = Auger PhotoElectron Coincidence Spectroscopy.
- **AR-APECS** = Angular Resolved Auger PhotoElectron Coincidence Spectroscopy.
- **BCC** = Body Centred Cubic lattice.
- **BCS** = Bardeen-Cooper-Schrieffer theory.
- **BLA** = Bare Ladder Approximation.
- **CLA** = Core Ladder Approximation.
- **CS** = Cini-Sawatzky.
- **CVV** = Core-Valence-Valence.
- **DFT** = Density Functional Theory.

- **FWHM** = Full Width at Half Maximum.
- **GA** = Gutzwiller Approximation.
- **HF** = Hartree-Fock.
- **HOPG** = Highly Ordered Pyrolytic Graphite.
- **KR** = Kotliar and Ruckenstein.
- **LDA** = Low Density Approximation.
- **LDLA** = Low Density Ladder Approximation.
- **MFA** = Mean Field Approximation.
- **RPA** = Random Phase Approximation.
- **SC** = Simple Cubic lattice.
- **SD** = Slater Determinant.
- **SFC-LDA** = SelF-Consistent Low Density Approximation.
- **SWCNT** = Single Wall Carbon NanoTubes.
- **TDGA** = Time Dependent Gutzwiller Approximation.
- **TEM** = Transmission Electron Microscopy.
- **XPS** = X-ray Photoemission Spectroscopy.

Bibliography

[1] S. Bellucci, M. Cini, P. Onorato and E. Perfetto, *Phys. Rev. B* **75**, 014523 (2007);

[2] E. Dagotto, *Rev. Mod. Phys.* **66**, 763 (1994);

[3] A. Balzarotti, M. Cini, E. Perfetto and G. Stefanucci, *J. Phys.: Cond. Matt.* **16**, R1387-R1422 (2004);

[4] N. F. Mott, *Proc. Roy. Soc. London A* **42**, 416 (1949);

[5] J. Hubbard, *Proc. Roy. Soc. London A* **276**, 2 (1959);

[6] P. W. Anderson, *Phys. Rev.* **115**, 2 (1959);

[7] M. Cini, *Effetto Auger*, Enciclopedia delle Scienze Fisiche, edited by Istituto della Enciclopedia Italiana Fondata da Giovanni Treccani (Rome,...), p.320;

[8] J. C. Riviére, *Development and Present State of the Theory of Auger Emission*, edited by United Kingdom Energy Authority (Harwell, 1982);

[9] *Lise Meitner*, Wikipedia, The Free Encyclopedia, URL: $http$: //en.wikipedia.org/wiki/Lise_Meitner;

[10] D. Chattarji, *The Theory of Auger Transitions*, edited by Academic Press (1976), pp. 20 - 27;

[11] J. C. Riviére, *Development and Present State of the Theory of Auger Emission*, edited by United Kingdom Energy Authority (Harwell, 1982), pp.6-41;

[12] H. Luth, *Solid Surface, Interface and Thin Films*, edited by Springer (2001), Panel III, p. 59;

[13] O. Gunnarsson and K. Schonhammer, *Phys. Rev. B* **22**,3710 (1980);

[14] H. W. Haak, *Auger-Photoelectron Coincidence Spectroscopy: a Study of Correlation Effects in Solids*, Degree Thesis, Gröningen University (1983);

[15] O. Gunnarsson and K. Schönhammer, *Phys. Rev. Lett.* **46**, 859 (1981);

[16] G. Stefani, *Synchrotron Radiation: Fundamentals, Methodologies and Applications*,

Conference Proceedings vol.**82**, edited by S. Mobilio and G. Vlaic (SIF, Bologna 2003), p. 319;

[17] G. Stefani, R. Gotter, A. Ruocco, F. Offi, F. Da Pieve, S. Iacobucci, A. Morgante, A. Verdini, A. Liscio, H. Yao and R. A. Bartynski, *J. El. Spec. Rel. Phen.* **141**, 149-159 (2004);

[18] J. C. Riviére, *Development and Present State of the Theory of Auger Emission*, edited by United Kingdom Energy Authority (Harwell, 1982), pp.46-68;

[19] G. Wentzel, *Z. Physik* 43, 524 (1927);

[20] E. H. S. Burhop, *The Auger Effect and Other Radiationless Transitions*, Cambridge University Press, London (1952);

[21] W. N. Asaad, *Proc. Phys. Soc.* **A249**, 555 (1959);

[22] M. A. Listengarten, *Bull. Acad. Sci. USSR, Phys. Ser.* **25**, 803 (1961); M. A. Listengarten, *ibid.* **26**, 182 (1962);

[23] M. H. Chen and B. Crasemann, *Phys. Rev.* **A8**, 7 (1973);

[24] D. L. Walters and C. P. Bhalla, *Phys. Rev.* **A3**, 519 (1971);

[25] D. L. Walters and C. P. Bhalla, *Phys. Rev.* **A3**, 1919 (1971);

[26] D. L. Walters and C. P. Bhalla, *Atomic Data* **3**, 301 (1971);

[27] E. U. Condon and G. H. Shortley, *The Theory of Atomic Spectra*, edited by Cambridge University Press (2nd edition, 1963), Chap. XI, p.266;

[28] H. Aksela and S. Aksela, *J. Phys. B: Atom. Molec. Phys* **7**, 1262 (1974);

[29] G. Breit, *Phys. Rev.* **34**, 553 (1929);

[30] G. Breit, *Phys. Rev.* **36**, 383 (1930);

[31] G. Breit, *Phys. Rev.* **39**, 616 (1932);

[32] J. J. Lander, *Phys. Rev.* **6**, 1382 (1953);

[33] C. J. Powell, *Phys. Rev. Lett.* **30**, 1179 (1973);

[34] M. Cini, *Solid State Commun.* **20**, 605 (1976);

[35] M. Cini, *Solid State Commun.* **24**, 681 (1977);

[36] G. A. Sawatzky, *Phys. Rev. Lett.* **39**, 504 (1977);

[37] P. J. Feibelman and E. J. McGuire, *Phys. Rev. B* **15**, 3575 (1977);

[38] A. M. Basset, T. E. Gallon, J. A. D. Matthewand M. Prutton, *Surf. Sci.* **35**, 63 (1973);

[39] P.Weightman, J. F. McGilp and C. E. Johnson, *J. Phys. C* **9**, L585 (1976);

[40] A. M. Baro, M. Salmeron and J. M. Rojo, *J. Phys. F* **5**, 826 (1975);

[41] H. H. Madden and J. E. Huston, *Solid State Commun.* **21**, 1081 (1977);

[42] P.J. Feibelman and E. J. McGuire, *Phys. Rev. B* **17**, 690 (1978);

[43] P. W. Anderson, *Phys. Rev.* **124**, 41 (1961);

[44] M. Cini, *Topics and Methods in Condensed Matter Theory, From Basic Quantum Mechanics to the Frontiers of Research*, edited by Springer-Verlag Hardcover (1st edition, 2007), p. 106;

[45] J. Hubbard, *Proc. Roy. Soc. A* **276**, 238 (1963);

[46] M. Cini, *Phys. Rev. B* **17**, 2788 (1978);

[47] C. J. Powell, *Solid State Commun.* **26**, 557 (1978);

[48] P. Weightman, *Reports on Progress in Phys. 45*, 753 (1982);

[49] P. Weightman and P. T. Andrews, *J. Phys. C 12*, 943 (1979);

[50] P. Weightman and P. T. Andrews, *J. Phys. C 13*, 3529 (1980);

[51] A. Pernaselci and M. Cini, *J. El. Spec. Rel. Phen.* **82**, 79 (1996);

[52] M. Cini, *Phys. Rev. B* **17**, 2486 (1978);

[53] M. Cini and A. D'Andrea, *Phys. Rev. B* **29**, 6540 (1983);

[54] C. Verdozzi, M. Cini, J. F. McGilp, G. Mondio, D. Norman, J. A. Evans, A. D. Laine, P. S. Fowles, L. Duò and P. Weightman, *Phys. Rev. B* **43**, 9550 (1991);

[55] R. J. Cole, C. Verdozzi, M. Cini and P. Weightman, *Phys. Rev. B* **49**, 13329 (1994);

[56] C. Verdozzi, M. Cini, J. A. Evans, R. J. Cole, A. D. Laine, P. S. Fowles, L. Duo and P. Weightman, *Europhys. Lett.* **16**, 743 (1991);

[57] M. Cini and C. Verdozzi, *Phys. Scr.* **T41**, 67 (1992);

[58] M. Cini, *Topics and Methods in Condensed Matter Theory, From Basic Quantum Mechanics to the Frontiers of Research*, edited by Springer-Verlag Hardcover (1st edition, 2007), p. 111;

[59] C. Verdozzi and M. Cini, *Phys. Rev. B* **51**, 7412 (1995);

[60] M. Cini and A. D'Andrea, *J. Phys. C: SOlid State Phys.* **16**, 4469-4478 (1983);

[61] M. Cini, *Surf. Sci.* **87**, 483 (1979);

[62] M. Cini and C. Verdozzi, *Il Nuovo Cimento* **9**, 1 (1987);

[63] M. Cini and C. Verdozzi, *J. Phys.: Condens. Matter* **1**, 7457-7470 (1989);

[64] M. Cini and C. Verdozzi,*Auger Spectroscopy and Electronic Structure*, edited by G. Cubiotti, G. Mondio and K. Wandelt, Springer Series in Surface Sciences **18** (Springer-Verlag Berlin, Heidelberg 1989), p. 122;

[65] A. Kotani and J. Toyozawa, *J. Phys. Soc. Jpn.* **37**, 912 (1974);

[66] L. A. Feldkamp and L. C. Davis, *Phys. Rev. B* **22**, 3644 (1980);

[67] V. Galitzkii, *Sov. Phys. JETP* **7**, 104 (1958);

[68] G. Treglia, F. Ducastelle and D. Spanjard, *J. Phys. (Paris)* **41**, 281 (1980);

[69] G. Treglia, M. C. Desionqueres, F. Ducastelle and D. Spanjard, *J. Phys. C* **14**, 4347 (1981);

[70] J. R. Schrieffer and D. C. Mattis, *Phys. Rev.* **140**, A1412 (1965);

[71] V. Drchal and J. Kudrnovsky, *J. Phys. F.* **14**, 2443 (1984);

[72] P. T. Andrews, T. Collins and P. Weightman, *J. Phys. C* **14**, L957 (1981);

[73] M. Cini and A. D'Andrea, *Auger Spectroscopy and Electronic Structure*, edited by G. Cubiotti, G. Mondio and K. Wandelt, Springer Series in Surface Sciences **18** (Springer-Verlag Berlin, Heidelberg 1989), p. 139;

[74] J. Fitchek, R. Patrick and S. M. Bose, *Phys. Rev. B* **26**, 6390 (1982);

[75] D. R. Jennison, *Chem. Phys. Lett.* **69**, 435 (1980);

[76] P. Hedegaard and F. U. Hillebrecht, *Phys. Rev. B* **34**,3045 (1986);

[77] D. K. G. De Boer, C. Haas and G. A. Sawatzky, *J. Phys. F: Metal Phys.* **14**, 2769 (1984);

[78] D. D. Sarma, S. R. Barman, S. Nimkar and H. R. Krishnamurthy, *Phys. Sci. T* **41**, 184 (1992);

[79] M. Cini and V. Drchal, *J. Phys. C: Cond. Matter* **6**, 8549 (1994);

[80] M. Cini and V. Drchal, *J. El. Spec. Rel. Phen.* **72**, 151-155 (1995);

[81] A. Marini and M. Cini, *Phys. Rev. B* **60**, 11391 (1999);

[82] C. Verdozzi, M. Cini and A. Marini, *J. El. Spec. Rel. Phen.* **117-118**, 41-55 (2001);

[83] M. Cini, *Topics and Methods in Condensed Matter Theory, From Basic Quantum Mechanics to the Frontiers of Research*, edited by Springer-Verlag Hardcover (1st edition, 2007), p. 270;

[84] M. C. Gutzwiller, *Phys. Rev.* **137**, A1726 (1965);

[85] V. Z. Vulovic and E. Abrahams, *Phys. Rev. B* **36**, 2614 (1987);

[86] T. Ogawa, K. Kanda and M. Matsubara, *Progr. Theor. Phys.* **53**, 614 (1975);

[87] D. Vollhardt, *Rev. Mod. Phys.* **56**, 99 (1984);

[88] W. F. Brinkman and T. M. Rice, *Phys. Rev. B* **2**, 4302 (1970);

[89] P. W. Anderson, *Solid State Phys* **14**, 99 (1963);

[90] T. A. Kaplan, P. Horsch and P. Hulde, *Phys. Rev. Lett.* **49**, 889 (1982);

[91] J. Bonner and M. E. Fisher, *Phys. Rev.* **135**, A640 (1964);

[92] F. Takano and M. Uchinami, *Progr. Theor. Phys.* **53**, 1267 (1975);

[93] W. Langer, M. Plischke and D. Mattis, *Phys. Rev. Lett.* **23**, 1448 (1969);

[94] M. Cyrot, *J. Phys.* **33**, 125 (1972);

[95] J. Florencio and K. A. Chao, *Phys. Rev. B* **14**, 3121 (1976);

[96] R. Dichtel,J. Jelitto and H. Koppe, *Z. Phys.* **246**, 248 (1971);

[97] R. Dichtel,J. Jelitto and H. Koppe, *Z. Phys.* **251**, 173 (1972);

[98] J. Bardeen, L. N. Cooper and J. R. Schrieffer, *Phys. Rev.* **108**, 1175 (1957);

[99] A. B. Migdal, *Zh. Eksp. Teor. Fiz.* **32**,399 (1957);

[100] A. B. Migdal, *Sov. Phys. - JETP* **5**,333 (1957);

[101] J. M. Luttinger, *Phys. Rev.* **119**, 1153 (1960);

[102] G. Kotliar and A. E. Ruckenstein, *Phys. Rev. Lett.* **57**, 1362 (1986);

[103] S. E. Barnes, *J. Phys. F* **6**, 1375 (1976);

[104] S. E. Barnes, *J. Phys. F* **7**, 2637 (1977);

[105] P. Coleman, *Phys. Rev. B* **29**, 3035 (1984);

[106] N. Read and D. Newns, *J. Phys. C* **16**, 3273 (1973);

[107] E. Arrigoni and G. C. Strinati, *Cond. Matt.* **9501132v2**, (1995);

[108] W. Metzner and D. Vollhardt, *Phys. Rev. Lett.* **62**, 324 (1989);

[109] F. Gebbhard, *Phys. Rev. B* **41**, 9452 (1990);

[110] R. Raimondi (private communication);

[111] G. Seibold and J. Lorenzana, *Phys. Rev. Lett.* **86**, 2605 (2001);

[112] P. Ring and P. Schuck, *The Nuclear Many-Body Problem* (Springer-Verlag, Berlin Heidelberg, 1980);

[113] H. Ehrenreich and M.H.Cohen, *Phys. Rev.* **115**, 786 (1959);

[114] G. Seibold, F. Becca and J. Lorenzana, *Phys. Rev. B* **67**, 085108 (2003);

[115] H. Yokoyama and H. Shiba, *J. Phys. Soc. Jpn.* **56**, 3582 (1987);

[116] E. H. Lieb and F. Y. Wu, *Phys. Rev. Lett.* **20**, 1445 (1968);

[117] G. Fano, *Phys. Rev. B* **42**, 6877 (1990);

[118] M. Cini and C. Verdozzi, *Solid State Commun.* **57**, 657 (1986);

[119] G. Seibold, F. Becca and J. Lorenzana, *Phys. Rev. Lett.* **100**, 016405 (2008);

[120] J. W. Negele and H. Orland, *Quantum Many-Particle Systems*, Frontiers in Physics (Addison-Wesley, 1988);

[121] J. P. Blaizot and G. Ripka, *Quantum Theory of Finite Systems* (MIT Press, Cambridge, MA, 1986);

[122] J. O. Sofo and C. A. Balseiro, *Phys. Rev. B* **45**, 377 (1992);

[123] S. Ugenti, M. Cini, E. Perfetto, F. Da Pieve, C. Natoli, R. Gotter, F. Offi, A. Ruocco, G. Stefani, F. Tommasini, G. Fratesi, M. I. Trioni and G. P. Brivio, *J. Phys.: Conf. Ser.* **100**, 072020 (2008);

[124] R. Gotter, A. Ruocco, A. Morgante, D. Cvetko, L. Floreano, F. Tommasini and G. Stefani *Nucl. Instrum. Methods A* **467-468**, 1468 (2001);

[125] URL http://physics.nist.gov/PhysRefData/DFTdata/Tables/ptable.html;

[126] S. P. Kowalczyk, R. A. Pollak, F. R. McFeely, L. Ley and D. A. Shirley, *Phys. Rev. B* **8**, 2387 (1973);

[127] J. B. Mann, *Atomic Structure Calculations I. Hartree-Fock Energy Results for the Elements Hydrogen to Lawrencium*, Los Alamos Scientific Report No. LASL-3690, (1967) unpublished;

[128] M. Cococcioni and S. De Gironcoli, *Phys. Rev. B* **71**, 0535105 (2005);

[129] I. V. Solovyev, P. H. Dederichs and V. I. Anisimov, *Phys. Rev. B* **50**, 16861 (1994);

[130] E. Jensen, R. A. Bartynski, S. L. Hulbert, E. D. Johnson and R. Garrett, *Phys. Rev. Lett.* **62**, 71 (1989);

[131] Lo I. Yin, I. Adler, T. Tsang, M. H. Chen, D. A. Ringers and B. Crasemann, *Phys. Rev. A* **9**, 1070 (1974);

[132] R. Gotter, A. Ruocco, F. Offi, F. Da Pieve, A. Verdini, H. Yao, R. A. Bartinsky and G. Stefani, *Private Comm.* (2007);

[133] E. Antonides, E. C. Janse and G. A. Sawatzky, *Phys. Rev. B* **15**, 1669 (1977);

[134] O. Gunnarsson,O.K. Andersen, O. Jepsen and J. Zaanen, Phys.Rev. **B39**, 1708 (1989);

[135] I. Anisimov, J. Zaanen and O.K.Andersen, *Phys. Rev. B* **44**, 943 (1991);

[136] I. Anisimov, I.V. Solovyev, M.A.Korotin, M.T. Czyzyk and G.A. Sawatzky, *Phys. Rev. B* **48**, 16929 (1993);

[137] G. Fratesi, M. I. Trioni, G. P. Brivio, S. Ugenti, E. Perfetto and M. Cini, *Phys. Rev. B* **78**, 205111 (2008);

[138] G. Fratesi, M. I. Trioni, G. P. Brivio, S. Ugenti, E. Perfetto and M. Cini, *arXiv:0811.3872v1 [cond-mat.str-el]* (2008);

[139] B. H. Bransden and C. J. Joachain, *Physics of Atoms and Molecules*, edited by Longman, p. 198;

[140] E. U. Condon and G. H. Shortley, *The Theory of Atomic Spectra* (Cambridge University Press, 1951), p. 123 and p.267;

[141] URL http://physics.nist.gov/PhysRefData/DFTdata/Tables/ptable.html;

[142] J. F. Janak, *Phys. Rev. B* **18**, 7165 (1978);

[143] M. Cini, *Corso di Fisica ATomica e Molecolare*, Edizioni Nuova Cultura (secod edition, 1998), Chapter 8;

[144] D. A. Shirley, *Phys. Rev. A* **7**, 1520 (1973);

[145] J. P. Perdew, K. Burke, and M. Ernzerhof, Physical Review Letters 77, 3865 (1996);

[146] Lo I Yin, I. Adler, M. H. Chen and B. Crasemann, *Phys. Rev. A* **7**, 897 (1973);

[147] F. Aryasetiawan and O. Gunnarsson, *Reports on Progress in Physics* **61**, 237 (1998);

[148] A. Marini, G. Onida and R. D. Sole, *Phys. Rev. Lett.* **88**, 016403 (2002);

[149] M. Cococcioni and S. De Gironcoli, *Phys. Rev. B* **71**, 035105 (2005);

[150] E. Perfetto, M. Cini, S. Ugenti, P. Castrucci, M. Scarselli, M. De Crescenzi, F. Rosei e M. A. El Khakani, *Phys. Rev. B* **76**, 233408 (2007);

[151] E. Perfetto, M. Cini, S. Ugenti, P. Castrucci, M. Scarselli, M. De Crescenzi, F. Rosei e M. A. El Khakani, *arXiv:0710.3721v1 [cond-mat.str-el]* (2007);

[152] E. Perfetto, M. Cini, S. Ugenti, P. Castrucci, M. Scarselli and M. De Crescenzi, *J. Phys.: Conf. Ser.* **100**, 052082 (2008);

[153] J. E. Houston, J. W. Rogers, R. R. Rye, F. L. Hutson and D. E. Remaker, *Phys. Rev. B* **34**, 1215 (1986);

[154] URL: $http://$www.pocographiteonline.com/servlet/StoreFront;

[155] K. S. Novoselov, A. K. Geim, S. V. Morozov, D. Jiang, M. I. Katsnelson, I. V. Grigorieva, S. V. Dubonos and A. A. Firsov, *Nature (London)* **438**, 197 (2005);

[156] Y. Zhang, Y. W. Tan, H. L. Stormer and P. Kin, *Nature (London)* **438**, 201 (2005);

[157] I. Takesue, J. Haruyama, N. Kobayashi, S. Chiashi, S. Maruyama, T. Sugai and H. Shinohara, *Phys. Rev. Lett.* **96**, 057001 (2006);

[158] Z. K. Tang, L. Zhang, N. Wang, X. X. Zhang, G. H. Wen, G. D. Li, J. N. Wang, C. T. Chan and P. Sheng, *Science* **292**, 2462 (2001);

[159] N. Braidy, M. A. Khakani and G. A. Botton, *Carbon* **40**, 2835 (2002);

[160] P. Castrucci, M. De Crescenzi, M. Scarselli, M. Diociaiuti, P. Chistolini, M. A. El Khakani and F. Rosei, *Appl. Phys. Lett.* **87**, 103106 (2005);

[161] R. Saito, M. Fujita, G. Dresselhaus and M. S. Dresselhaus, *Phys. Rev. B* **46**, 1804 (1992);

[162] J. E. Houston, D. E. Remaker, J. W. Rogers Jr., R. R. Rye and F. L. Hutson, *Phys. Rev. Lett.* **56**, 1302 (1986);

[163] M. Cini, *Phys. Rev. B* **17**, 2788 (1978);

[164]

[165] C. Verdozzi and M. Cini, *Phys. Rev. B* **51**, 7412 (1995);

[166] J. B. Mann, *Atomic Structure Calculations*, National Technical Information Service (Springfield, VA, 1967);

[167] S. Bellucci, M. Cini, P. Onorato and E. Perfetto, *Phys. Rev. B* **75**, 014523 (2007);

[168] J. G. Bednorz and K. A. Müller, *Z. Phys. B* **64**, 189 (1986);

[169] G. Seibold, *private communication* (2008);

[170] D. Van Der Marel, J. Van Elp, G. A. Sawatzky and D. Heitmann, *Phys. Rev. B* **37**, 5136 (1988);

[171] A. Balzarotti, M. De Crescenzi, N. Motta, F. Patella and A. Sgarlata, *Phys. Rev. B* **38**, 6461 (1988);

[172] R. Bar-Deroma, J. Felsteiner, R. Brener, J, Ashkenazi and D. Van Der Marel, *Phys. Rev. B* **45**, 2361 (1992);

[173] URL:$http://$www.wolfram.com;

[174] URL:$http://$www.python.org;

[175] E. K. U. Gross, E. Runge, O. Heinonen, *Many Particle Physics*, p.174 (Adam Hilger,1991);

[176] G. Seibold and J. Lorenzana, *Phys. Rev. Lett.* **86**, 2605 (2001);

[177] G. Seibold, F. Becca and J. Lorenzana, *Phys. Rev. Lett.* **100**, 016405 (2000);

[178] A. K. McMahan, J. F. Annett and R. M. Martin, *Phys.Rev. B* **42**, 6268 (1990);

[179] M. Cini, F. Maracci and R. Platania, *J. El. Spec. Rel. Phen.* **41**, 37-58 (1986);

[180] S. Ugenti, M. Cini, J. Lorenzana, G. Seibold, E. Perfetto and G. Stefanucci, *The First Application of TDGA to High T_c Superconductors*, in preparation;

[181] M. Cini, E. Perfetto, G. Stefanucci and S. Ugenti, *Phys. Rev. B* **76**, 205412 (2007);

[182] M. Cini, E. Perfetto, G. Stefanucci and S. Ugenti, *J. Phys.: Cond. Matt.* **20**, 474209 (2008);

[183] M. Cini, E. Perfetto, G. Stefanucci and S. Ugenti, *J. Phys.: Conf. Ser.* **100**, 0720198 (2008);

[184] C. P. Lund, S. M. Thurgate and A. B. Wedding, *Phys. Rev. B* **55**, 5455 (1997);

[185] URL: $http://$www.webelements.com/webelements/elements/text/periodictable/bind.html;

[186] URL: $http://$www.chembio.uoguelph.ca/educmat/ATOMDATA/bindener/elecbind.htm;

[187] S. M. Thurgate, *Aust. J. Phys.* **50**, 745 (1997);

[188] S. Aksela and J. Sivonen, *Phys. Rev. A* **25**, 1243 (1982);

[189] M. Davies, D. R. Jennison and P. Weightman, *J. Phys. C* **17**, L107 (1984);

[190] A. G. Kochur, D. Petrini and E. P. Da Silva, *Astron. Astrophys.* **365**, 248 (2001);